CLASSICAL REPRESENTATION OF QUANTUM SYSTEMS AT EQUILIBRIUM

By

SANDIPAN DUTTA

A DISSERTATION PRESENTED TO THE GRADUATE SCHOOL
OF THE UNIVERSITY OF FLORIDA IN PARTIAL FULFILLMENT
OF THE REQUIREMENTS FOR THE DEGREE OF
DOCTOR OF PHILOSOPHY

UNIVERSITY OF FLORIDA

2013

To my parents

ACKNOWLEDGMENTS

First and foremost, I would like to thank my advisor and mentor Professor Jim Dufty without whose guidance and encouragement this work would not have been possible. I would also like to acknowledge Jeffery Wrighton for helping me with the computations. Further, I would like to thank my committee members Professor Cheng, Professor Ladd, Professor Muttalib and Professor Reitze for their support. This work was made possible by the grants from DOE.

TABLE OF CONTENTS

LIST OF FIGURES

Abstract of Dissertation Presented to the Graduate School
of the University of Florida in Partial Fulfillment of the
Requirements for the Degree of Doctor of Philosophy

CLASSICAL REPRESENTATION OF QUANTUM SYSTEMS AT EQUILIBRIUM

By

Sandipan Dutta

August 2013

Chair: James W Dufty
Cochair: Hai-Ping Cheng
Major: Physics

A quantum system at equilibrium is represented by an effective classical system, chosen to reproduce thermodynamic and structural properties. The motivation is to allow application of classical strong coupling theories and classical simulations like molecular dynamics and Monte Carlo to quantum systems at strong coupling. The correspondence is made at the level of the grand canonical ensembles for the two systems. The effective classical system is defined in terms of an effective temperature, local chemical potential, and pair potential. These are determined formally by requiring the equivalence of the grand potentials and their functional derivatives of the quantum and representative classical systems. The mapping is inverted using the classical density functional theory to solve for these three parameters. Practical forms of these formal solutions are obtained using the classical liquid state theories like hypernetted chain approximation (HNC). The mapping is applied to the ideal Fermi gas is demonstrated and the details of the thermodynamics of the effective system is derived explicitly. As the next application we consider the uniform electron gas and an explicit form for the effective interaction potential is obtained in the weak coupling limit. The pair correlation functions are calculated using the HNC equations and compared with path integral Monte Carlo data and other theoretical models like Perrot Dharma-wardana. Excellent agreement is obtained over a wide range of temperatures and densities. The last application is to the shell structure of harmonically bound charges. We show that in the mean

field limit, the quantum effects of degeneracy and diffraction produce shells at very low temperatures.

CHAPTER 1
INTRODUCTION

The literature on the thermodynamics of quantum systems at zero and very high temperatures is vast and well developed. Many experiments and simulations have been performed around room temperature and very high temperatures. Since room temperature is usually small compared to the Fermi energy of most systems, which is in the order of ten thousand kelvin, these systems can be successfully described by zero temperature theories like the Fermi liquid theory [1–3] or the zero-temperature density functional theory (DFT) [1, 4–6]. On the other extreme, at very high temperatures, weak coupling theories like Debye-Huckel are quite successful. Very recently a new class of quantum systems called ”warm dense matter” (complex ion-electron systems) [7–10] , has emerged for which the traditional zero and high temperature theories fail. Although the ions are typically semi-classical, the electrons can have moderate to strong coupling and degeneracy. This is roughly the regime at which the temperatures are comparable to the Fermi temperature and the densities are close to solid. The typical temperatures and densities for warm dense matter are shown below in Figure 1-1. As of now we have a host of experimental data and simulation methods like the path integral Monte Carlo (PIMC) [11], but we lack an effective theory. The basic problem lies in the conditions for which both the strong coupling and the strong quantum effects occur together at finite temperatures. New theoretical ideas and methods are needed now to explain the physics of some of the interesting phenomena associated with such systems. The general objective here is to address this problem with a new method based on exploiting strong coupling classical many-body methods for application to these quantum systems.

The zero temperature theories are difficult to extend to finite temperatures. The Fermi liquid theory is based on the picture that the energy levels of the interacting system can be adiabatically modified into the weakly interacting system [1–3], which is usually true only at very low temperatures. The quasi-particles, on which the Fermi liquid

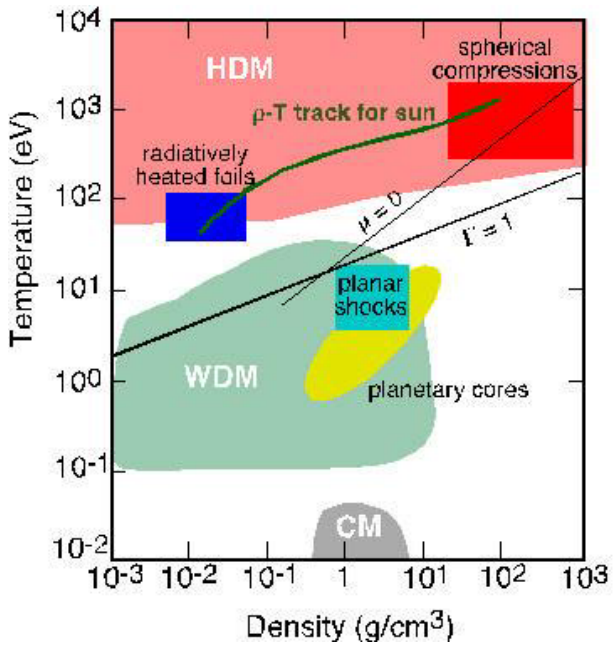

Figure 1-1. The temperature density plot showing the regime of the warm dense matter [12].

theory is based, have short lifetimes at finite temperatures and this is where the theory breaks down. Another successful zero temperature theory is the Kohn Sham formulation of density functional theory [1, 4–6], which is based on the filling up of the lowest energy Kohn-Sham orbitals at zero temperature. At finite temperatures more and more of these orbitals are filled and the calculations become increasingly difficult. At moderately high temperatures the practical calculations do not converge. Furthermore, the form of the exchange-correlation part of the free energy is not known at finite temperatures, hence the orbitals do not capture the physics accurately. Other methods like the local field correction theories [1, 13], which adds correlations to weakly coupled theories like the random phase approximation (RPA), fail at the metallic densities and low temperatures where they give negative pair correlations at short distances. Dynamical mean field theory assumes first that the problem of interest can be represented (approximately) by a lattice model [14–18]. This lattice system is then mapped exactly onto an impurity problem that can be solved approximately. It is not clear how this approach can be applied to the disordered, fluid-like states of WDM.

A completely different approach is the attempt to apply effective strong coupling methods of classical statistical mechanics to quantum systems using effective "quantum potentials" [19–33]. The quantum potentials are defined to incorporate selected quantum effects into the classical systems. Molecular Dynamics (MD) is very successful in describing the dynamics and the correlations for classical systems [32]. MD is also be used with the quantum potentials to study strong correlations in quantum systems. Molecular Dynamics and classical Monte Carlo methods are far less computationally intensive than quantum simulations like path integral Monte Carlo (PIMC). In addition, there exists a large literature in liquid state theory like hypernetted chain approximation (HNC) and Percus Yevick (PY) which successfully describe the strong correlations in classical systems [32]. These equations are easy to solve numerically, which led us to adopt the modified classical methods instead of the traditional quantum theories.

Recently Perrot and Dharma-wardana (PDW) introduced an effective temperature as well as a quantum potential to provide a model that can describe the equilibrium properties of hydrogen and the uniform electron gas for a wide range of temperatures and densities [29, 33, 34]. They split their effective potential for the uniform electron gas into a noninteracting term, also called the Pauli potential, and a regularized Coulomb term, for which they use the Deustch potential. Writing the potential in this way implies that the exact ideal gas exchange effects are recovered in the limit the interactions are zero. They introduced the concept of the effective temperature $T_c = \sqrt{T^2 + T_0^2}$ which remains finite at T=0. The quantity T_0 is determined by equating the exchange-correlation energy of the quantum system at $T = 0$ obtained from simulation data to the excess energy of the classical systems. This effective temperature T_c captures additional quantum many-body effects beyond those of the effective pair potential. Their other idea was to use their effective potential in the classical liquid state theory like the hypernetted chain approximation (HNC) to predict the pair correlation functions for the

uniform electron gas at equilibrium. Their phenomenological work provided an additional motivation for more systematic work.

The general objective addressed in this work is to develop a systematic theory to explain the thermodynamics of the strongly correlated quantum plasmas that will work for a wide range of temperatures and densities. Our approach is to construct an effective classical system that will represent the thermodynamics of the quantum system we want to describe [35]. The particles in the quantum system interact through a potential $\phi(\mathbf{r}, \mathbf{r}')$ in the presence of an external potential $\phi_{ext}(\mathbf{r})$. In the grand ensemble the relevant thermodynamic variables are the temperature T and chemical potential μ. The effective classical system has the corresponding effective potentials $\phi_c(\mathbf{r}, \mathbf{r}')$ and $\phi_{c,ext}(\mathbf{r})$ at the effective thermodynamic variables T_c and μ_c respectively. The unknown effective potentials and thermodynamic variables for the effective system are determined by mapping the thermodynamics of the classical system to that of the quantum system. Since we have to determine three unknown parameters we need three equivalent conditions. We set the pressure, density and pair correlation functions for the quantum and the classical system equal to each other.

To solve for the effective parameters, we invert the mapping defined above. The inversion is done within the classical density functional theory which relates the external potential and the interaction potential to the densities and the pair correlation functions respectively [44, 45]. Exact inversion is very difficult since that would involve the solution of the classical many-body problem. However within approximations like the integral equations in liquid state theory like HNC and Percus-Yevick this can be done to a good approximation [32]. The effective temperature is determined from the virial equation for pressure and the equivalence conditions of the pressures.

In this way we have the effective potentials and the classical thermodynamical variables in terms of the quantum quantities: pressure, density and pair correlation function. It seems like calculating the pressure, density and pair correlations themselves

would involve solving the full quantum many body problem and hence little progress has been made. However there exist some known limits from which the exact expressions for these quantities can be evaluated as approximations. The effective parameters, calculated with these approximate quantum quantities, are then put into some strong coupling classical theories to obtain the desired thermodynamical quantities. Thus the correlations in the resultant quantities are incorporated in two steps: the quantum correlations are incorporated in the effective parameters in some simple quantum approximation, such as weak coupling RPA, and then stronger correlations are obtained through the evaluation of properties by a chosen strong coupling classical method like HNC equations or MD simulations.

As a first application we consider the ideal Fermi gas. Although the ideal Fermi gas is a simple non-interacting system, the corresponding effective classical system is complicated because of the interactions coming from the Pauli exclusion statistics. The effective temperature stays finite because of the finite energies of the Fermions at zero temperatures. Some results for the average internal energy and the entropy which are true for the ideal Fermi systems is recovered for its classical counterpart.

The next application is to the uniform electron gas or ”jellium”. The effective potential is constructed to include the exchange effects through the Pauli potential and the Coulomb effects through the weak coupling RPA limit. The pair correlation functions are then calculated with this effective potential using the HNC equations. The agreement between these results and the quantum simulation data from PIMC and PDW model is quite good over a wide range of temperatures and densities. These results are next applied to the charges confined in a harmonic trap. Such systems are important for modeling laser cooled ions in a harmonic trap and electrons in quantum dots. The HNC equations were successfully used by Wrighton et al. [46] to predict the shell formation in classical Coulomb systems in a harmonic trap. Their results agreed quite well with the classical MC simulations as shown below in Figure 1-2 and provided motivation to

extend our work to confined systems. For classical Coulomb systems in a harmonic trap only the strong correlations produce shells. Consequently we do not get any shell structure in the mean field limit for any value of the coupling constant [46]. Here we explore the possible origins of shell formation due to the quantum effects of diffraction and degeneracy. We use the effective potentials to include appropriate quantum effects and solve for the density using the HNC equations. Even at the mean field level we get shells at very low temperatures and densities (large coupling constant).

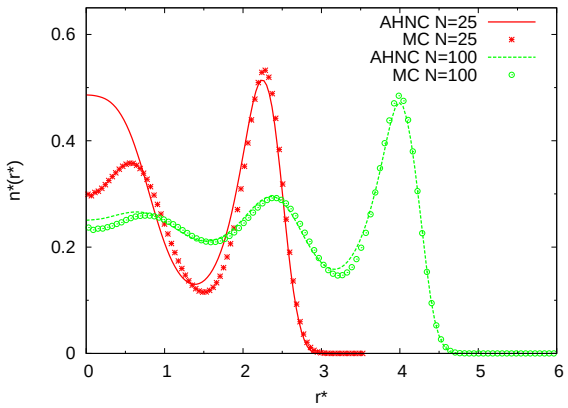

Figure 1-2. The comparison between the density profile obtained by Wrighton et al. and that of the classical MC is shown. The bridge terms need to be added to the HNC equations to get good agreement [46].

The rest of the Chapters are arranged in the following way:

1. In Chapter 2 we explore in further detail some of the available theories that treat strong correlations in both the classical and quantum systems. First we look at the Fermi liquid theory, its central concepts, formalism and limitations. The RPA with the local field corrections is briefly discussed in particular the earliest one, the STLS scheme. We briefly look into the density functional theory (DFT) for both classical and quantum as our model is based on these concepts. Lastly we look into the history and development of quantum potentials and the most successful applications of this approach. We discuss in detail the recent classical theory by Perrot and Dharma-wardana.

2. Chapter 3 sets up the theoretical framework on which the rest of this work is built. We construct an effective classical system that describes the thermodynamics of a given quantum system. We define the effective potentials and effective thermodynamic variables for the effective classical system by equating the three thermodynamic quantities of the classical and the quantum system. The map is

inverted using the classical density functional theory and the virial equation. The peculiarity of the thermodynamics of the effective system is discussed. Finally the classical mapping is applied to the ideal Fermi gas.

3. In Chapter 4 we explore the effective system for the uniform electron gas or ”jellium”. For the uniform electron gas we separate the interaction potential into an ideal gas and a Coulomb term, which is determined using weak coupling RPA. We use the HNC equations to calculate the pair correlation functions. We compare these pair correlations with those of the Perrot-Dharmawardana model and the simulation data from PIMC. The regime of the validity of this model is briefly discussed. Other thermodynamic quantities like the pressure and chemical potential are also predicted using this model and compared with other data.

4. In Chapter 5, first the existing classical theoretical models for shell formation are briefly reviewed. The classical map is then generalized to the confined quantum systems. The density profile for the effective system is calculated and the quantum effects of diffraction and degeneracy on the shell formation is discussed in the mean field limit. In the mean field limit, the classical Coulomb systems do not produce shells at any value of the coupling constant in a harmonic trap. However, we show that quantum diffraction and exchange effects lead to shell formation in this limit.

5. In Chapter 7, we briefly mention some possible applications of this map to the correlated quantum systems like the spin polarized electron gas and the lattice systems. The complete results for these systems have not been fully worked out with our map yet.

CHAPTER 2
CORRELATIONS IN QUANTUM SYSTEMS

This Chapter is divided into two sections. In the first section 2.1 we briefly review the quantum theories like the Fermi liquid theory, the RPA with the local field corrections, the density functional theory (DFT) and the dynamical mean field theory (DMFT). We discuss how the correlations and many-body effects are built into these theories. Although these theories are very successful at their respective domains, in the warm dense matter conditions where we are interested in they fail. In the second section 2.2 we look at the classical method to describe the quantum correlations using the quantum potentials. The quantum potentials are used in classical strong coupling theories like classical DFT, liquid state theories, Molecular Dynamics and classical Monte Carlo simulations to describe correlations in quantum systems. The recent success of the semi-classical formalism by Perrot and Dharma-wardana for uniform quantum systems and the classical strongly coupled liquid state formalism by Wrighton et al. provided motivation to look to classical methods for our work. We discuss briefly the Perrot Dharma-wardana model.

2.1 Quantum Theories For Electron Systems

In this section we briefly look into some of the quantum theories that are commonly used to study electron systems.

2.1.1 Fermi Liquid Theory

Fermi Liquid theory is widely used to study correlations in Fermi systems at very low temperatures [1–3]. We start with a non-interacting system and then turn on the interactions adiabatically. In case of no energy level crossing, this interacting system will have a set of eigenvalues which is in one-to-one correspondence with those of the non-interacting system. Thus the theory maps strongly coupled systems to weakly coupled systems, with the strong correlations absorbed into the effective masses and other parameters of the ”quasi-particles”. The sharply defined single particle energy

states get broadened by switching on the interactions, the width of which are given by the inverse lifetime of the quasi-particles. The Fermi liquid theory successfully describes strongly correlated quantum systems at very low temperatures. However it breaks down at finite temperatures due to two reasons: i) the higher energy states get filled and the Fermi surface is not well defined ii) the quasi-particles become very unstable.

2.1.2 Random Phase Approximation With Local Field Corrections

The response functions are widely used to study the collective and many-particle excitations and their associated equilibrium structure factors, in and around the equilibrium [1]. The fluctuation dissipation theorem [37, 38] relates the response functions to the structure factor, from which the other thermodynamic quantities are calculated. The simplest method for the response function calculation is the random phase approximation (RPA) which holds for weakly coupled systems [51]. To include strong correlations the local field corrections are added to the RPA.

When a test charge moves through an electron gas, it is not only influenced by the external potential ϕ_{ext} but also by the density fluctuations due to the motion of the test charge. Hence the particle sees an effective potential : $\int d\mathbf{r}'\phi_{ext}(\mathbf{r}', \omega)/\epsilon(\mathbf{r}, \mathbf{r}', \omega)$, i.e. the external potential modified by the medium. The Fourier transform of the dielectric function, ϵ in the effective potential for an uniform electron gas is given by :

$$\epsilon(\mathbf{k}, \omega) = 1 - \phi(\mathbf{k})\chi_{nn}(q, \omega) \tag{2–1}$$

where χ_{nn} is the proper density-density response function and ϕ the interaction potential.

Under the random phase approximation [1], we keep only the non-interacting part of the proper response function also called the Lindhard function. Further details about the structure factor and other thermodynamic quantities in the RPA approximation are given in the Appendix D. As a result RPA works for weakly interacting systems. The situation is remedied by introducing the local field correlations $G(q, \omega)$ to add the many-body effects missing in RPA due to neglecting the non-ideal gas terms. This is accomplished

by replacing the interaction potential $\phi(q)$ of the system by $\phi(q)(1 - G(q,\omega))$ in all the RPA computations. This not only preserves the simple form of the RPA but at the same time adds the exchange and correlation effects. The local field corrections are related to the response functions by the identity:

$$\phi(q)G(q,\omega) = \frac{1}{\chi(q,\omega)} - \frac{1}{\chi_0(q,\omega)} \tag{2–2}$$

where the χ_0 is the non-interacting response function. The first attempt to estimate the form of the field corrections was by Hubbard [40]. He assumed a frequency independent form for G for the same spins:

$$G(q) = \frac{q^2}{q^2 + k_F^2} \tag{2–3}$$

and $G = 0$ for different spins. The field corrections have some exact analytical limits, such as $q \to 0$, $G(q,\omega) \to 0$ and $q \to \infty$, $G(q,\omega) \to 1$.

Among the earliest methods to calculate the field techniques is the STLS scheme [13]. In STLS the field corrections are calculated self consistently from the static structure factor and the fluctuation dissipation theorem at zero temperature.

$$\begin{aligned} S(q) &= -\frac{\hbar}{\pi n}\int d\omega \Im\chi_{nn}(\mathbf{q},\omega) \\ \chi_{nn}(\mathbf{q},\omega) &= \frac{\chi_0(\mathbf{q},\omega)}{1 - v_q\left[1 - G(\mathbf{q},\omega)\right]\chi_0(\mathbf{q},\omega)} \\ G(q) &= -\frac{1}{n}\int \frac{d\mathbf{q}'}{(2\pi)^3}\frac{\mathbf{q}.\mathbf{q}'}{q^2}\frac{v_{q'}}{v_q}\left[S(\mathbf{q}' - \mathbf{q}) - 1\right] \end{aligned} \tag{2–4}$$

While the STLS improves the pair correlation functions from the RPA, they still go negative close to the origin at metallic densities. The correlation energy is in good agreement with Monte Carlo simulations and exhibit the correct r_s^{-1} behavior at large values of r_s. The plasmon dispersion relation which is obtained from the poles of the density-density response function goes negative at metallic densities. Also the compressibility sum rule is violated at those regimes. The zero temperature Equations

(2–4) have been extended to finite temperatures by Tanaka and Ichimaru [39–41]. The only difference at finite temperatures is the static structure factor equation gets modified by a Bose distribution term:

$$S(q) = -\frac{\hbar}{\pi n}\int d\omega coth(\beta\hbar\omega)\Im\chi_{nn}(\mathbf{q},\omega) \tag{2–5}$$

The finite temperature STLS again breaks down at metallic densities and suffers the same problem as the STLS [39].

2.1.3 Dynamical Mean Field Theory

Dynamical mean field theory (DMFT) is used to study strongly correlated lattice systems [14–17]. The DMFT associates a single-site effective dynamics through a local Green's function $\mathcal{G}_0(i\omega_n)$ which does not depend on the momentum. $\mathcal{G}_0$ is related to the on-site Green's function $G(i\omega_n)$, which is calculated later, through

$$\mathcal{G}_0(i\omega_n) = i\omega_n + \mu + G(1\omega_n)^{-1} - R[G(i\omega_n)]] \tag{2–6}$$

A Hubbard Hamiltonian [42] and an imaginary-time action functional S_{eff} defined for the lattice system. This formalism is solved by mapping it to an Anderson impurity model (AM) [18]. DMFT can be used to determine the stability of long ranged systems, the understanding the Hubbard model and the Mott insulator transition and high temperature superconductors. However it is not clear how this theory can be applied to the warm dense matter systems.

2.1.4 Hohenberg Kohn Density Functional Theory

The thermodynamics of a many-particle quantum system is determined from the grand potential Ω through

$$\beta\Omega(\Psi) = -\sum_{N=0}^{\infty} z^N \left\langle \Psi_N | e^{-\beta(\widehat{K_N}+\widehat{V}+\int d\mathrm{r}\widehat{n}(\mathrm{r})\phi_{ext}(\mathrm{r})} | \Psi_N \right\rangle \tag{2–7}$$

where Ψ_N, K_N, V and ϕ_{ext} are the N-particle many-body wave function, kinetic, interaction and the external potential respectively. The Hohenberg-Kohn-Mermin theorem

provides an alternate description of the thermodynamics in terms of the equilibrium density of the system [4–6]. The theorem claims that the ground state density uniquely determines the external potential that gives rise to it [43]. The theorem has been extended to finite temperatures by Mermin [6]. The proof of the theorem is based on minimizing the grand potential with respect to the density matrix. The grand potential functional is given by:

$$\beta\Omega[\rho] = -Tr\left(\hat{\rho}\left(\hat{H} - \mu\hat{N} + In\hat{\rho}\right)\right) \tag{2–8}$$

The grand potential is given by: $\Omega = -\frac{1}{\beta} In\, Tr\left(exp(-\beta(\hat{H} - \mu\hat{N}))\right)$ and the equilibrium density matrix by: $\hat{\rho_0} = exp(-\beta(\hat{H} - \mu\hat{N}))/Tr\left(exp(-\beta(\hat{H} - \mu\hat{N}))\right)$. The Mermin theorem states that $\Omega[\hat{\rho}] > \Omega[\hat{\rho_0}]$ for all density matrices $\hat{\rho}$. The practical implementation of Mermin's theorem however is very complicated as it involves the solution of the operator equations.

Kohn and Sham developed an elegant representation of the DFT which gives the exact result at the level of a non-interacting system [5]. Their approach involves solving single particle orbital equations with Kohn-Sham potentials and provides a practical implementation of the DFT theory at zero temperature. Kohn and Sham wrote their potential as a Hartree part and the rest called the exchange-correlation part. However the exchange-correlation potential is unknown. The Kohn-Sham approach is not practical at finite temperatures since the computations do not converge.

2.2 Classical Methods: Quantum Potentials

In this section we look into various techniques to incorporate quantum effects, in particular quantum exchange and diffraction, into classical systems. This is done using the quantum potentials. The quantum potentials are the potentials used in classical systems that incorporate quantum effects by appropriate parameterization or forms for these potentials. For example a quantum potential replacing the classical Coulomb potential is a Deutsch potential [21] that regularizes the Coulomb potential at the origin,

removing the classical singularity due to the diffraction effects. The parameters in the quantum potentials are determined using simulation data or exact known limits for the quantum systems. In the rest of the section we look into various ways to build the quantum potentials. These potentials are then put into some classical strong coupling theories like the classical DFT, classical liquid state theories and the classical simulations to strong correlations.

The effective potential ϕ^{eff} is a combination of N particle potentials ϕ_N^{eff}, which are defined in terms of the N particle Slater sums W_N for the quantum systems by:

$$\frac{1}{N!\lambda^N}\int dr^{(N)}\, W_N(r^{(N)}) = Tr\left[exp(-\beta\hat{H})\right]$$

$$\beta\phi_N^{eff}(r^{(N)}) = -ln(W_N(r^{(N)}))$$

$$\phi^{eff} = \sum_{i<j}^{N}\phi_2^{eff}(r_{ij}) + \sum_{i<j<k}^{N}\phi_3^{eff}(r_{ij}, r_{jk}, r_{ki}) + ... \tag{2–9}$$

(2–10)

For most practical applications the higher order potentials are neglected.

Uhlenbeck and Gropper [19] were the first to use an effective potential for the ideal Fermi (Boson) systems at very high temperatures to explain the exchange effects in an unpolarized gas:

$$\beta\phi^{eff}(r) = -ln\left(1 \mp \frac{1}{2}exp(-2\pi r^2/\lambda^2)\right) \tag{2–11}$$

This was later extended to all degeneracies by Lado for ideal quantum fluids [24]. The quantum effects of the spin statistics in Fermions due to Pauli's exclusion principle turns out to be repulsive while for the Bosons it is attractive.

An interesting choice for the definition of quantum potentials is through the use of the two particle density matrix $\hat{\rho}$. The effective potential is defined by

$$\rho_{ij} = \frac{(m_i m_j)^{3/2}}{(2\pi\hbar\beta)^3}exp(-\frac{m_i}{2\hbar^2\beta}(\mathbf{r}_i - \mathbf{r}'_j)^2)exp(-\frac{m_j}{2\hbar^2\beta}(\mathbf{r}_i - \mathbf{r}'_j)^2)exp(-\beta\phi_{ij}) \tag{2–12}$$

where ρ_{ij} is the two particle density matrix in coordinate representation.

In the weak coupling limit the diagonal element of the density matrix can be calculated exactly:

$$\triangle_K(\mathbf{x}_{ij}) = \frac{q_i q_j}{\lambda_{ij} x_{ij}} \left[1 - exp(-x_{ij}^2) + \sqrt{\pi} x_{ij} \left(1 - erf(x_{ij})\right)\right] \tag{2–13}$$

which is called the Kelbg potential, where $x_{ij} = r_{ij}/\lambda_{ij}$. The Kelbg form can be generalized by adding an extra parameter, γ_{ij} to give some effects of the bound states. Adding this extra parameter preserves the first derivative of the Kelbg potential but at the same time controls the height of the potential at the origin. To determine the parameter γ_{ij}, the effective potential is defined as : $exp(-\beta\phi_{ij}) \equiv S_{ij}$, where S_{ij} is the binary Slater sum of particles i and j. From this we obtain:

$$\gamma_{ij} = -\frac{\sqrt{\pi}}{\lambda_{ij}} \frac{q_i q_j \beta}{ln[S_{ij}(\mathbf{r}_{ij} = 0, \beta)]} \tag{2–14}$$

In particular the electron-electron Slater sum at the origin is given by:

$$S_{ee}(\mathbf{r}_{ee} = 0, \beta) = 2\sqrt{\pi}\epsilon_{ee} \int_0^\infty \frac{exp(-x^2)xdx}{1 - exp(-\pi\epsilon_{ee}/x)} \tag{2–15}$$

where $\epsilon_{ee} = q_i q_j \beta/\lambda_{ij}$. With this new parameter γ_{ij} the modified Kelbg looks like:

$$\triangle_K(\mathbf{x}_{ij}) = \frac{q_i q_j}{\lambda_{ij} x_{ij}} \left[1 - exp(-x_{ij}^2) + \sqrt{\pi}\frac{x_{ij}}{\gamma_{ij}} \left(1 - erf(x_{ij}\gamma_{ij})\right)\right] \tag{2–16}$$

Using this potential Filinov [27, 28] could explain the formation of hydrogen atoms using classical statistical mechanics. As discussed above the quantum potentials used in MD or classical MC simulations can be used to describe strong correlations for quantum systems. The classical density functional theory is another theoretical tool to do the same. Since our formalism is based on classical DFT we will discuss this theory in detail in the subsection 2.2.1.

2.2.1 Classical DFT

Just like the quantum DFT, the classical DFT provides a formalism to include strong correlations in classical systems [44, 45]. The reason for the discussion of the classical DFT in this Chapter is to broaden the scope of the classical methods of the quantum potentials and the PDW formalism. This section provides a quick overview of the classical DFT that will be discussed in detail in Chapter 3. The quantum effects will be incorporated through the appropriate thermodynamic quantities in the classical DFT equations. In classical DFT the grand potential functional is written as:

$$\Omega[n;\phi_{ext}] = F[n] + \int d\mathbf{r}\, n(\mathbf{r})\,(\phi_{ext}(\mathbf{r}) - \mu) \tag{2–17}$$

where $F[n] = \sum_{N=0}^{\infty} \int \left(\hat{K}_N + \hat{V}_N + k_b T ln(N! h^{DN}) + k_B T Inf[\phi_{ext}[n]]\right) d\mathbf{p}^N d\mathbf{q}^N$ in D dimensions. The Euler-Lagrange equation is:

$$\frac{\delta F[n]}{\delta n(\mathbf{r})} = \mu - \phi_{ext}(\mathbf{r}) \tag{2–18}$$

Next the $F[n]$ is written as the ideal gas part F_{id} and the excess part F_{ex} [45]. It can be shown that $\delta F_{id}/\delta n(\mathbf{r}) = In(n(\mathbf{r})\lambda^D)$.

The N th order correlation function is defined as:

$$c_N(\mathbf{r}_1, \mathbf{r}_2, \ldots, \mathbf{r}_N) = -\frac{\delta^N \beta F_{ex}[n]}{\delta n(\mathbf{r}_N)\delta n(\mathbf{r}_{N-1})\ldots\delta n(\mathbf{r}_1)} \tag{2–19}$$

The second order correlation function is called the direct correlation function and is related to the pair correlation function g through the Ornstein Zernike equation:

$$g(\mathbf{r}_1, \mathbf{r}_2) - 1 = c_2(\mathbf{r}_1, \mathbf{r}_2) + \int d\mathbf{r}_3\,(g(\mathbf{r}_1, \mathbf{r}_3) - 1)\, n(\mathbf{r}_3) c_2(\mathbf{r}_3, \mathbf{r}_2) \tag{2–20}$$

Using the above expressions the excess free energy at density $n(\mathbf{r})$ can be written in terms of that at density $n_0(\mathbf{r})$ as:

$$\begin{aligned}\beta F_{ex}[n] = \beta F_{ex}[n_0] + \int d\mathbf{r}_1 \left[\beta\mu - ln\left(n_0(\mathbf{r}_1)\right) - \beta\phi_{ext}(\mathbf{r}_1; n_0)(n(\mathbf{r}_1 - n_0(\mathbf{r}_1))\right) \\ -\frac{1}{2}\int_0^1 d\lambda \int_0^\lambda d\lambda' \int d\mathbf{r}_1 d\mathbf{r}_2\, c_2(\mathbf{r}_1, \mathbf{r}_2; n'_\lambda) \frac{\partial n_{\lambda'}(\mathbf{r}_1)}{\partial\lambda'} \frac{\partial n_{\lambda'}(\mathbf{r}_2)}{\partial\lambda'}\end{aligned} \tag{2–21}$$

where $n_\lambda(\mathbf{r}) = (1-\lambda)n_0(\mathbf{r}) + \lambda n(\mathbf{r})$. The above expression for excess free energy is still difficult to calculate because of the non-local dependence on density. In most cases the reference density is chosen to be uniform density $n_0(\mathbf{r}) = n_0$ and also the nonlocal density is replaced by the local density. One such theories, Ramakrishnan-Yussouff, can predict the freezing of liquids. The replacement of the non-local density dependence by the corresponding local one is also called hypernetted chain approximation. Further details is given in Appendix A. The classical DFT provides a useful formalism to include many-body effects at finite temperature. The calculations are easier as we do not have to solve the eigenvalue equation as Kohn-Sham DFT.

2.2.2 Perrot Dharma-wardana Method

Perrot and Dharma-wardana provided a computationally simple and novel method for calculating the pair correlation functions and other thermodynamic quantities for the uniform electron gas (UEG) using only the information about the correlation energy E_c obtained from PIMC at zero temperature [29, 33, 34]. They used classical liquid state theory, the HNC approximation to obtain the pair correlation function $g(r)$ for the UEG by putting in quantum many-body effects through a quantum potential $\phi_c(r)$ and an effective temperature T_c. The effective potential is written as a combination of Pauli potential $\phi^{(0)}$ and the Deustch potential

$$\beta_c\phi_c(r) = (\beta_c\phi_c)^{(0)}(r) + \frac{\Gamma_c}{r}\left(1 - exp(-r/\lambda_c)\right) \tag{2–22}$$

The Deustch potential is a simpler fitting function than the Kelbg potential in Equation (2–16). The Pauli potential $\phi^{(0)}$ contains the exchange effects and the Deustch potential

contains the Coulomb effects along with diffraction. The PDW potential is parameterized by the effective temperature T_c through the effective coupling constant Γ_c and the thermal wavelength λ_c. Since the leading energy dependence on temperature is quadratic, the effective temperature is assumed of the form $T_c = \sqrt{T^2 + T_0^2}$. T is the temperature of the actual quantum system and T_0 is the temperature of the classical fluid when the temperature of the quantum system is zero. At a given density n, T_0 is determined by setting the correlation energy $E_c(n)$ of UEG equal to the excess energy of the classical system at the temperature T_0. T_0 is fitted to a form $1/(a + b\sqrt{r_s} + cr_s)$, where $r_s = (3/(4\pi n))^{1/3}$. The coefficients a, b and c are obtained from variational Monte Carlo and diffusion Monte Carlo fitting data for E_c for r_s ranging from 1 and 10. Using this effective potential $\phi_c(r)$ and temperature T_c in the HNC equations

$$g(r) = exp(-\beta_c \phi_c(r) + g(r) - 1 - c(r)) \tag{2–23}$$

they were able to successfully reproduce the pair correlation functions for UEG in two and three dimensions at zero temperature. The function $c(r)$ in Equation (2–22) is obtained using the Ornstein-Zernike equation

$$g(r) - 1 = c(r) + n \int d\mathbf{r}'(g(|\mathbf{r} - \mathbf{r}'|) - 1)c(r') \tag{2–24}$$

The details about the HNC equations are discussed further in Chapter 3. The pair correlation functions, the specific heat and other thermodynamic quantities calculated using this model agree quite well with the data from the quantum simulations.

2.3 Why We Chose Classical Approach Instead Of Quantum theories (Our Motivation)

All the quantum theories discussed in the section 2.1 fail in the regime of warm dense matter. Either the concepts they are based on can not be easily extended to finite temperatures like the Fermi liquid theory and DFT or their prediction of some of the fundamental thermodynamic quantities is wrong like the STLS theory. Quantum

simulations like PIMC is computationally more intensive than the classical Molecular Dynamics and Monte Carlo. In the classical theories we do not have to solve the eigenvalues as the operator formalism of the quantum theories. The formalism by Perrot and Dharma-wardana show that using appropriate quantum potentials and the concept of effective temperature, the classical theories can successfully predict the uniform electron gas over a wide range of temperature and densities. Wrighton et al. used the HNC equations to study the shell formation in strongly correlated classical systems. The density profile predicted by them is in excellent agreement with the classical MC data. These two works provided us confidence that the classical methods are going to work for the ”warm dense matter” conditions for jellium and can be further extended to confined quantum systems. The Perrow Dharma-wardana model is however phenomenological and it is not clear what kind of physics gives such good agreement. In the next Chapter we build a systematic theory based on the classical approach incorporating some exact limits of the quantum systems. As is seen later our classical formalism successfully predicts the essential thermodynamics of the uniform electron gas and some interesting physics for the confined systems.

CHAPTER 3
THE EFFECTIVE CLASSICAL SYSTEM

In this Chapter we construct a formalism to describe quantum correlations, develop practical ways of implementing it and then apply it to the case of the ideal Fermi gas. We explicitly build an effective classical system having the thermodynamics and the equilibrium structure of the quantum system we want to describe [35]. The thermodynamics of the effective system depends on three parameters: effective interaction potential ϕ_c, effective local chemical potential μ_c and effective temperature T_c. These parameters are determined by mapping selected quantum properties onto the classical system. The explicit calculation of these parameters is only formal because it requires a solution to the classical many body problem. For practical applications we introduce approximations like the weak coupling classical approximation and the random phase approximation for the quantum systems as illustrated in Chapters 4. In this Chapter we apply this formalism to the ideal Fermi gas and interpret the results, as a first illustration.

3.1 Definition Of The Representative Classical System

3.1.1 Thermodynamics From Statistical Mechanics

Consider a quantum system of N particles inside a volume V in an external potential ϕ_{ext}. The particles are interacting though a pair-potential ϕ. We chose the Grand canonical description for the system, hence the thermodynamics of the system needs two parameters, the inverse temperature β and the chemical potential μ. The Hamiltonian of the system does not depend on the internal degrees of freedom like spin. It is of the form:

$$H = K + \Phi + \Phi_{ext} \tag{3–1}$$

where K denotes the total kinetic energy,

$$K = \sum_{i=1}^{N} \frac{p_i^2}{2m} \tag{3–2}$$

Φ is the total interaction potential energy among particles, Φ_{ext} is the total external potential acting on the system.

$$\Phi = \frac{1}{2}\sum_{ij}^{N}\phi(\mathbf{q}_i, \mathbf{q}_j), \qquad \Phi_{ext} = \sum_{i=1}^{N}\phi_{ext}\left(\mathbf{q}_i\right) \tag{3–3}$$

These can be written in the equivalent forms :

$$\hat{\Phi}_{ext} = \sum_{i=1}^{N}\phi_{ext}(\hat{q}_i) = \int d\mathbf{r}\phi_{ext}(\mathbf{r})\hat{n}(\mathbf{r})$$
$$\hat{\Phi} = \sum_{i\neq j}^{N}\phi(\hat{q}_i, \hat{q}_j) = \int d\mathbf{r}\,d\mathbf{r}'\phi(\mathbf{r}, \mathbf{r})\hat{g}(\mathbf{r}, \mathbf{r}') \tag{3–4}$$

$$\tag{3–5}$$

where $\hat{n}(\mathbf{r}) = \sum_{i=1}^{N}\delta(\hat{q}_i - \mathbf{r})$ and $\hat{g}(\mathbf{r}, \mathbf{r}') = \hat{n}(\mathbf{r})\hat{n}(\mathbf{r}') - \hat{n}(\mathbf{r})\delta(\mathbf{r} - \mathbf{r}')$. In the Grand ensemble the Hamiltonian occurs in combination with the chemical potential

$$\hat{H} - \mu N = \hat{K} + \hat{\Phi} + \hat{\Phi}_{ext} \tag{3–6}$$
$$= \hat{K} + \int d\mathbf{r}\,d\mathbf{r}'\phi(\mathbf{r}, \mathbf{r})\hat{g}(\mathbf{r}, \mathbf{r}') - \int d\mathbf{r}\left(\mu - \phi_{ext}(\mathbf{r})\right)\hat{n}(\mathbf{r}) \tag{3–7}$$

The quantity in the above equation $\mu - \phi_{ext}(\mathbf{r})$ is called the local chemical potential and is denoted by the symbol $\mu(\mathbf{r})$.

All thermodynamic quantities can be derived from the grand potential Ω [47]. It depends on three thermodynamic parameters: the inverse temperature β, the local chemical potential $\mu(\mathbf{r})$, and the volume V, and is given by

$$\Omega(\beta \mid \mu, \phi) = -\beta^{-1}\ln\sum_{N} Tr_N e^{-\beta\left(\hat{H} - N\mu\right)} \tag{3–8}$$

The symbol Tr_N denotes a trace over the N particle antisymmetric wave-functions for Fermions or symmetric wave-functions for Bosons. From the Equations (3–6) and (3–8) we see that Ω is a function of the inverse temperature β and functionals of the interaction potential ϕ and local chemical potential μ. From now on we use the

$(parameters \mid functionals)$ notation to make the distinction between the parameter and functional dependence. The dependence on the volume V is left implicit. In the grand ensemble the pressure $p(\beta \mid \mu, \phi)$ is related to the grand potential by:

$$p(\beta \mid \mu, \phi) V = -\Omega(\beta \mid \mu, \phi) \tag{3–9}$$

The first order derivatives of the grand potential give the internal energy $E(\beta \mid \mu, \phi)$ and average number density $n(\mathbf{r};\beta \mid \mu, \phi)$ and average pair correlation function $g(\mathbf{r}, \mathbf{r}'; \beta \mid \mu, \phi)$

$$E(\beta \mid \mu, \phi) = \frac{\partial \beta \Omega(\beta \mid \mu, \phi)}{\partial \beta} \mid_{\beta\mu(\mathrm{r})} \tag{3–10}$$

$$n(\mathbf{r};\beta \mid \mu, \phi) V = -\frac{\delta \Omega(\beta \mid \mu, \phi)}{\delta \mu(\mathbf{r})} \mid_{\beta} \tag{3–11}$$

$$\begin{aligned} \frac{\delta \Omega(\beta \mid \mu, \phi)}{\delta \phi(\mathbf{r}, \mathbf{r}')} \mid_{\beta,\mu} &\equiv n(\mathbf{r};\beta \mid \mu, \phi) n(\mathbf{r}';\beta \mid \mu, \phi) g(\mathbf{r}, \mathbf{r}';\beta \mid \mu, \phi) \\ &= \langle \widehat{n}(\mathbf{r}) \widehat{n}(\mathbf{r}'); \beta \mid \mu, \phi \rangle - n(\mathbf{r};\beta \mid \mu, \phi) \delta(\mathbf{r} - \mathbf{r}') \end{aligned} \tag{3–12}$$

as can be seen from Equation (3–6). Higher order derivatives provide the fluctuations (susceptibilities) and structure functions. In particular, the second functional derivative with respect to $\mu(\mathbf{r})$ is related to the response function $\chi(\mathbf{r}, \mathbf{r}';\beta \mid \mu)$

$$\begin{aligned} \frac{1}{\beta} \frac{\delta^2 \Omega(\beta \mid \mu, \phi)}{\delta \mu(\mathbf{r}) \delta \mu(\mathbf{r}')} \mid_{\beta} &= -\chi(\mathbf{r}, \mathbf{r}';\beta \mid \mu, \phi) \\ &= -\frac{1}{\beta} \int_0^{\beta} d\beta' \left\langle e^{\beta' H} \delta \widehat{n}(\mathbf{r}) e^{-\beta' H} \widehat{n}(\mathbf{r}'); \beta \mid \mu, \phi \right\rangle \end{aligned} \tag{3–13}$$

where $\delta \widehat{n}(\mathbf{r}) = \widehat{n}(\mathbf{r}) - n(\mathbf{r})$, and $\langle X; \beta \mid \mu, \phi \rangle$ denotes an equilibrium grand canonical average of the quantity X.

Next we consider a classical system with N particles interacting via a pair potential ϕ_c and acted on by an external potential $\phi_{ext,c}$ and confined to the same volume V. The system has a chemical potential μ_c and inverse temperature β_c. The Hamiltonian H_c

has the same form as in Equation (3–1) except that the potential energy functions in Equation (3–3) are different, and denoted by

$$\Phi_c = \frac{1}{2}\sum_{i\neq j}^{N}\phi_c(\mathbf{q}_i,\mathbf{q}_j), \qquad \Phi_{c,ext} = \sum_{i=1}^{N}\phi_{c,ext}\left(\mathbf{q}_i\right) \tag{3–14}$$

The local chemical potential is $\mu_c(\mathbf{r})$

$$\mu_c(\mathbf{r}) \equiv \mu_c - \phi_{c,ext}\left(\mathbf{r}\right) \tag{3–15}$$

The classical grand potential is defined in terms of these quantities by

$$\beta\Omega_c(\beta_c \mid \mu_c,\phi_c) = -\ln\sum_{N}\frac{1}{\lambda_c^{3N}N!}\int d\mathbf{q}_1..d\mathbf{q}_N e^{-\beta_c\left(\Phi_c-\int dr\mu_c(r)\widehat{n}(r)\right)} \tag{3–16}$$

Here, $\lambda_c = \left(2\pi\beta_c\hbar^2/m\right)^{1/2}$ is the thermal de Broglie wavelength associated with the temperature β_c. The integration for the partition function is taken over the N particle configuration space.

The thermodynamical quantities for the classical system are determined in the same way as in Equations (3–9) - (3–11) for the quantum system.

$$p_c(\beta_c \mid \mu_c,\phi_c)V = -\Omega_c(\beta_c \mid \mu_c,\phi_c) \tag{3–17}$$

$$E_c(\beta_c \mid \mu_c,\phi_c) = \frac{\partial\beta_c\Omega_c(\beta_c \mid \mu_c,\phi_c)}{\partial\beta_c}\mid_{\beta_c\mu_c,\phi_c} \tag{3–18}$$

$$n_c(\mathbf{r};\beta_c \mid \mu_c,\phi_c) = -\frac{\delta\Omega(\beta_c \mid \mu_c,\phi_c)}{\delta\mu_c(\mathbf{r})}\mid_{\beta_c,\phi_c} \tag{3–19}$$

$$\begin{aligned}\frac{1}{\beta_c}\frac{\delta^2\Omega(\beta_c \mid \mu_c,\phi_c)}{\delta\mu_c(\mathbf{r})\delta\mu_c(\mathbf{r}')}\mid_{\beta_c,\phi_c} &\equiv -\chi_c(\mathbf{r},\mathbf{r}';\beta_c \mid \mu_c,\phi_c)\\ &= -\left\langle\delta\widehat{n}(\mathbf{r})\widehat{n}(\mathbf{r}');\beta_c \mid \mu_c,\phi_c\right\rangle_c\end{aligned} \tag{3–20}$$

$$\frac{\delta\Omega(\beta_c \mid \mu_c, \phi_c)}{\delta\phi_c(\mathbf{r}, \mathbf{r}')}\,|_{\beta_c,\mu_c} \equiv n_c(\mathbf{r};\beta_c \mid \mu_c, \phi_c)\, n_c(\mathbf{r}';\beta_c \mid \mu_c, \phi_c)\, g_c(\mathbf{r}, \mathbf{r}';\beta_c \mid \mu_c, \phi_c)$$

$$= \langle \delta\widehat{n}(\mathbf{r})\widehat{n}(\mathbf{r}');\beta_c \mid \mu_c, \phi_c\rangle_c - n_c(\mathbf{r};\beta_c \mid \mu_c, \phi_c)\,\delta(\mathbf{r}-\mathbf{r}') \qquad (3\text{–}21)$$

The difference from the Equations (3–9) - (3–11), is the ensemble averaging for a classical system is done by integrating over the phase space. The Equations (3–17) - (3–21) have an additional constraint that the derivatives are taken at constant pair potential ϕ_c. This is necessary because we will see later that the interaction potential of the classical system ϕ_c depends on the temperature β_c and μ_c. See Section 3.2 below for further elaboration.

3.1.2 Construction Of The Effective Classical System: Classical - Quantum Correspondence Conditions

Our goal in this section is to construct an effective classical system that would have some selected thermodynamic properties as the quantum system we want to describe. The thermodynamics of this effective system is unknown at this stage, because the three ingredients of the grand potential: the effective inverse temperature, β_c, the local chemical potential $\mu_c(\mathbf{r})$, and the interaction potential among the particles $\phi_c(\mathbf{r}, \mathbf{r}')$ are still unknown. Determining these quantities involve expressing them as functions or functionals of the corresponding quantum quantities: β, $\mu(\mathbf{r})$, and $\phi(\mathbf{r}, \mathbf{r}')$. Since we have three unknown quantities for the effective system, we need three equivalent conditions relating the effective classical and quantum system. This is accomplished by requiring the numerical equivalence of two independent thermodynamic properties and one structural property for the classical and quantum systems. One choice is the equality of the grand potentials, since the grand potentials completely determine the thermodynamics of any system. The two additional choices are equivalence of its first functional derivatives with respect to the local chemical potential and the interaction

potential.

$$\Omega_c(\beta_c \mid \mu_c, \phi_c) \equiv \Omega(\beta \mid \mu, \phi) \tag{3–22}$$

$$\frac{\delta\Omega_c(\beta_c \mid \mu_c, \phi_c)}{\delta\mu_c(\mathbf{r})} \mid_{\beta_c,\phi_c} \equiv \frac{\delta\Omega(\beta \mid \mu, \phi)}{\delta\mu(\mathbf{r})} \mid_{\beta} \tag{3–23}$$

$$\frac{\delta\Omega_c(\beta_c \mid \mu_c, \phi_c)}{\delta\phi_c(\mathbf{r}, \mathbf{r}')} \mid_{\beta_c,\mu_c} \equiv \frac{\delta\Omega(\beta \mid \mu, \phi)}{\delta\phi(\mathbf{r}, \mathbf{r}')} \mid_{\beta,\mu} \tag{3–24}$$

The equivalence conditions can be expressed in terms of physical quantities. In the grand canonical ensemble, the grand potential is proportional to the pressure, and its first derivatives with respect to the pair and external potentials are the density and the pair correlation functions respectively, as seen from the Equations (3–4) and (3–6). So the Equations (3–22) and (3–24) can be reinterpreted as:

$$p_c(\beta_c \mid \mu_c, \phi_c) \equiv p(\beta \mid \mu, \phi) \tag{3–25}$$

$$n_c(\mathbf{r};\beta_c \mid \mu_c, \phi_c) \equiv n(\mathbf{r};\beta \mid \mu, \phi) \tag{3–26}$$

$$g_c(\mathbf{r}, \mathbf{r}';\beta_c \mid \mu_c, \phi_c) \equiv g(\mathbf{r}, \mathbf{r}';\beta \mid \mu, \phi) \tag{3–27}$$

The equivalence of the pair correlation functions above follows in two steps: i) from the Equation (3–4) $\frac{\delta\Omega}{\delta\phi_c(\mathrm{r},\mathrm{r}')} = n(\mathbf{r})n(\mathbf{r}')g(\mathbf{r}, \mathbf{r}')$ and ii) the equivalence of the densities. The Equation (3–24) can also be interpreted in terms of the equivalence of density fluctuations

$$\langle\delta\widehat{n}(\mathbf{r})\widehat{n}(\mathbf{r}');\, \beta_c \mid \mu_c, \phi_c\rangle_c \equiv \langle\delta\widehat{n}(\mathbf{r})\widehat{n}(\mathbf{r}');\, \beta \mid \mu, \phi\rangle \tag{3–28}$$

In summary, the classical - quantum correspondence conditions are the equivalence of the pressures, densities, and pair correlation functions.

There are some alternate scenarios for the choice of the equivalence conditions. An alternative choice to Equation (3–24) would be to equate the second functional derivatives of the grand potential with respect to the local chemical potential, which from

Equations (3–9)-(3–11) implies: $\chi_c(\mathbf{r},\mathbf{r}';\beta_c \mid \mu_c,\phi_c) \equiv \chi(\mathbf{r},\mathbf{r}';\beta \mid \mu,\phi)$. However, we run into problems because the classical response function has a singular contribution proportional to $\delta(\mathbf{r}-\mathbf{r}')$ that is not present in the quantum response function, which makes the map complicated. Using the equivalence of the classical and quantum forms for the pair correlation functions do not have this problem.

In this way the three Equations (3–25) determine, formally, the classical parameters β_c, μ_c, and ϕ_c as functions of β, and functionals of $\mu(\mathbf{r})$, and $\phi(\mathbf{r},\mathbf{r}')$

$$\beta_c = \beta_c(\beta \mid \mu,\phi), \qquad \mu_c = \mu_c(\mathbf{r};\beta \mid \mu,\phi), \qquad \phi_c = \phi_c(\mathbf{r},\mathbf{r}';\beta \mid \mu,\phi) \tag{3–29}$$

So far we have defined an effective classical system and provided equivalent conditions to calculate the details of its thermodynamics. It is necessary to invert these equivalence conditions to determine the three parameters as is done in Section 3.1.3.

3.1.3 Inversion Of The Correspondence Conditions

The classical density functional theory provides a way to invert the two equivalent conditions in Equations (3–25) for density and pair correlation functions, to solve for the effective potentials in Equation (3–29). This formalism relates the interaction potential and the external potential to the pair correlation function and density, respectively. See Appendix A for further details.

$$\begin{aligned} \ln g_c(\mathbf{r},\mathbf{r}') = -\beta_c\phi_c(\mathbf{r},\mathbf{r}') + \int_0^1 d\alpha \int d\mathbf{r}'' c_c^{(2)}(\mathbf{r},\mathbf{r}'' \mid n_c + \alpha n_c (g_c - 1)) \\ \times n_c(\mathbf{r}'')\left(g_c(\mathbf{r}'',\mathbf{r}') - 1\right) \quad , \end{aligned} \tag{3–30}$$

$$\ln\left(n_c(\mathbf{r})\lambda_c^3\right) = \beta_c\mu_c(\mathbf{r}) + \int_0^1 d\alpha \int d\mathbf{r}'' c_c^{(2)}(\mathbf{r},\mathbf{r}'' \mid \alpha n_c) n_c(\mathbf{r}'') \tag{3–31}$$

where the constant λ_c in Equation (3–31) is the thermal de Broglie wavelength evaluated at the classical temperature β_c defined below , $\lambda_c = \left(2\pi\hbar^2\beta_c/m\right)^{1/2}$. The function c_c in Equations (3–30) and (3–31) is the direct correlation function and it is determined from

the pair correlation function g_c via the Ornstein-Zernike equation:

$$\left(g_c\left(\mathbf{r},\mathbf{r}'\right)-1\right)=c_c\left(\mathbf{r},\mathbf{r}'\mid n_c\right)+\int d\mathbf{r}''c_c\left(\mathbf{r},\mathbf{r}''\mid n_c\right)n_c\left(\mathbf{r}''\right)\left(g_c\left(\mathbf{r}'',\mathbf{r}'\right)-1\right)\quad , \tag{3–32}$$

The virial equation for the classical pressure (obtained by differentiating $\Omega_c(\beta_c \mid \mu_c,\phi_c)$ with respect to the volume) is

$$\beta_c p_c(\beta_c\mid\mu_c,\phi_c)=\frac{1}{V}\int d\mathbf{r}n_c(\mathbf{r})\left[1+\frac{1}{3}\mathbf{r}\cdot\nabla\beta_c\mu_c\left(\mathbf{r}\right)-\frac{1}{6}\int d\mathbf{r}'n_c(\mathbf{r}')g_c(\mathbf{r},\mathbf{r}')\mathbf{r}'\cdot\nabla'\beta_c\phi_c(\mathbf{r},\mathbf{r}')\right] \tag{3–33}$$

It provides the third inversion of the pressure equivalence in Equation (3–25) to solve for the effective temperature β_c. See Appendix A for further elaboration.

In Section 3.1.4 we get explicit forms for the effective potentials and the effective temperature in terms of the quantum quantities. We rewrite the Equations (3–30) and (3–31) and then use the equivalence conditions in Equations (3–25) to replace all the classical pair correlations g_c and densities n_c by the corresponding quantum quantities g and n:

$$\beta_c\mu_c(\mathbf{r})=\frac{3}{2}\ln\left(\frac{\beta_c}{\beta}\right)+\ln\left(n\left(\mathbf{r}\right)\lambda^3\right)-\int_0^1 d\alpha\int d\mathbf{r}''c^{(2)}(\mathbf{r},\mathbf{r}''\mid\alpha n)n\left(\mathbf{r}''\right) \tag{3–34}$$

$$\begin{aligned}\beta_c\phi_c(\mathbf{r},\mathbf{r}')=-\ln g(\mathbf{r},\mathbf{r}')+\int_0^1 d\alpha\int d\mathbf{r}''c^{(2)}(\mathbf{r},\mathbf{r}''\mid n+\alpha n\left(g-1\right))\\ \times n\left(\mathbf{r}''\right)\left(g(\mathbf{r}'',\mathbf{r}')-1\right)\quad ,\end{aligned} \tag{3–35}$$

$$c^{(2)}\left(\mathbf{r},\mathbf{r}'\mid n\right)=\left(g\left(\mathbf{r},\mathbf{r}'\right)-1\right)-\int d\mathbf{r}''c^{(2)}\left(\mathbf{r},\mathbf{r}''\mid n\right)n\left(\mathbf{r}''\right)\left(g\left(\mathbf{r}'',\mathbf{r}'\right)-1\right) \tag{3–36}$$

On the left hand side of the Equations (3–34) and (3–35) we have the effective local chemical potential and interaction potential for the classical systems that we wanted to calculate. The right hand sides of these equations depend only on the quantum quantities, n and g. The $c^{(2)}$ is defined by the Ornstein-Zernicke equation, Equation

(3–32), in terms of the quantum pair correlation function g by the equivalence condition in Equation (3–25).

Finally, an equation for β_c/β is obtained by using the equivalence of the classical and quantum pressures $p_c = p$, Equation (3–25), to write

$$\frac{\beta_c}{\beta} = \frac{\beta_c p_c}{\beta p} \tag{3–37}$$

or with Equation (3–33)

$$\frac{\beta_c}{\beta} = \frac{1}{\beta p V}\int d\mathbf{r}\, n(\mathbf{r})\left[1 + \frac{1}{3}\mathbf{r}\cdot\nabla\beta_c\mu_c(\mathbf{r}) - \frac{1}{6}\int d\mathbf{r}'\, n(\mathbf{r}')g(\mathbf{r},\mathbf{r}')\mathbf{r}'\cdot\nabla'\beta_c\phi_c(|\mathbf{r}-\mathbf{r}'|)\right] \tag{3–38}$$

Equations (3–34), (3–35), (3–36), and (3–38) then determine the classical parameters as β_c/β, $\beta_c\mu_c(\mathbf{r})$, and $\beta_c\phi_c(\mathbf{r},\mathbf{r}')$ from the properties of the given quantum system

$$\beta_c = \beta_c\left(\beta \mid n, g\right), \qquad \mu_c(\mathbf{r}) = \mu_c(\mathbf{r}, \beta \mid n, g), \qquad \phi_c(\mathbf{r},\mathbf{r}') = \phi_c(\mathbf{r},\mathbf{r}', \beta \mid n, g) \tag{3–39}$$

which is equivalent to Equation (3–29) (corresponding to a change of variables from μ, ϕ to n, g for the quantum system).

Although these equations look simple, the calculation of $\beta_c\phi_c$, $\beta_c\mu_c$ and β_c is difficult because we still need to solve the classical many-body problem hidden inside the functional $c^{(2)}(\mathbf{r},\mathbf{r}'' \mid \cdot)$. An exact calculation would involve solving the higher order correlation functions and there is no simple way to determine these functions. Hence we will have to introduce some approximations for practical applications.

Till now the formalism is exact. In Section 3.1.4 approximations are introduced to solve the classical many-body problem. These are called the hypernetted chain approximation (HNC) which forms a closed set of equations replacing Equations (3–34) and (3–35). The general course we will follow is: i) First simplify the many-body terms in the correlation functions $c^{(2)}(\mathbf{r},\mathbf{r}'' \mid \cdot)$ using the HNC equations. ii) use approximations to calculate the quantum inputs in the map: pressure, density and pair correlations.

The type of approximation will be specific to the quantum system we want to describe. Then put these into the Equations (3–34), (3–35) and (3–38) to get ϕ_c, μ_c and β_c. iii) Use these effective parameters to calculate properties of interest using various tools in classical statistical mechanics (liquid state theory, density functional theory, molecular dynamics, classical Monte Carlo).

3.1.4 Hypernetted Chain Approximation

Hypernetted chain approximatin is a closure relation that relates the pair correlation function and density to the interaction potential and the external potential through the use of the Ornstein-Zernike equation, Equation (3–32). This involves replacing the non-local density dependence of the correlation functionals in Equations (3–30) and (3–31) by the local density dependence:

$$c_c^{(2)}(\mathbf{r}, \mathbf{r}'' \mid \alpha n_c) \to c_c^{(2)}(\mathbf{r}, \mathbf{r}'' \mid n_c), \qquad c_c^{(2)}(\mathbf{r}, \mathbf{r}'' \mid n_c + \alpha n_c (g_c - 1)) \to c_c^{(2)}(\mathbf{r}, \mathbf{r}'' \mid n_c) \quad (3\text{–}40)$$

Then Equations (3–30) and (3–31) become

$$\ln\left(n_c(\mathbf{r})\,\lambda_c^3\right) = \beta_c \mu_c(\mathbf{r}) + \int d\mathbf{r}' c_c^{(2)}(\mathbf{r}, \mathbf{r}' \mid n_c) n_c(\mathbf{r}'). \quad (3\text{–}41)$$

$$\ln g_c(\mathbf{r}, \mathbf{r}' \mid n_c) = -\beta_c \phi_c(\mathbf{r}, \mathbf{r}') + \int d\mathbf{r}'' c_c^{(2)}(\mathbf{r}, \mathbf{r}'' \mid n_c) n_c(\mathbf{r}'') \left(g_c(\mathbf{r}'', \mathbf{r}' \mid n_c) - 1\right) \quad (3\text{–}42)$$

Together with the Ornstein-Zernicke equation, Equation (3–32), they form a closed set of equations that determine the density and pair correlation function for the given potentials. This is the HNC of liquid state theory, generalized to spatially inhomogeneous systems [54]. It is known to give very good results for uniform Coulomb systems [32] and for inhomogenous, confined Coulomb systems even at strong coupling conditions [46, 49].

The effective potentials in Equations (3–34) and (3–35) have the following form within HNC approximation:

$$\beta_c \mu_c(\mathbf{r}) = \ln\left(n(\mathbf{r})\,\lambda_c^3\right) - \int d\mathbf{r}'' c^{(2)}(\mathbf{r}, \mathbf{r}'' \mid n) n(\mathbf{r}'') \tag{3–43}$$

$$\beta_c \phi_c(\mathbf{r}, \mathbf{r}') = -\ln(1 + h(\mathbf{r}, \mathbf{r}' \mid n)) + h(\mathbf{r}, \mathbf{r}' \mid n) - c(\mathbf{r}, \mathbf{r}' \mid n) \tag{3–44}$$

and the Ornstein-Zernicke equation, Equation (3–35a), is unchanged

$$c^{(2)}(\mathbf{r}, \mathbf{r}' \mid n) = h(\mathbf{r}, \mathbf{r}' \mid n) - \int d\mathbf{r}'' c^{(2)}(\mathbf{r}, \mathbf{r}'' \mid n)\, n(\mathbf{r}'')\, h(\mathbf{r}'', \mathbf{r}' \mid n) \tag{3–45}$$

The "hole function", $h(\mathbf{r}, \mathbf{r}' \mid n)$ has been introduced for notational simplicity

$$h(\mathbf{r}, \mathbf{r}' \mid n) = g(\mathbf{r}, \mathbf{r}' \mid n) - 1 \tag{3–46}$$

Similar approximations have to be made in Equation (3–38) for β_c/β, to provide practical forms to determine β_c/β for given appropriate quantum input.

For uniform systems, the second term of Equation (3–43) is simply related to the static structure factor $S(k)$

$$\int d\mathbf{r}'' c^{(2)}(\mathbf{r}, \mathbf{r}'' \mid n) n(\mathbf{r}'') \to n \int d\mathbf{r}'' c^{(2)}(\mathbf{r} - \mathbf{r}'', n) = 1 - \frac{1}{S(k=0)} \tag{3–47}$$

For the uniform systems like jellium and the ideal Fermi fluids at zero temperature, $S(k)$ vanishes as $k \to 0$ and this contribution to $\beta_c \mu_c$ diverges. Therefore for such systems, instead of Equation (3–43) an alternative form derived using a coupling constant integration and the HNC approximation [45] is used,

$$\beta_c \mu_c = \ln\left(n_c \lambda_c^3\right) - n \int d\mathbf{r} \left(c(r, n) + \beta_c \phi_c(r) - \frac{1}{2} h(r, n) \left(h(r, n) - c(r, n) \right) \right) \tag{3–48}$$

3.2 Peculiarity Of The Thermodynamics Of The Effective System

The definition of the equivalent classical system assures that the pressure and density in the grand ensemble give the correct quantum results (in principle), e.g.

$$p_c(\beta_c \mid \mu_c, \phi_c)V = -\Omega_c(\beta_c \mid \mu_c, \phi_c) = p(\beta \mid \mu, \phi)V = -\Omega(\beta \mid \mu, \phi) \tag{3–49}$$

However proper care should be taken with the functional derivatives for the effective classical system. The effective parameters ϕ_c, β_c and μ_c are coupled and are not independent variables as those of the quantum system. As a result while taking the derivatives in Equations (3–17)- (3–21) we have to hold the potential ϕ_c constant. Since all three quantities are coupled, a small variation in one would change the others. Therefore, the variation of the pressure leads to (in the following the volume V is always held constant)

$$\begin{aligned}\delta\left(p_c V\right) = &\left[\frac{\partial p_c V}{\partial \beta_c} \mid_{\mu_c,\phi_c} + \int d\mathbf{r} d\mathbf{r}' \frac{\delta p_c V}{\delta \phi_c(\mathbf{r}, \mathbf{r}')} \mid_{\beta_c,\mu_c} \frac{\partial \phi_c(\mathbf{r}, \mathbf{r}')}{\partial \beta_c} \mid_{\mu_c}\right] \delta\beta_c \\ &+ \int d\mathbf{r} \left[\frac{\delta p_c V}{\delta \mu_c(\mathbf{r})} \mid_{\beta_c,\phi_c} + \int d\mathbf{r}' d\mathbf{r}'' \frac{\delta p_c V}{\delta \phi_c(\mathbf{r}', \mathbf{r}'')} \mid_{\beta_c,\mu_c} \frac{\delta \phi_c(\mathbf{r}', \mathbf{r}'')}{\delta \mu_c(\mathbf{r})} \mid_{\beta_c}\right] \delta\mu_c(\mathbf{r}) \\ &\equiv \widetilde{S}_c dT_c + \int d\mathbf{r} \widetilde{n}_c(\mathbf{r}) \delta\mu_c(\mathbf{r})\end{aligned} \tag{3–50}$$

The second equality defines the classical thermodynamic entropy and thermodynamic density in terms of the grand potential

$$\begin{aligned}T_c \widetilde{S}_c &= -\beta_c \left[\frac{\partial p_c V}{\partial \beta_c} \mid_{\mu_c,\phi_c} + \int d\mathbf{r} d\mathbf{r}' \frac{\delta p_c V}{\delta \phi_c(\mathbf{r}, \mathbf{r}')} \mid_{\beta_c,\mu_c} \frac{\partial \phi_c(\mathbf{r}, \mathbf{r}')}{\partial \beta_c} \mid_{\mu_c}\right] \\ &= \beta_c \frac{\partial \Omega_c}{\partial \beta_c} \mid_{\mu_c}\end{aligned} \tag{3–51}$$

$$\begin{aligned}\widetilde{n}_c(\mathbf{r}) &= \left[\frac{\delta p_c V}{\delta \mu_c(\mathbf{r})} \mid_{\beta_c,\phi_c} + \int d\mathbf{r}' d\mathbf{r}'' \frac{\delta p_c V}{\delta \phi_c(\mathbf{r}', \mathbf{r}'')} \mid_{\beta_c,\mu_c} \frac{\delta \phi_c(\mathbf{r}', \mathbf{r}'')}{\delta \mu_c(\mathbf{r})} \mid_{\beta_c}\right] \\ &= -\frac{\delta \Omega_c}{\delta \mu_c(\mathbf{r})} \mid_{\beta_c}\end{aligned} \tag{3–52}$$

Similarly, the classical internal energy is defined by

$$\begin{aligned}\widetilde{E}_c &\equiv T_c\widetilde{S}_c + \int d\mathbf{r}\widetilde{n}_c(\mathbf{r})\mu_c(\mathbf{r}) - p_c V \\ &= \frac{\partial\beta_c\Omega}{\partial\beta_c}\,|_{\mu_c} - \int d\mathbf{r}\beta_c\mu_c(\mathbf{r})\frac{\delta\Omega_c}{\delta\beta_c\mu_c(\mathbf{r})}\,|_{\beta_c} \qquad (3\text{–}53)\\ &= \frac{\partial\beta_c\Omega_c}{\partial\beta_c}\,|_{\beta_c\mu_c}\end{aligned}$$

(3–54)

Note that derivatives in the last equalities of Equations (3–51) - (3–53) do not have the restriction of constant ϕ_c.

These same relationships hold for the quantum properties as well, since they are the general definitions of thermodynamics for the chosen variables, μ and β. In the quantum case ϕ is independent of the thermodynamic variables and hence is constant in the variations. This leads to the equivalent expressions in terms of equilibrium averages

$$n(\mathbf{r}) = -\frac{\delta\Omega}{\delta\mu(\mathbf{r})}\,|_{\beta} = \langle\widehat{n}(\mathbf{r})\rangle\,, \qquad E = \frac{\partial\beta\Omega}{\partial\beta}\,|_{\beta\mu} = \left\langle\widehat{H}\right\rangle \qquad (3\text{–}55)$$

However, in the classical case the above leads to

$$\widetilde{n}_c(\mathbf{r}) = \langle\widehat{n}(\mathbf{r})\rangle_c - \int d\mathbf{r}'\,d\mathbf{r}''\frac{\delta\Omega_c}{\delta\phi_c(\mathbf{r}',\mathbf{r}'')}\,|_{\beta_c,\mu_c}\,\frac{\delta\phi_c(\mathbf{r}',\mathbf{r}'')}{\delta\mu_c(\mathbf{r})}\,|_{\beta_c} \qquad (3\text{–}56)$$

$$\widetilde{E} = \langle H\rangle_c + \int d\mathbf{r}'\,d\mathbf{r}''\frac{\delta\beta_c\Omega_c}{\delta\phi_c(\mathbf{r}',\mathbf{r}'')}\,|_{\beta_c\mu_c}\,\frac{\delta\phi_c(\mathbf{r}',\mathbf{r}'')}{\delta\beta_c\mu_c(\mathbf{r})}\,|_{\beta_c} \qquad (3\text{–}57)$$

For example, the thermodynamic density, $\widetilde{n}_c(\mathbf{r})$, differs from the average density of the text above, $n_c(\mathbf{r})$, because the latter is defined as a derivative of the grand potential at constant ϕ_c.

3.3 Example - Ideal Fermi Gas

As a first application of the above map, we consider the simplest quantum system, the ideal Fermi gas. For now we consider an inhomogeneous unpolarized ideal Fermi

system and calculate all the quantum inputs that go into the effective quantities.

$$H - \mu N \rightarrow \int d\mathbf{r} \left(\frac{\hat{p}^2}{2m} - \mu(\mathbf{r}) \right) \hat{n}(\mathbf{r}) \tag{3–58}$$

Since for a non-interacting system the hamiltonian is the sum of single particle Hamiltonians, all the thermodynamic quantities of the system can be written in terms of the corresponding thermodynamic quantities of a single particle system [47].

$$p(\beta \mid \mu) V \equiv p(\beta \mid \mu, \phi = 0) V = \beta^{-1}(2s+1) \int d\mathbf{r} \, \langle \mathbf{r} | \ln \left(1 + e^{-\beta \left(\frac{\widehat{p}^2}{2m} - \mu(\widehat{\mathbf{r}}) \right)} \right) | \mathbf{r} \rangle \tag{3–59}$$

$$n(\mathbf{r}, \beta \mid \mu) \equiv n(\mathbf{r}, \beta \mid \mu, \phi = 0) = (2s+1) \, \langle \mathbf{r} | \left(exp \left(\beta \left(\frac{\widehat{p}^2}{2m} - \mu(\widehat{\mathbf{r}}) \right) \right) + 1 \right)^{-1} | \mathbf{r} \rangle \tag{3–60}$$

$$g(\mathbf{r}, \mathbf{r}'; \beta \mid \mu) \equiv g(\mathbf{r}, \mathbf{r}'; \beta \mid \mu, \phi = 0) \tag{3–61}$$

$$= 1 - \frac{1}{2s+1} \frac{n(\mathbf{r}, \mathbf{r}') n(\mathbf{r}', \mathbf{r})}{n(\mathbf{r}, \mathbf{r}) n(\mathbf{r}', \mathbf{r}')}, \qquad n(\mathbf{r}, \mathbf{r}') = \langle \mathbf{r} | \left(exp \left(\beta \left(\frac{\widehat{p}^2}{2m} - \mu(\widehat{\mathbf{r}}) \right) \right) + 1 \right)^{-1} | \mathbf{r}' \rangle \tag{3–62}$$

where $\langle \mathbf{r} | \, X \, | \mathbf{r}' \rangle$ denotes a matrix element in coordinate representation, and s is the spin.

To further simplify the operator equations, Equations(3–59)-(3–61), we have to introduce a complete set of wave-functions ψ_n and solve the energy eigenvalues ϵ_n for the single particle hamiltonian $(\widehat{p}^2/2m) - \mu(\hat{q})$.

$$p(\beta \mid \mu) V = \beta^{-1}(2s+1) \sum_{n=0}^{\infty} ln(1 + exp(-\beta(\epsilon_n - \mu))) \tag{3–63}$$

$$n(\mathbf{r}, \beta \mid \mu) = (2s+1) \left(exp \left(\beta \left(\epsilon_n - \mu \right) \right) + 1 \right)^{-1} |\psi_n(\mathbf{r})|^2 \tag{3–64}$$

$$g(\mathbf{r}, \mathbf{r}'; \beta \mid \mu) = 1 - \frac{1}{2s+1} \frac{n(\mathbf{r}, \mathbf{r}') n(\mathbf{r}', \mathbf{r})}{n(\mathbf{r}, \mathbf{r}) n(\mathbf{r}', \mathbf{r}')}, \qquad n(\mathbf{r}, \mathbf{r}') = \sum_{n=0}^{\infty} \left(exp \left(\beta \left(\epsilon_n - \mu \right) \right) + 1 \right)^{-1} \psi_n^{\star}(\mathbf{r}) \psi_n(\mathbf{r}') \, , \tag{3–65}$$

For slowly varying external potentials a practical approximation is obtained by replacing the operator $\mu(\hat{q})$ by its eigenvalue $\mu(\mathbf{r})$, also known as a "local density approximation", which is equivalent to replacing the non-local density dependence by the local density as seen below. This approximation usually works well for systems when no discrete bound states are formed. The expectation values above then can be calculated as simple integrals

$$p(\beta \mid \mu) \rightarrow \frac{1}{V} \int d\mathbf{r}\,(2s+1)\,\frac{1}{h^3} \int d\mathbf{p} \frac{\mathbf{p}^2}{2m} \left(e^{\beta(\frac{p^2}{2m} - \mu(\mathrm{r}))} + 1 \right)^{-1} \tag{3–66}$$

$$n(\mathbf{r}, \beta \mid \mu) \rightarrow (2s+1)\,h^{-3} \int d\mathbf{p} \left(e^{\beta(\frac{p^2}{2m} - \mu(\mathrm{r}))} + 1 \right)^{-1} \tag{3–67}$$

$$n(\mathbf{r}, \mathbf{r}') \rightarrow \frac{1}{h^3} \int d\mathbf{p}\, e^{\frac{i}{\hbar}\mathrm{p}\cdot(\mathrm{r}-\mathrm{r}')} \left(e^{\beta(\frac{p^2}{2m} - \mu(\mathrm{R}))} + 1 \right)^{-1}, \qquad \mathbf{R} = \frac{\mathbf{r}+\mathbf{r}'}{2} \tag{3–68}$$

The results in Equation (3–66) are the familiar finite temperature Thomas-Fermi approximations for the thermodynamics, while Equation (3–68) is its extension to structure [55]. The expressions for $n(\mathbf{r}, \beta \mid \mu)$ and $n(\mathbf{r}, \mathbf{r}')$ are no longer functionals of $\mu(\mathbf{r})$, but rather local functions of $\mu(\mathbf{r})$ and $\mu(\mathbf{R})$, respectively. Practical fits for $n(\mathbf{r}, \beta \mid \mu)$ and this inversion are given in Appendix B, along with simplification of $n(\mathbf{r}, \mathbf{r}')$. The comparison of the density obtained using the LDA with the exact density calculation in Equation (3–64) is shown in Figure (3-1) at $r_s = 10$ for 100 particles. For small r_s and large number of particles in the trap, LDA agrees well with the exact density calculation. At very low temperatures and large values of r_s, LDA densities differ from the actual densities close to the origin. The details of the wavefunctions used to generate the plot is given in Appendix F.

Even though the quantum system is non-interacting, the corresponding classical system is non-trivial because $\phi_c(\mathbf{q}_i, \mathbf{q}_j) \neq 0$. This is because the classical pair interactions are required to reproduce the effects of the quantum statistics. We are still required

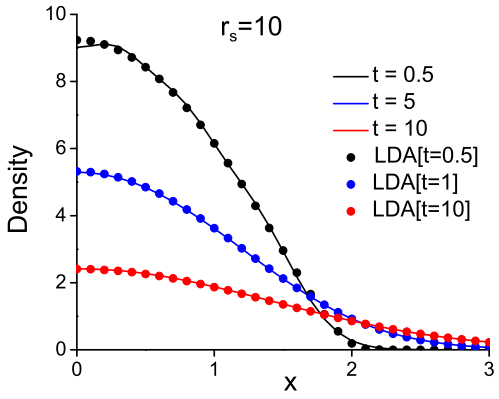

Figure 3-1. The comparison of the exact density (as in Equation (3–64)) for the ideal Fermi gas for 100 particles in a harmonic trap with that obtained using LDA (Equation (3–67)).

to solve the complicated classical many body problem. This is addressed within the HNC approximation described above by Equations (3–43) and (3–44) together with the Ornstein - Zernicke equation, Equations (3–45) and (3–38) for β_c/β. The effective potential and the effective temperature can be explicitly calculated numerically, however ϕ_c and β_c both depend on the external potential through the local chemical potential $\mu_c(\mathbf{r})$. To illustrate the above discussion in more detail we restrict ourselves to a uniform unpolarized ideal Fermi gas ($\mu(\mathbf{r}) = \mu$). For the uniform gas the Equations (3–61)-(3–68) for the effective parameters simplify to

$$\frac{\beta_c}{\beta} = \frac{n}{\beta p}\left[1 - \frac{1}{6}n\int d\mathbf{r} g(r)\mathbf{r}\cdot\nabla\beta_c\phi_c(r)\right] \tag{3–69}$$

$$\beta_c\mu_c = \ln\left(n_c\lambda_c^3\right) - n\int d\mathbf{r}\left(c(r) + \beta_c\phi_c(r) - \frac{1}{2}h(r)\left(h(r) - c(r)\right)\right) \tag{3–70}$$

$$\beta_c\phi_c(r) = -\ln\left(1 + h(r)\right) + h(r) - c(r) \tag{3–71}$$

$$c\left(r\right) = h\left(r\right) - n\int d\mathbf{r}' c\left(|\mathbf{r} - \mathbf{r}'|\right) h\left(r'\right) \tag{3–72}$$

The superscript (2) on $c^{(2)}(r)$ and the dependence of $c(r), h(r)$ on thermodynamic variables has been suppressed for simplicity. These last two equations can be solved for $\beta_c\phi_c(r)$ using $h(r)$ from Equations (3–61) and (3–68) in the uniform limit. With that result, β_c/β can be calculated from Equation (3–69), and then $\beta_c\mu_c$ determined from Equation (3–48).

The dimensionless potential $\beta_c\phi_c$ will be referred to as the Pauli potential. From now on we use only dimensionless parameters. The dimensionless distance is given by $r^* = r/r_0$, where r_0 is the mean distance between particles related to the uniform density by $4\pi r_0^3/3 = 1/n$. The plots of the Pauli potential at different temperatures are shown in Figure 3-2 as a function of the dimensionless coordinate r^*. The thermodynamics of a quantum system is parameterized by the temperature T and the density n. In our discussions we use dimensionless temperature t and dimensionless average inter-particle distance r_s instead. They are defined by $r_s = r_0/a_B$ where a_B is the Bohr radius, and $t = \beta_F/\beta$ for the temperature relative to the Fermi temperature ($\beta_F^{-1} = \epsilon_F = \hbar^2\left(3\pi^2 n\right)^{2/3}/2m$). For example, in these units $n\lambda^3 = 8/\left(3\pi^{1/2}t^{3/2}\right)$ and the classical limit occurs for $t >> 1$ where the distance between particles is large compared to the thermal de Broglie wavelength and the degeneracy effects are low. The thermodynamics of the ideal gas properties is independent of r_s and can be obtained as the $r_s \to 0$ limit of any quantum system. Figure 3-2 shows the Pauli potential for $t = 0$, 10^{-1}, 1, and 10.

The Pauli potential is repulsive because of the Pauli exclusion principle, finite at $r = 0$ for spin-less systems, and monotonically decreasing. The behavior is exponential at high temperatures , but an r^{-2} algebraic tail develops for low temperatures t, arising from the direct correlation function $c^{(2)}(r)$ in Equation (3–71). The grand potential does not exist for such a potential which decays slower than r^{-3} in three dimension [47] and it would appear that the equivalent classical system proposed here fails even for this simplest case of an ideal Fermi gas. However, we adopt the same technique that is

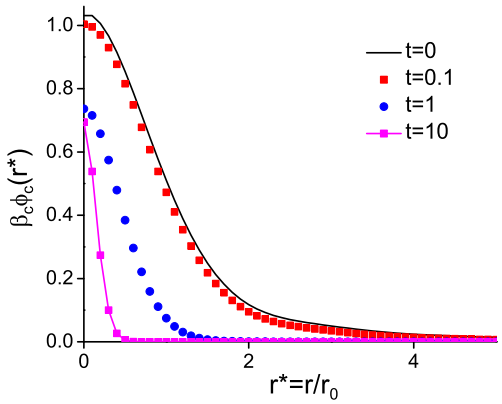

Figure 3-2. Ideal gas Pauli pair potential as a function of $r^* = r/r_0$ for $t = 0, 0.1, 1, 10$ [35].

used to cure the long ranged problem for the Coulomb systems by adding a uniform neutralizing background (one component plasma). The same procedure can be used here, i.e., a classical system is considered where a uniform compensating background term has been added to the Hamiltonian. Changing the Hamiltonian implies replacing $g_c(\mathbf{r}, \mathbf{r}')$ by $g_c(\mathbf{r}, \mathbf{r}') - 1$ in the pressure equation Equation (3–33), so that Equation (3–69) becomes

$$\frac{\beta_c}{\beta} = \frac{n}{\beta p}\left[1 - \frac{1}{6}n\int d\mathbf{r}\, h(r)\mathbf{r}\cdot\nabla\beta_c\phi_c(r)\right] \tag{3–73}$$

Figure 3-3 shows the classical temperature relative to the Fermi temperature, $\beta_F/\beta_c \equiv t_c$, as a function of t obtained from Equation (3–73). It is seen that the classical temperature T_c remains finite at $T = 0$, and crosses over to $T_c = T$ at high temperatures. The finiteness of T_c when $T = 0$ results because a quantum system has a finite average kinetic energy at $T = 0$. The PDW model postulates the phenomenological form $T_c = \left(T^2 + T_0^2\right)^{1/2}$. The model originally uses the average energy per particle at $T = 0$ to evaluate $T_0 = 2T_F/5$. The result from Equation (3–73) is quite close $T_c\,(t = 0) \sim 0.43\,T_F$. To compare the dependence at finite t, the PDW

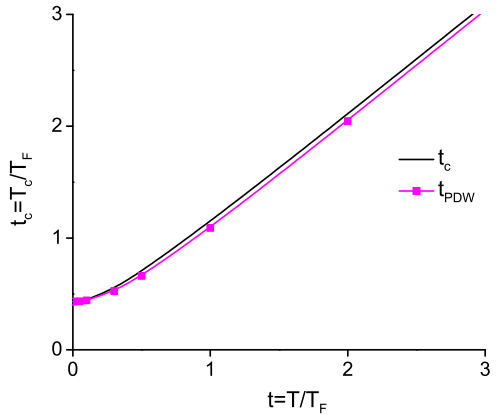

Figure 3-3. Ideal gas reduced classical temperature $t_c = T_c/T_F$ as a function of $t = T/T_F$. Also shown is the result of PDW [35].

form is also shown in Figure 3-3 with $T_0 = T_c\,(t = 0)$. It is seen that the results are quite similar although the PDW form has a somewhat faster cross over to the classical limit.

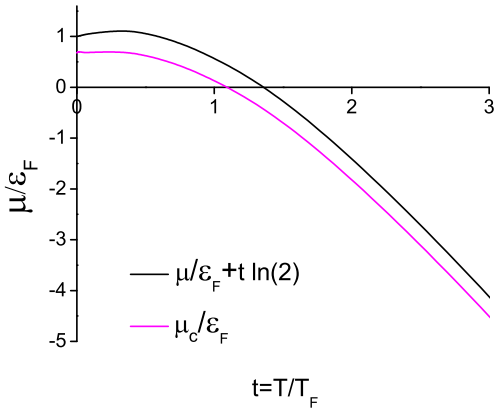

Figure 3-4. Ideal gas dimensionless chemical potential μ_c/ϵ_F as a function of t. Also shown is the corresponding quantum chemical potential $\mu/\epsilon_F + t\ln 2$ [35].

Since there is no external potential, the local chemical potential is a constant μ_c. Figure 3-4 shows similar results for μ_c/ϵ_F as a function of t obtained from Equation (3–70). Also shown is the result for the quantum μ/ϵ_F. Both forms depend only on t (independent of r_s). At high temperatures the chemical potential of the representative system goes over to $\ln(n\lambda^3)$ as in Equation (3–70) while the quantum chemical potential

goes over to $\ln(n\lambda^3/2)$. They differ by a constant amount of $\ln(2)$ at high temperatures due to the internal spin degrees of freedom in the quantum calculation. This is accommodated in the comparison shown in Figure 3-4.

Now that we have determined the effective potential and the effective temperature for the uniform ideal Fermi gas, it would be useful to look at the average internal energy of the system. For the ideal Fermi gas, the average energy is related to the pressure as $E = \frac{3}{2}pV$. First, note that all the dimensionless thermodynamic quantities for both the ideal Fermi gas and its effective classical system depend on only one thermodynamic parameter $z = e^{\beta\mu}$. In particular

$$\beta_c p_c \lambda_c^3 = G(z) \tag{3–74}$$

The specific form for $G(z)$ is not required for the present discussion. The corresponding quantum result is $\beta p \lambda^3 = f_{3/2}(z)$, where $f_{3/2}(z)$ is the Fermi integral of Appendix B, (B–19). Although $G(z)$ and $f_{3/2}(z)$ are quite different, the fact that they both depend only on z implies that the relationship among different thermodynamic properties is the same in both classical and quantum cases. For example, the energy per particle is determined from the pressure via the thermodynamic definition Equation (3–53) with Equation (3–70)

$$\begin{aligned} \widetilde{E}_c &= \frac{\partial \beta_c p_c V}{\partial \beta_c}|_{\phi_c,\beta_c\mu_c} = \frac{\partial G(z) V/\lambda_c^3}{\partial \beta_c}|_{\phi_c,\beta_c\mu_c} \\ &= -VG(z)\frac{\partial \lambda_c^{-3}}{\partial \beta_c}\ |_{z_c} = \frac{2}{3}p_c V \end{aligned} \tag{3–75}$$

The contribution from $\partial G(z)/\partial\beta_c\ |_{z_c,V}$ vanishes since $z = z(z_c)$. This follows on dimensional grounds since z is dimensionless, and there is no additional energy scale to make β_c dimensionless. Hence the classical calculation gives the known exact quantum result. This non-trivial result for a classical interacting system is a strong confirmation of the effective classical map defined here. As noted in Section 3.2, it can be verified that the classical average of the classical Hamiltonian does not give the correct relationship

to the pressure. Instead it is necessary to define the internal energy thermodynamically, as is done in Equation (3–75). In a similar way it is verified that the relationship of the classical entropy to the pressure and density is the same as in the quantum case

$$T_c S_c = \frac{5}{2} p_c V - \mu_c \overline{N}_c \tag{3–76}$$

This is a form of the Sackur-Tetrode equation valid for the quantum case. It is emphasized that these simple ideal quantum gas results are being retained for the more complex effective classical system with pair interactions via the Pauli potential.

3.4 Summary

1. We developed a formalism to describe the quantum correlations using classical methods.

2. We develop a formalism that constructs an effective classical system by mapping its thermodynamics to that of the quantum system we want to describe. The thermodynamics of the effective system is described completely by the effective interaction potential, the effective external potential and the effective temperature.

3. Since there are three unknowns, the two effective potentials and the effective temperature, we need three equivalent conditions to solve them. We do that by equating the pressure, density and the pair correlations for the effective classical and the quantum system.

4. The map is inverted using the classical density functional theory and further simplified using the HNC approximation.

5. The map is applied to the ideal Fermi gas. The effective quantities for its effective classical system have been calculated and plotted. The result $E = 3/2pV$, which is true for the quantum system, is recovered for the effective system also.

CHAPTER 4
UNIFORM ELECTRON GAS

The formalism developed in Chapter 3 is now applied to the uniform electron gas or "jellium" [48]. The calculation of the three parameters of the effective classical system for jellium needs three quantum inputs. However, getting the exact expressions for the quantum inputs for jellium (pressures and pair correlation functions) is considerably more difficult than for the ideal Fermi gas. Hence in this Chapter these quantities are calculated within the random phase approximation. More precisely, we define the effective parameters such that they preserve the ideal gas and the exact weak coupling limits. Once we determine the three parameters, they are used with the classical strong coupling HNC equations to obtain the pair correlation functions and other thermodynamic functions. The pair correlation functions are compared with other theories like PDW and STLS and simulation methods like PIMC. The agreement with the simulation data and PDW model is quite good. Other thermodynamic functions like the pressure and the chemical potential are also calculated.

4.1 Thermodynamics Of The Effective Classical System

The interacting electron gas or "jellium" is a system of electrons interacting via the Coulomb interactions embedded in an uniform neutralizing background. The neutralizing background is required for the thermodynamic stability of a system interacting with long ranged forces [47]. The uniform electron gas is the starting model for the study of electron interactions in the metals, lattices, and plasmas [52]. The corresponding classical system is called the one component plasma. In this Chapter we will look into both the thermodynamics and structure of "jellium". We construct the parameters of the effective classical system, $\beta_c = 1/k_B T_c$, $\mu_c(\mathbf{r})$, and $\phi_c(\mathbf{r}, \mathbf{r}')$, which are exact in the weak coupling limit. The effective interaction potential is then used in HNC equations to calculate the pair correlation function to further include classical strong coupling effects.

Once we obtain the pair correlation functions, the pressure and other quantities can be derived using the classical statistical mechanics.

To summarize the results of Chapter 3, the classical parameters for an uniform quantum system are defined as following. First the pair potential is obtained from the inversion of the HNC equation

$$\beta_c \phi_c(r) = -\ln\left(1 + h(r)\right) + h\left(r\right) - c\left(r\right) \tag{4–1}$$

where the direct correlation function c in the equation above is determined from the Ornstein-Zernike equation [32]:

$$c\left(r\right) = h\left(r\right) - n\int d\mathbf{r}' c(|\mathbf{r} - \mathbf{r}'|)h\left(r'\right) \tag{4–2}$$

The classical temperature is obtained from the correspondence condition of equal pressures, Equation (3–25), and the classical virial equation

$$\frac{\beta_c}{\beta} = \frac{\beta_c p_c}{\beta p} = \frac{n}{\beta p}\left[1 - \frac{n}{6}\int d\mathbf{r} h(r)\mathbf{r}\cdot\nabla\beta_c\phi_c(r)\right] \tag{4–3}$$

where we used the effective potential derived in Equation (4–1). The replacement of the pair correlation function $g(r)$ by the hole function $h(r) = g(r) - 1$ occurs because of the uniform neutralizing background [32]. The classical activity $\beta_c\mu_c$ is given by [45]

$$\beta_c\mu_c = \ln\left(n\lambda_c^3\right) - n\int d\mathbf{r}\left(c(r) + \beta_c\phi_c(r) - \frac{1}{2}h(r)\left(h(r) - c(r)\right)\right) \tag{4–4}$$

where $\lambda_c = (2\pi\beta_c\hbar^2/m)^{1/2}$. The functions g are all the quantum pair correlation functions. The classical pair correlation functions have been replaced by the quantum pair correlations by using the equivalence conditions in Equations (3–25).

In the following sections we consider a uniform electron gas with dimensionless temperature t and average interparticle dimensionless distance r_s. The objective here is to find a way to put appropriate approximations into the system for practical use.

4.1.1 Classical Potential $\beta_c\phi_c(r)$

The dominant exchange effects have already been included in the quantities calculated in Chapter 3 for the ideal Fermi gas. Therefore it is convenient to write [35] $\beta_c\phi_c(r)$ in the form

$$\beta_c\phi_c(r) = (\beta_c\phi_c(r))^{(0)} + \Delta(r) \tag{4–5}$$

where the first term is the Pauli potential and $\Delta(r)$ is the Coulomb interaction term. The Pauli potential captures the ideal gas exchange effects and the Coulomb term contains the modifications of the Coulomb interaction by both the exchange and the diffraction effects. Writing the effective potential in this way implies we recover the ideal gas results in the limit of zero interactions. In the classical limit, the Pauli potential vanishes and the Coulomb part becomes the Coulomb potential. In the weak coupling limit, the direct correlation function becomes proportional to the potential

$$\beta_c\phi_c(r) \to -c(r), \quad (\beta_c\phi_c(r))^{(0)} \to -c^{(0)}(r) \tag{4–6}$$

This gives an explicit form for the Coulomb term $\Delta(r) = -\left(c(r) - c^{(0)}(r)\right)$. Thus we propose an approximation for the effective potential:

$$\beta_c\phi_c(r) \to (\beta_c\phi_c(r))^{(0)} - \left(c(r) - c^{(0)}(r)\right)^{(w)} \tag{4–7}$$

where $\left(c(r) - c^{(0)}(r)\right)^{(w)}$ denotes a weak coupling calculation of the direct correlation functions from the Ornstein - Zernicke equation, Equation (4–2). This approximation clearly incorporates the ideal gas and weak coupling limits. For the classical OCP (Coulomb potential) this yields the Debye - Huckel approximation to $g(r)$. In the quantum case, the weak coupling limit $g^{RPA}(r)$ can be calculated explicitly using the random phase approximation [1]. To determine c we use g^{RPA} in the Ornstein -Zernike equation,

Equation (4–2).

$$c(r)^{(w)} = \frac{1}{n}\int \frac{d\mathbf{k}}{(2\pi)^3} e^{-i\mathbf{k}\cdot\mathbf{r}} \frac{S^{RPA}(k) - 1}{S^{RPA}(k)} \tag{4–8}$$

where $S^{RPA}(k)$ is the RPA static structure factor

$$S^{RPA}(k) = 1 + n\int d\mathbf{r} e^{i\mathbf{k}\cdot\mathbf{r}} h^{RPA}(r) \tag{4–9}$$

Finally the modified Coulomb potential $\Delta(r)$ in Equation (4–5) becomes

$$\Delta(r) \to \frac{1}{n}\int \frac{d\mathbf{k}}{(2\pi)^3} e^{-i\mathbf{k}\cdot\mathbf{r}} \left(\frac{1}{S^{RPA}(k)} - \frac{1}{S^{(0)}(k)}\right) \tag{4–10}$$

The definition of $S^{RPA}(k)$ in terms of the Lindhard function and the RPA dielectric function is given in Appendix D.

The proof of some of the limits of $\Delta(r) = \Delta(t, r_s, r^*)$ is given in Appendix D. The RPA structure factor behaves as $S^{RPA}(k) \propto k^2$ because of the perfect screening sum rule. A consequence of this is that for large $r^* = r/r_0$, $\Delta(r^*)$ has a Coulomb tail as shown in the Appendix D.

$$\lim_{r^*} \Delta(t, r_s, r^*) \to \Gamma_e(t, r_s)\, r^{*-1} \tag{4–11}$$

where $\Gamma_e(t, r_s)$ is an effective Coulomb coupling constant

$$\Gamma_e(t, r_s) = \frac{2}{\beta\hbar\omega_p \coth(\beta\hbar\omega_p/2)}\Gamma, \quad \Gamma \equiv \frac{\beta q^2}{r_0} \tag{4–12}$$

Here $\omega_p = \sqrt{4\pi n q^2/m}$ is the plasma frequency. The dimensionless parameter is $\beta\hbar\omega_p = (4/3)\left(2\sqrt{3}/\pi^2\right)^{1/3}\sqrt{r_s}/t$ so for fixed r_s the high and low temperature limits are

$$\Gamma_e \to \begin{cases} \Gamma, & \beta\hbar\omega_p << 1 \\ \left(\frac{4}{3}r_s\right)^{1/2}, & \beta\hbar\omega_p >> 1 \end{cases} \tag{4–13}$$

The coefficient of the Coulomb tail follows from the fact that the RPA incorporates the exact perfect screening sum rule [1, 50, 51]. It is illustrated for $r^*\Delta(t, r_s, r^*)$ in Figure 4-1 at $r_s = 5$ for several values of t.

Also shown in this figure are the results from the PDW classical potential which we briefly discussed in Section 2.2.2

$$(\beta_c\phi_c(r))^{PDW} = (\beta_c\phi_c(r))^{(0)} + \Delta^{PDW}(r) \tag{4–14}$$

The Pauli potential $(\beta_c\phi_c(r))^{(0)}$ as in is the same as in Equation (4–5) but its Coulomb part $\Delta^{PDW}(r)$ is given by the Deutsch potential [21]

$$\Delta^{PDW}(r) = \beta^{PDW}\frac{q^2}{r}\left(1 - e^{-r/\lambda^{PDW}}\right), \quad \lambda^{PDW} = \left(\frac{\beta^{PDW}\hbar^2}{\pi m}\right)^{1/2} \tag{4–15}$$

where $\beta^{PDW} = 1/k_B T^{PDW}$ and $T^{PDW} \equiv \left(T^2 + T_0^2\right)^{1/2}$. Thus the PDW potential depends on only one unspecified parameter T_0. Since the Pauli potential is independent of r_s, the density dependence in the potential occurs through T_0. The $T_0 = T_0(r_s)$ is obtained by requiring that the classical excess energy at T_0 matches the quantum exchange-correlation energy obtained from quantum simulation at $T = 0$. T_0 is fitted to a form [33, 34]

$$T_0 \simeq \frac{T_F}{a + b\sqrt{r_s} + cr_s} \tag{4–16}$$

with $a = 1.594$, $b = -0.3160$, and $c = 0.0240$ when diffusion Monte Carlo data is used. For variational Monte Carlo data, the fitting parameters are $a = 1.3251$, $b = -0.1779$ and $c = 0.0$. The PDW potential is quite similar to the approximate form of our potential in Equation (4–7) at $r_s = 5$. Greater discrepancies occur for both larger and smaller r_s except at higher temperatures. Further comments on this comparison are given below.

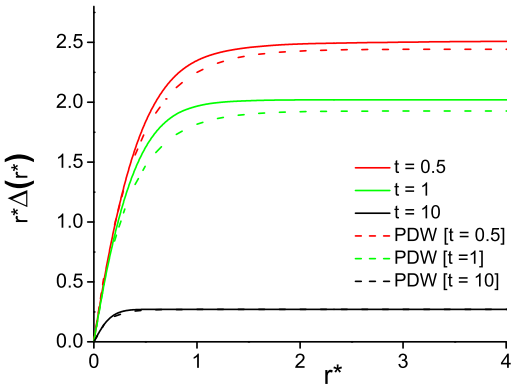

Figure 4-1. Demonstration of crossover for $r^*\triangle(t, r_s, r^*)$ to Coulomb with effective coupling constant $\Gamma_e(t, r_s)$ given by Equation (4–12), for $r_s = 5$ and $t = 0.5, 1$ and 10 [48]. Also shown are the corresponding results for $r^*\triangle_{PDW}(t, r_s, r^*)$.

Close to the origin $r^* << 1$, $\Delta(t, r_s, r^*)$ approaches a finite value so the Coulomb potential is regularized.

$$\Delta(t, r_s, 0) = \frac{1}{n}\int \frac{d\mathbf{k}}{(2\pi)^3}\left(\frac{1}{S^{RPA}(k)} - \frac{1}{S^{(0)}(k)}\right) \tag{4–17}$$

The integral converges because the RPA static structure factors for large k approach 1 as k^{-4} due to quantum effects (cusp condition [57]). Finally, another limit obtained in the Appendix D is that for large r_s and large t (low density, high temperature) in which case the Kelbg potential [20] is recovered

$$\lim_{t, r_s >> 1} \Delta(t, r_s, r^*) \to \Delta_K(t, r^*) = \frac{\Gamma}{r^*}\left(1 - \exp(-r^{*2}/a^2) + \sqrt{\pi}r^*/a(1 - \mathrm{erf}(r^*/a))\right) \tag{4–18}$$

with $a = \lambda/(\sqrt{2\pi}r_0)$. The Kelbg potential is obtained as the weak coupling limit of the effective potential defined using the two particle density matrix. The details are given in Chapter 2. This limit is approached to within 10 percent at $t = 10$ and $1 \leq r_s \leq 10$.

NOTE: i) There are two ways to calculate the RPA static structure factor $S^{RPA}(k)$. One way is to use the definition of the static structure factor as a frequency integral of the dynamic structure factor. At small momentum k values, the integrand (the dynamic structure factor) starts developing sharp peaks. The peaks occur because of the plasma

oscillations where the dielectric function (the denominator of the integrand) becomes very small. The numerical estimation of the integration is very difficult at small momentum. To overcome this problem we used the frequency summation representation of the static structure given in [39]. The explicit form of the integral and the frequency sums are given in the Appendix D.

ii) When expressed in terms of the density, the degeneracy parameter z that occurs in the Fermi function in the structure factor calculation depends on the chemical potential of the ideal Fermi gas, not that for jellium. This choice of z preserves the exact screening sum rule.

4.1.2 Classical Effective Temperature And Chemical Potential

The approximate temperature and chemical potential equations are obtained following the same logic of splitting the thermodynamic quantities into an ideal gas term and an interaction term. The interaction term is determined from the weak coupling forms of these quantities.

$$\beta_c = \beta_c^{(0)} + \left(\beta_c^{RPA} - \beta_c^{RPA,(0)}\right) \tag{4–19}$$

$$\beta_c\mu_c = \left(\beta_c\mu_c\right)^{(0)} + \left(\beta_c\mu_c\right)^{RPA} - \left(\beta_c\mu_c\right)^{RPA,(0)} \tag{4–20}$$

where $\beta_c^{(0)}$ and $\left(\beta_c\mu_c\right)^{(0)}$ denote the ideal gas results of [35], and from Equations (4–3) and (4–4)

$$\beta_c^{RPA} = \frac{n\left[1 - \frac{n}{6}\int d\mathbf{r} h^{RPA}(r)\mathbf{r}\cdot\nabla\left(\beta_c\phi_c(r)\right)^{RPA}\right]}{p^{RPA}} \tag{4–21}$$

$$\left(\beta_c\mu_c\right)^{RPA} = \frac{3}{2}\ln\left(\frac{\beta_c^{RPA}}{\beta}\right) + \ln\left(n\lambda^3\right)^{RPA} + \frac{1}{2}n\int d\mathbf{r} h^{RPA}(r)\left(h^{RPA}(r) + \left(\beta_c\phi_c(r)\right)^{RPA}\right) \tag{4–22}$$

The RPA results for p^{RPA} and $\left(n\lambda^3\right)^{RPA}$ are computed from the Pade fits of reference [52].

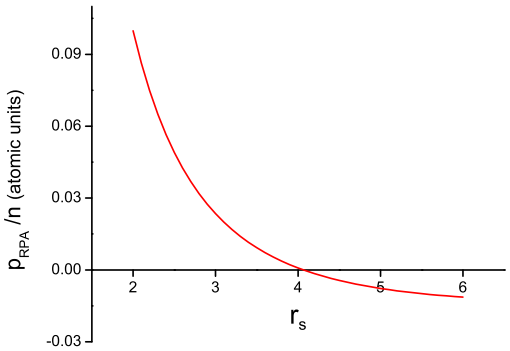

Figure 4-2. Quantum RPA pressure p^{RPA} at $t = 0$ as a function of r_s [48] .

The pressure for jellium becomes negative at large r_s and small t [52, 53]. For real systems, the pressure is positive as follows from the convexity of the free energy as a function of the volume. This convexity does not hold for jellium [45, 47]. The pressure of the effective classical system at the corresponding temperature and densities is still positive. From the Equation (4–21) we get unphysical results like negative temperatures. Since p^{RPA} in the Equation (4–21) is a monotonic function of t, for some temperature $t = t_0$, $p^{RPA} = 0$. This situation occurs for $r_s \geq 4$. Therefore for jellium, this is one of the equivalence conditions that should be replaced by a different condition (e.g., equivalence of internal energies). Instead, the analysis here is restricted to $t > t_0\,(r_s)$ to assure positive pressure. Figure 4-3 shows $t_c = T_c/T_F$ as a function of t calculated from Equation (4–19) for $r_s = 0, 1, 3, 4,$ and 5. Figure 4-4 shows the corresponding results for μ_c/ϵ_F calculated from Equation (4–20).

4.2 Radial Distribution Function And Thermodynamics

We can use the approximate effective potential given by the Equations (4–5) and (4–10) in MD or use the Equations (4–1) and (4–2) to calculate the pair correlation functions $g(r)$. The resulting function g has two kinds of correlations built into it: i) the weak coupling correlations in RPA (ring diagrams) through S^{RPA} and ii) classical strong coupling effects (e.g., molecular dynamics simulation, HNC equations). Here we will

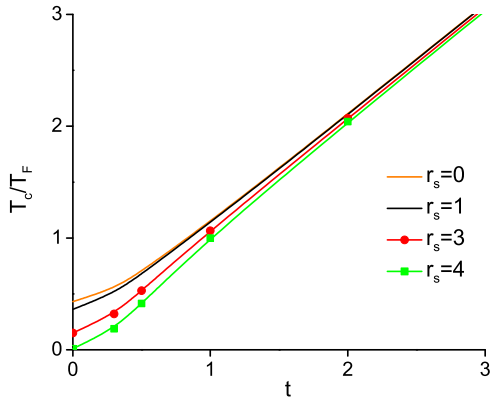

Figure 4-3. Classical reduced temperature T_c/T_F as a function of t for $r_s = 0, 1, 3$ and 4 [48].

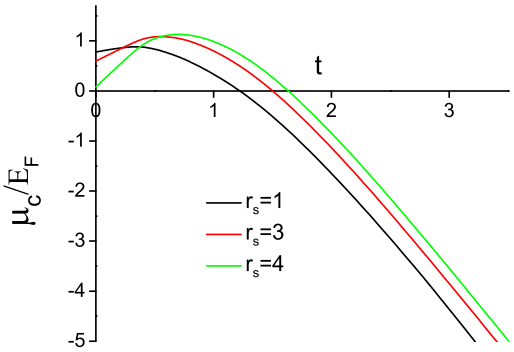

Figure 4-4. Dimensionless classical chemical potential μ_c/E_F as a function of t for $r_s = 1, 3, 5$ [48].

solve for g using the HNC approximation Equations (4–1) and (4–2)

$$\ln g(r) = -\beta_c\phi_c(r) + h(r) - c(r), \qquad c(r) = h(r) - n\int d\mathbf{r}' c(|\mathbf{r} - \mathbf{r}'|)h(r') \tag{4–23}$$

The effective potential in the formalism in Chapter 3 is defined using the HNC equations which takes the quantum pair correlation function as input. But the Equation (4–23) produces the pair correlation function as the output. Although it looks like a circular logic, the fact is we constructed $\beta_c\phi_c$ using only the weak coupling form of the HNC equations. The quantum input for $\beta_c\phi_c$ and $g(r)$ is calculated using the RPA theory,

hence the final pair correlation from the Equation (4–23) contains the effects from the weak quantum correlations and the strong classical correlations. The form of the HNC equations guarantees $g(r)$ always stays positive just as noted in [33]. In contrast the pair correlation function becomes negative at short distances for large values of r_s and low temperatures in typical calculations based on static local field corrections to RPA.

The computation of $g(r)$ from Equation (4–23) has been done using Ng's method [58] by splitting the interaction potential into a long ranged and a short ranged part following that reference. The Equations (4–7) and (4–23) do not use the pressure or temperature calculations. Hence they do not have the restriction to positive pressures and the associated restriction on r_s. The results are shown in Figure 4-5 for the case of $r_s = 6$ at $t = 0.5, 1, 4$ and 8. Also shown are the results from the recent restricted PIMC [11]. The agreement is quite good. Figure 4-6 shows the same conditions as Figure 4-5 for comparison with the results of PDW. The agreement is remarkable even though they have very different origins. This agreement between the predictions here, PIMC, and PDW extends to other state conditions as well, except for small t and very large r_s.

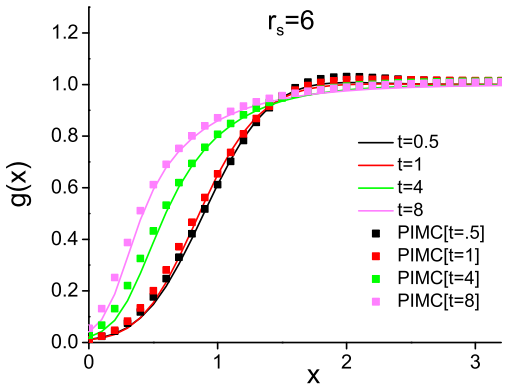

Figure 4-5. Radial distribution function $g(r^*)$ for $r_s = 6$ at $t = 0.5, 1, 4, 8$. Also shown are the results of PIMC [48].

Other theoretical models for $g(r)$ are based on modifying the dielectric formalism of the RPA by including "local field" corrections. The STLS model [13] is one of the

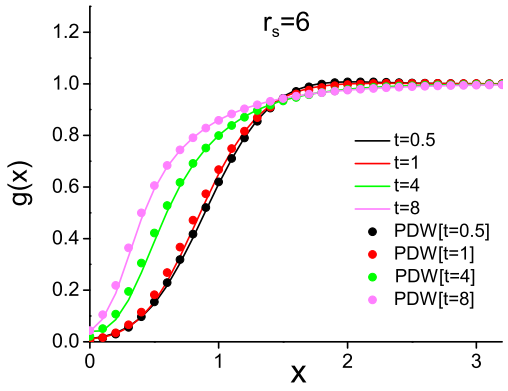

Figure 4-6. Radial distribution function $g(r^*)$ for $r_s = 6$ at $t = 0.5, 1, 4, 8$. Also shown are the results of PDW [48].

earliest self-consistent at $T = 0$, later generalized to finite temperature by Tanaka and Ichimaru (TI) [39]. We briefly looked at both the RPA and STLS scheme in Section 2.1.2. At metallic densities and low temperatures TI found that the pair correlation functions become negative as shown in Figure 4-7. The RPA results are significantly more negative in this range. Figure 4-7 shows the comparison of the pair correlation function from our model with TI at $r_s = 5$ at $t = 0.5, 1$ and 10 . Both RPA and its improved TI overestimate the size of the electron correlation hole [1] at larger values for r_s.

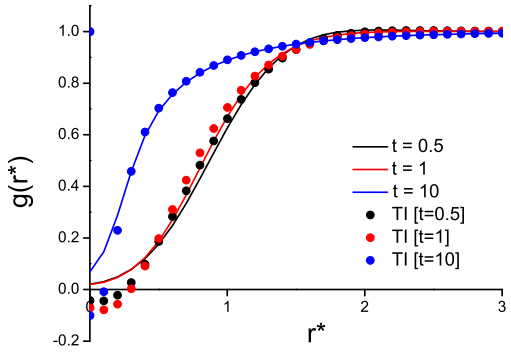

Figure 4-7. Radial distribution function $g(r^*)$ for $r_s = 5$ at $t = 0.5, 1$ and 10. Also shown are the results of Tanaka-Ichimaru [48].

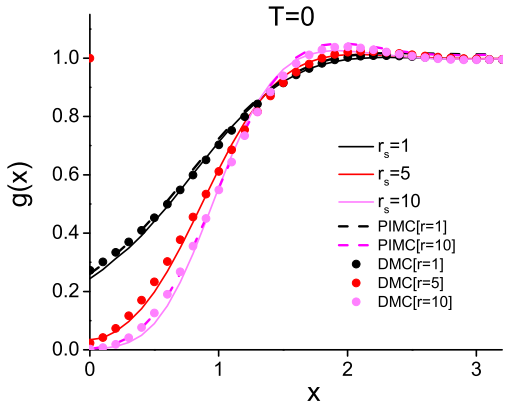

Figure 4-8. Radial distribution function $g(r^*)$ for $t = 0$ at $r_s = 1, 5, 10$. Also shown are results from PIMC and diffusion Monte Carlo. The PIMC and diffusion Monte Carlo plots are indistinguishable [11, 48].

The PDW $g(r)$ is in good agreement with diffusion MC data at $t = 0$ [33] for $r_s = 1, 5, 10$. The PDW model depends on one parameter T_0 which contains all the quantum many-body effects. It is determined by fitting the classical excess energy to the $t = 0$ exchange/correlation energy from MC data. It is impressive that this provides good results for $g(r)$ across a range of both r_s and t. Figure 4-8 shows a comparison of the results of the present analysis with the same $T = 0$ diffusion MC data [56], and also the recent PIMC for $T = 0.065$ at $r_s = 1, 10$. The good agreement is quite surprising since there is no MC parametrization in the present analysis and all quantum input is via the RPA and ideal gas exchange. However, it is recalled that the RPA preserves the exact quantum mechanics of the perfect screening sum rule that governs the cross over to the exact large r^* Coulomb limit. This is discussed further in Section 4.1.1.

4.2.1 Thermodynamics

The predicted pressure, p_c in atomic units, for the effective classical system is obtained from

$$\frac{\beta_c p_c}{n_c} = 1 - \frac{1}{6} n \int d\mathbf{r} h(r) \mathbf{r} \cdot \nabla \beta_c \phi_c(r) \tag{4–24}$$

using the effective temperature, Equation (4–21), and the full pair correlation function obtained from the Equation (4–23). Figure 4-9 shows this as a function of t for $r_s = 1, 3$ and 5. Also shown are the corresponding results for modified RPA (using the fits from reference [53]).

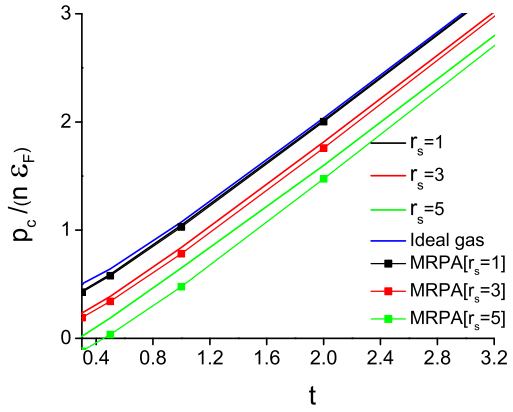

Figure 4-9. Dimensionless classical pressure $p_c/(n\epsilon_F)$ as a function of t for $r_s = 1, 3, 5$. Also shown are the corresponding modified RPA results [48].

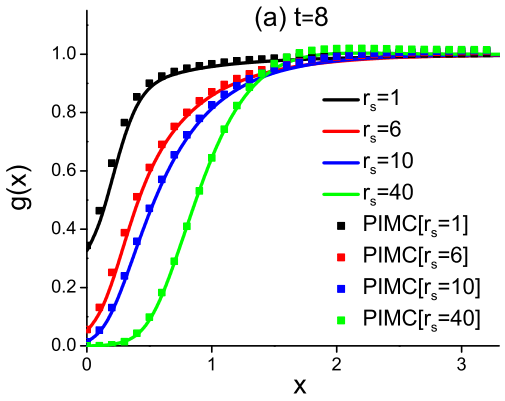

Figure 4-10. The pair correlation function is calculated using the modified Kelbg potential at $t = 8$ for $r_s = 1$, 6, 10 and 40. Comparison with the PIMC is also shown [59].

4.3 Kelbg Fitting For The Effective Potential $\beta_c\phi_c$

The calculation of the effective potential ϕ_c in the Equation (4–7) is complicated as it involves computing the RPA structure and then the direct correlation function.

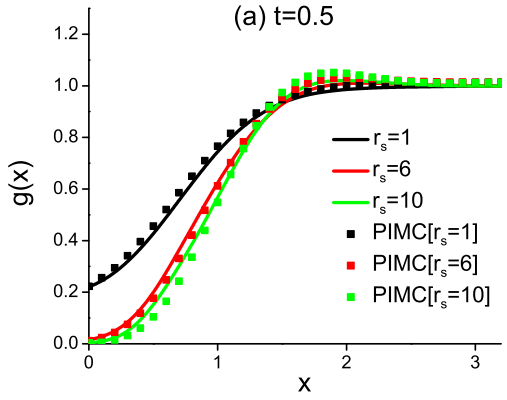

Figure 4-11. The pair correlation function is calculated using the modified Kelbg potential at $t = 0.5$ for $r_s = 1$,6, 10 and 40. Comparison with the PIMC is also shown [59].

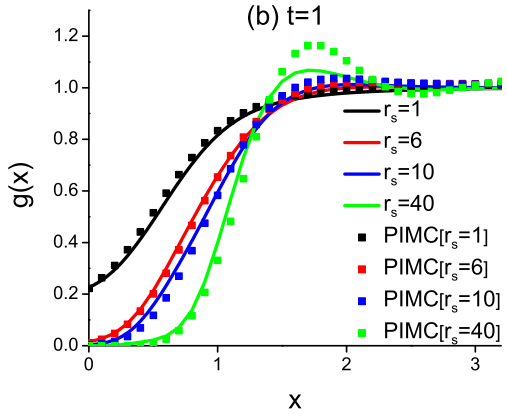

Figure 4-12. The pair correlation function is calculated using the modified Kelbg potential at $t = 1$ for $r_s = 1$,6, 10 and 40. Comparison with the PIMC is also shown [59].

For practical application it would be more convenient to obtain a fitting function for the potential. ϕ_c has an exact Kelbg form at high temperatures as proved in Appendix D. The effective potential is required to have a Coulomb tail which has the coupling coefficient determined by the exact screening sum rule. The effective coupling constant is given by the form in the Equation (4–12). First, the weak coupling Kelbg form Equation

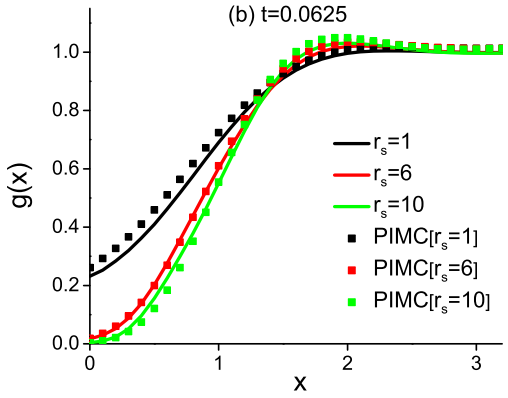

Figure 4-13. Comparison of the pair correlation functions for the modified Kelbg potential at $t = 0$ for $r_s = 1$,6, 10 and 40 with PIMC at $t = 0.0625$ and diffusion Monte Carlo at $t = 0$ [59].

(4–18) is improved by including another parameter γ [27]

$$\triangle_K(r^*) = \frac{\Gamma}{r^*}\left(1 - exp(-(ar^*)^2) + \sqrt{\pi}\frac{(ar^*)}{\gamma}erfc(\gamma ar^*)\right) \tag{4–25}$$

where $\gamma = -\frac{(\pi\Gamma r_s)^{1/2}}{ln(S(\Gamma r_s))}$ and $a = (r_s/\Gamma)^{1/2}$. The function S is the two electron Slater sum at the origin.

$$S(x) = -(4x)^{1/2}\int_0^\infty dye^{-y^2}\frac{y}{1 - e^{\pi\sqrt{x}/y}} \tag{4–26}$$

The new parameter γ affects the height of the modified potential in Equation (4–25) at the origin while it keeps the first derivative of the potential the same as the original Kelbg potential, Equation (4–18).

Second, in order for this effective potential to agree with the correct large distance behavior of the original effective potential, Equation (4–7), the Coulomb coefficient Γ in Equation (4–25) should be replaced by the effective coupling constant Γ_e, Equation (4–12). We propose the form of the effective potential [59]

$$\beta_c\phi_c(r^*) = (\beta_c\phi_c)^{(0)}(r^*) + \triangle_K(r^*) \tag{4–27}$$

This effective potential can be used in the HNC equations, Equations (4–23), to obtain the pair correlation functions $g(r)$ at various temperatures and densities. The comparison of the pair correlation functions with the PIMC data is shown below. The agreement is good at relatively high temperature $t = 8$ for $1 \leq r_s \leq 40$ as shown in Figure 4-10. Figures 4-11 and 4-12 show the comparison at $t = 0.5$ and 1 respectively. Again the agreement is good except at very low densities $r_s = 40$. It estimates the location of the peak of the pair correlation function g correctly but underestimates its height. Also shown in Figure 4-13 is the comparison of g with that of PIMC at $t = 0.0625$ and diffusion Monte Carlo at zero temperature. From the figures it is seen that g has a weak dependence on the temperature for $r_s > 1$ and $t \leq 0.5$.

4.4 Summary

1. We constructed the effective classical system for jellium.

2. The effective interaction potential ϕ_c is written as sum of the exchange term (Pauli potential) and Coulomb interaction term. The explicit form of the Coulomb term is obtained using weak coupling classical theory and quantum random phase approximation. The result is a regularized Coulomb potential at small r^*, and a Coulomb tail whose coefficient is determined by the exact screening sum rule.

3. The pair correlations were calculated using the HNC equations and the effective potential and compared with the PDW theory and PIMC.

4. The effective temperature and the effective chemical potential are also calculated within the weak coupling approximations. Then the full pressure and chemical potential were calculated from the HNC equations.

CHAPTER 5
SHELL FORMATION IN NONUNIFORM SYSTEMS

This Chapter gives a brief overview of the classical theories of the shell formation due to classical correlations. This is then used as the basis for studying quantum effects on the shell formation via the effective classical system. Zero temperature classical DFT is used to obtain the ground state density by minimizing the energy functional [60]. The contributions of the correlations are included using LDA and fits for the correlation energies for uniform system [61]. The shell models phenomenologically construct the energy functional that are parameterized by the number of shells, their position and the number of charges in each shell and then minimized it to solve for these parameters. Wrighton et al. [46, 49] successfully used classical DFT and HNC to include the correlations at finite temperatures. The shell formation due to strong quantum correlations in ultra-cold atoms in a trap and quantum dots is studied only at zero temperature. Since there are no finite temperature theories to explain the shells in these systems, we will extend our formalism in Chapter 3 to the confined quantum systems. We briefly look into the mechanism of the shell formation: quantum effects and quantum correlations. We primarily use the model of Wrighton et al. and the classical map of Chapter 3 and 4 to study quantum effects in the shell formation in a harmonic trap. The effective potentials and correlation functions of the previous Chapters are used in the HNC equations to calculate the density profile of the effective system. The density of classical systems depends on two parameters, the number of particles in the trap and the strength of the potential (coupling constant). This dependence will be discussed for the classical systems following the discussion in reference [46, 49] and will be extended to the quantum systems in the mean field theory.

5.1 Zero Temperature Classical Density

Just as in the zero temperature quantum DFT, the average energy of a classical system is minimized at the equilibrium density profile in classical DFT [60]. To obtain

the density profile we write the average energy as a functional of the density. Let us consider a system of N particles in an external potential $\phi_{ext}(\mathbf{r})$ and interacting via $\phi(\mathbf{r}, \mathbf{r}')$. The Hamiltonian is given by:

$$\hat{H} = \sum_{i=1}^{N} \frac{\hat{p}_i^2}{2m} + \int d\mathbf{r} \phi_{ext} \hat{n}(\mathbf{r}) + \int d\mathbf{r} d\mathbf{r}' \phi(\mathbf{r}, \mathbf{r}') \hat{g}(\mathbf{r}, \mathbf{r}') \tag{5–1}$$

The average energy is given by:

$$\begin{aligned} E &= \langle \hat{H} \rangle \\ &= \frac{3}{2} k_B T + N \int d\mathbf{r} \phi_{ext} n(\mathbf{r}) + \frac{N(N-1)}{2} \int d\mathbf{r} d\mathbf{r}' \phi(\mathbf{r}, \mathbf{r}') g(\mathbf{r}, \mathbf{r}') n(\mathbf{r}) n(\mathbf{r}') \end{aligned} \tag{5–2}$$

where $\langle \hat{n}(\mathbf{r}) \rangle = n(\mathbf{r})$ is the average density and $\langle \hat{g}(\mathbf{r}, \mathbf{r}') \rangle = g(\mathbf{r}, \mathbf{r}') n(\mathbf{r}) n(\mathbf{r}')$ is the average pair correlation function. Since the pair correlation functions are difficult to calculate, Henning et al. [61] included correlations through a local density approximation. This is done in the following steps: Start with energy expression for the uniform system: $\int d\mathbf{r} d\mathbf{r}' \phi(\mathbf{r}, \mathbf{r}') g(\mathbf{r}, \mathbf{r}') n(\mathbf{r}) n(\mathbf{r}') \rightarrow n^2 \int d\mathbf{r} d\mathbf{r}' \phi(\mathbf{r} - \mathbf{r}') \left(h(\mathbf{r} - \mathbf{r}') + 1\right) = V n^2 \phi(\mathbf{k}) + E_{corr}$. The correlation part of energy E_{corr} is given for Yukawa potential by an approximate form by Totsuji et al [62]: $E_{corr} = -1.44 q^2 n^{4/3} exp(-0.375 \kappa n^{-1/3} + 0.000074 (\kappa n^{-1/3})^4)$. Using LDA the uniform density n is replaced by non-uniform density $n(\mathbf{r})$. The energy is now minimized to solve for the ground state density. Even after including the correlations through LDA, it fails to produce any shell structure. However it agrees quite well with the averaged shell densities from the simulations.

5.2 Shell Models

Shell models attempt to explain the location and number of the shells and the number of particles in a shell by minimizing the energy function [63–65]. It assumes a density represented by a set of nested shells

$$n_{SM}(\mathbf{r}) = \sum_{\nu=1}^{L} N_\nu \frac{\delta(|\mathbf{r}| - R_\nu)}{4\pi R_\nu^2} \tag{5–3}$$

where L represents the total number of thin shells, located at a radius R_ν and with number of particles N_ν in the ν th shell. The energy is defined as a function of this shell model density n_{SM}. For Yukawa systems ($\frac{q^2}{r} exp(-\kappa r)$), the average total energy is the sum of three terms [64, 65]

$$E_{SM} = E_{ext} + E_{intra} + E_{inter} \tag{5–4}$$

$$E_{ext} = \sum_{nu=1}^{L} N_\nu \phi_{ext}(R_\nu) \tag{5–5}$$

$$E_{intra} = \sum_{nu=1}^{L} N_\nu \frac{q^2 e^{\kappa R_\nu}}{R_\nu} \frac{sinh(\kappa R_\nu)}{\kappa R_\nu} \frac{N_\nu}{2} \tag{5–6}$$

$$E_{inter} = \sum_{nu=1}^{L} N_\nu \frac{q^2 e^{\kappa R_\nu}}{R_\nu} \sum_{\mu<\nu}^{L} \frac{sinh(\kappa R_\mu)}{\kappa R_\mu} N_\mu \tag{5–7}$$

$$\tag{5–8}$$

E_{ext} is the contribution due to the trapping potential ϕ_{ext}, E_{intra} is the intra-shell model [60] and E_{inter} is the inter-shell energy. The parameters L, R_ν and N_ν are obtained by minimizing E_{SM} with respect to the parameters under the constraint $\sum_{\nu=1}^{L} N_\nu = N$ [63]. The results for the Coulomb systems are recovered by taking the $\kappa \to 0$ limit. The shell model quite accurately predicts the population of each shell as well as their location at the zero temperature [63]. However their extension to the finite temperatures is not straightforward.

5.3 Finite Temperature Formalism

Wrighton et al. [46, 49] developed an interesting formalism based on classical density functional theory to describe correlations in classical systems. They used the HNC equations for the density:

$$\ln\left(n\left(\mathbf{r}\right)\lambda^3\right) = \beta\mu - \beta\phi_{ext}(\mathbf{r}) + \int d\mathbf{r}'' c(\mathbf{r}, \mathbf{r}'') n\left(\mathbf{r}''\right) \tag{5–9}$$

The equation has two inputs the local chemical potential $\mu(\mathbf{r})$ and the direct correlation function $c(\mathbf{r}, \mathbf{r}')$. To simplify calculation they replaced the nonuniform correlations $c(\mathbf{r}, \mathbf{r}')$

by the uniform correlations of OCP systems $c_{OCP}(\mathbf{r}-\mathbf{r}')$. The results here are specialized to their work on the Coulomb systems in harmonic traps. Thus the interaction potential is $\phi(r) = \frac{\Gamma}{r^*}$ and the local chemical potential $\beta\mu - \frac{\Gamma}{2}(r^*)^2$, $r^* = r/r_0$, $\Gamma = \beta q^2/r_0$. The uniform correlations for such system are obtained from the HNC equations for the pair correlation functions for the one component plasma and the Ornstein-Zernike equation, Equation (4–2). At the mean field level, which means replacing $c(r^*) \to -\Gamma/r^*$, they did not get any shells for any value of the coupling constant Γ, as shown in Figure 5-1. However including the correlations in the HNC equations produced shells for strong coupling $\Gamma >> 1$ as shown in Figure 5-3.

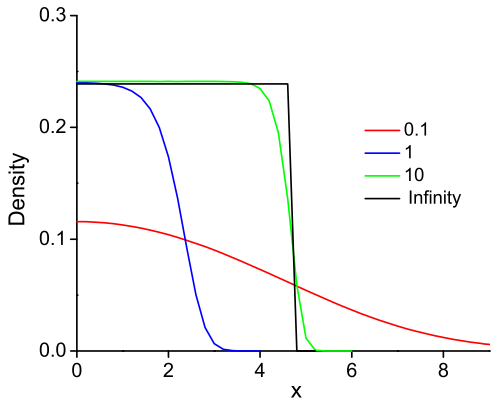

Figure 5-1. Mean field classical density profile for $N = 100$ particles for various values of Γ. The mean field Coulomb limit $\Gamma \to \infty$ is a step function [46].

We generalize their results to the quantum systems. We will use the same equation, Equation (5–9), but the quantum information is incorporated via the two inputs, the effective local chemical potential μ_c and the direct correlations c for jellium calculated in Chapter 4. In the rest of this Chapter, we address the question whether the quantum effects can produce shell structure in the mean field limit. The effective local chemical potential μ_c is no longer harmonic, but is modified by quantum effects as is shown below. Hence an interesting preliminary exploration would be to generate the density profile for some general external polynomial potentials at mean field and see the

effects of their shape on the possibility of shell formation. The effective local chemical potential corresponding to the classical harmonic trap changes its shape at different temperatures and densities. Knowing the effects of the shape of the external potential on the shell formation would help us study the influence of the quantum effects at different temperature and density range.

5.3.1 Shell Formation In A Polynomial Potential

Consider a classical system of N particles interacting via a potential ϕ confined by a trap potential ϕ_{ext}. The total potential energy of the Hamiltonian is given by the Equation (5–1). The radius of the trap R, which is the average position of the outermost particle, is defined to be the position where the forces due to the interaction potential of other particles on the outermost particle is balanced by the force due to the trap potential $-\nabla\phi_{ext}(\mathbf{r})$. For the particular case of Coulomb interactions $\phi(r) = q^2/r$ and a class of external potentials labeled by a parameter α, $\phi_{ext}(\mathbf{r}, \alpha)$, the force balance condition gives

$$\phi'_{ext}(R, \alpha) = (N-1)\frac{q^2}{R^2} \quad , \tag{5–10}$$

Using the following identities:

$$\begin{aligned} 4\pi n r_0^3/3 &= 1 \\ 4\pi n R^3/3 &= N \\ \Rightarrow R^3 &= r_0^3 N \quad , \end{aligned} \tag{5–11}$$

and the last equation from Equation (5–10), we get

$$r_0^2 N^{2/3} \phi'_{ext}(r_0 N^{1/3}, \alpha) = (N-1)q^2 \tag{5–12}$$

The dimensionless potential energy for the system is:

$$\beta\phi(r_i) = \Gamma\left(\frac{N^{1/3}}{r_0}\sum_i \frac{\phi_{ext}(\mathbf{r}_i^* r_0, \alpha)}{\phi'_{ext}(r_0 N^{1/3}, \alpha)} + \frac{1}{2}\sum_{i\neq j}\frac{1}{|\mathbf{r}_i^* - \mathbf{r}_j^*|}\right) \tag{5–13}$$

,

where $\Gamma = \beta q^2/r_0$. In particular for a polynomial external potential of the form $\phi_{ext}(\mathbf{r}, \alpha) = \alpha r^n$, the total potential becomes:

$$\beta\phi = \Gamma\left(\frac{N^{(2-n)/3}}{n}\sum_i r_i^{*n} + \frac{1}{2}\sum_{i\neq j}\frac{1}{|\mathbf{r}_i^* - \mathbf{r}_j^*|}\right) \tag{5–14}$$

,

In particular for a harmonic trap we have the total potential:

$$\beta\phi = \Gamma\left(\frac{1}{2}\sum_i r_i^{*2} + \frac{1}{2}\sum_{i\neq j}\frac{1}{|\mathbf{r}_i^* - \mathbf{r}_j^*|}\right) \tag{5–15}$$

(5–16)

We can now calculate the density profile from the Equation (5–9). For most experiments and simulations it is more convenient to use the average number of particles in the trap N instead of the chemical potential μ. The conversion between the two is done using the equation $\int d\mathbf{r}\, n(\mathbf{r}, \mu) = N$. The result is:

$$\begin{aligned} n(\mathbf{r}) &= N\frac{exp(-\Gamma U(\mathbf{r}))}{\int d\mathbf{r}' exp(-\Gamma U(\mathbf{r}'))} \\ \Gamma U(\mathbf{r}) &= \beta\phi_{ext}(\mathbf{r}) + N\frac{\int d\mathbf{r}' exp(-\Gamma U(\mathbf{r}'))c_{OCP}(|\mathbf{r} - \mathbf{r}'|)}{\int d\mathbf{r}' exp(-\Gamma U(\mathbf{r}'))} \end{aligned} \tag{5–17}$$

where $\Gamma = \beta q^2/r_0$. All the above equations can be written in terms of the dimensionless distance $\mathbf{x} = \mathbf{r}/r_0$. We can calculate the density profile for various polynomial potentials as in Equation (5–14): $\beta\phi_{ext}(\mathbf{x}) = \Gamma\frac{N^{(2-n)/3}}{n}x^n$ in the mean field limit i.e. replacing $c_{OCP}(\mathbf{r} - \mathbf{r}')$ by $-\beta\phi(\mathbf{r} - \mathbf{r}')$, of the Equation (5–17). The results are shown in Figure 5-2.

The plots show that in the mean field limit we do not get any shell for the linear and harmonic traps as found by Wrighton et al. [46]. However higher order trap polynomials produce shells i.e. when the effective local chemical potential is steeper than the harmonic potential we get shells.

For the rest of the section, we focus on only the harmonic trap potentials. The above results can be generalized beyond the mean field by including the correlations

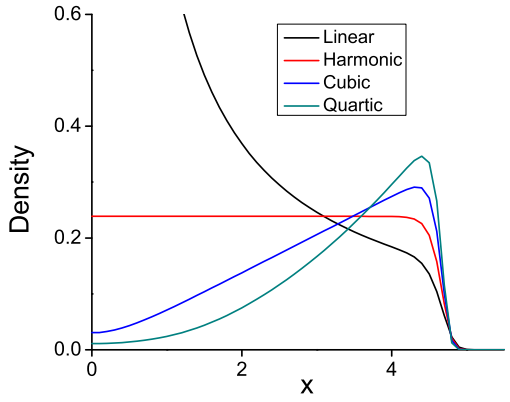

Figure 5-2. The density profile in the mean field limit of Coulomb systems in different polynomial trap potentials for $\Gamma = 40$

from the uniform OCP, c_{OCP}. The density profile depends on two parameters Γ and N, so it is interesting to see how the density changes as these parameters are changed. For fixed number of particles in the trap N, the sharpness of the shells increases as we increase Γ but the number and the position of shells remains unchanged [46] as shown in Figure 5-3

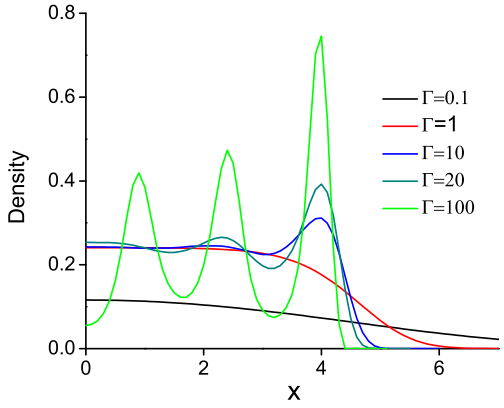

Figure 5-3. The variation of the density profile with the coupling constant Γ for 100 particles in the trap [46].

In the other case at a constant Γ, the number of shells increases as we changing N as is shown in Figure 5-4.

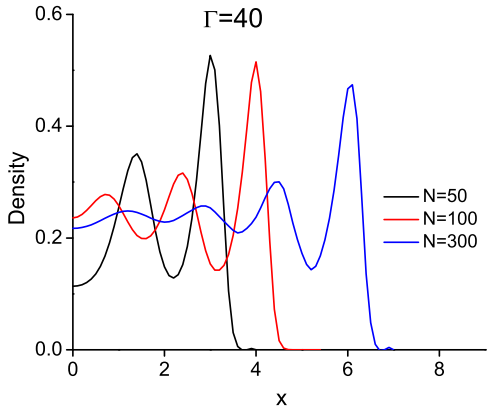

Figure 5-4. The variation of the density profile with the number of particles in the trap for $\Gamma = 100$ [46].

Figure 5-5 shows how the shells are filled and when new shells are formed. The number of particles in each shell varies as $N^{2/3}$. From these results we conclude that

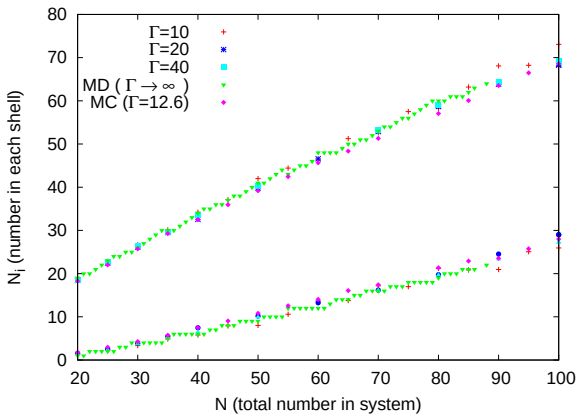

Figure 5-5. The filling of the shells and the dependence of the population in each shell on the total number of particles in the trap is shown. Also shown are the corresponding MC and MD data [46].

only the strong correlations $\Gamma >> 1$ produce shell structure. The singularity of the Coulomb potential at the origin destroys the shells for classical particles in the mean field limit. The shells in a harmonic trap are equi-spaced and the position of the shells varies as $N^{2/3}$. The HNC equations provide a good description of the strong correlations in the classical systems as shown in Figure 1-2 and Figure 5-5.

5.4 Shell Formation In Quantum Systems

For quantum systems we still can use the classical equations to obtain the density profile [46]. Using the effective local chemical potential $\mu_c(\mathbf{r})$ from Chapter 3 and the uniform correlations c for jellium calculated in Chapter 4 we can incorporate appropriate quantum effects.

$$ln\left(n(\mathbf{r})\lambda_c^3\right) = \beta_c\mu_c(\mathbf{r}) + \int d\mathbf{r}'c(|\mathbf{r}-\mathbf{r}'|)n(\mathbf{r}') \tag{5–18}$$

An equivalent representation is in terms of the average number of particles in the trap N similar to the discussion in Equation (5–17). The density is then given by:

$$\begin{aligned} n(\mathbf{r}) &= N\frac{exp(-\beta U(\mathbf{r}))}{\int d\mathbf{r}'exp(-\beta U(\mathbf{r}'))} \\ \beta U(r) &= \beta_c\mu_c(\mathbf{r}) - \int d\mathbf{r}'c(|\mathbf{r}-\mathbf{r}'|)n(\mathbf{r}') \end{aligned} \tag{5–19}$$

Without the diffraction and exchange effects, the local chemical potential in Equation (5–18) is harmonic. As a first estimate of quantum effects on the effective local chemical potential, we neglect the Coulomb interactions among the particles and consider the effective local chemical potential with only the exchange effects.

5.4.1 Effective Local Chemical Potential For Ideal Fermi Gas

The local chemical potential for the ideal Fermi gas is given by:

$$(\beta_c\mu_c)^{(0)}(\mathbf{r}) = ln\left(n^{(0)}(\mathbf{r})(\lambda_c^{(0)})^3\right) - \int d\mathbf{r}'c^{(0)}(|\mathbf{r}-\mathbf{r}'|)n^{(0)}(\mathbf{r}') \tag{5–20}$$

where $n^{(0)}$ and $c^{(0)}$ are the density and direct correlation functions of the ideal Fermi gas calculated in Chapter 3. The density $n^{(0)}$ can be calculated in two ways: by summing over all the eigenfunctions of the harmonic Hamiltonian, or by a local density approximation. Some fitting functions for the latter is given in Appendix B. The details of the density expressions are provided in Chapter 3. The density profile calculated in two different ways do not differ much as discussed in Section 3.3.

The local chemical potential $(\beta\mu)^{(0)}$ is calculated using Equation (5–20) with the densities calculated using LDA Equations (3–66,3–67,3–68). The plots of $(\beta\mu)^{(0)}$ for r_s and temperatures $t = 0.5$ and 10 for $N = 100$ particles are shown in Figure 5-6:

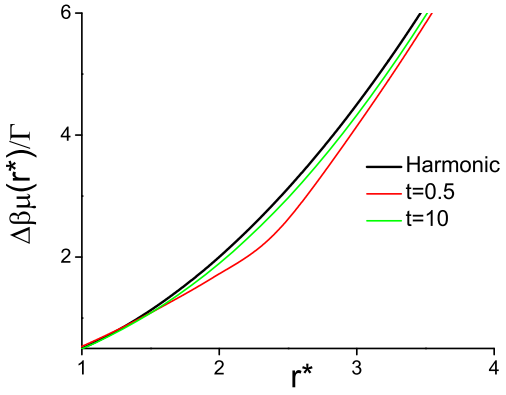

Figure 5-6. Effective classical trap potential $\triangle\beta_c\mu_c(\mathbf{r}^*)/\Gamma = (\beta_c\mu_c(\mathbf{r}^*) - \beta_c\mu_c(\mathbf{0}))/\Gamma$ as a function of r^* for $t = 0.5, 10$ [48]. Also shown is the harmonic potential.

It can be seen from Figure 5-6 that $(\beta\mu)^{(0)}$ differs from the harmonic potential at intermediate distances at very low temperatures. At large distances it has a harmonic asymptote.

5.4.2 The Quantum Effects On The Shell Formation In The Mean Field Theory

For classical Coulomb systems in a harmonic trap we do not get shells in the mean field for any value of the coupling constant as discussed in Section 5.3. In this section we study the quantum effects on the shell formation in the mean field limit. First we consider the diffraction effect. Diffraction effects are put into classical systems by using a regularized Coulomb potential for the interaction potential. In our case we choose the Kelbg potential for the interaction potential and the harmonic potential for the external potential. Thus our system has only diffraction effects. In the mean field limit we get shells at very low temperatures as shown in Figure 5-7 for $\Gamma = 3$ at $t = 0.1, 0.5$ and 1. The shell formation is because of the fact that the Kelbg potential is regularized at the

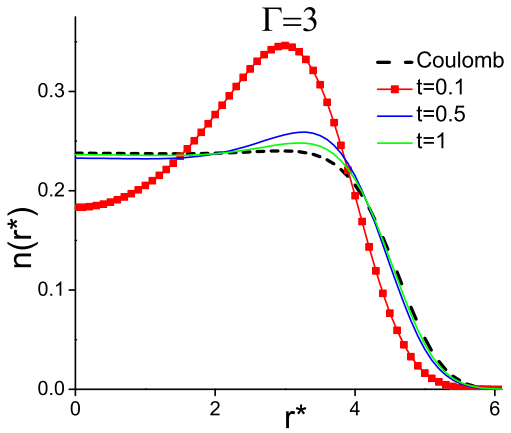

Figure 5-7. Diffraction mean field approximate density profile for $\Gamma = 3$ and $t = 0.1, 0.5, 1$ [48].

origin and at very low temperatures it can mimic the strong correlations of the classical OCP as shown in Figure 5-8.

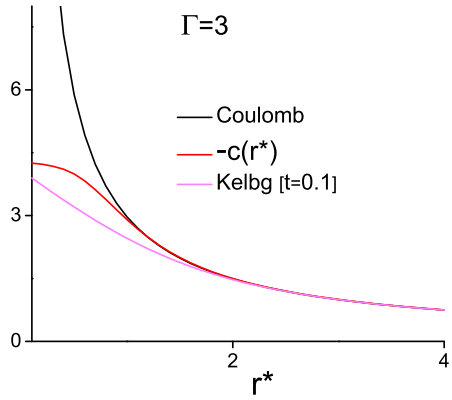

Figure 5-8. Comparison of $-c(r^*)$ and $V_K(r^*)$ at $t = 0.1, 0.27$ both corresponding to $\Gamma = 3$ [48]. Also shown is the Coulomb limit $\beta q^2/r$.

To study the degeneracy effects, we neglect the diffraction effects by using the Coulomb potential as the interaction potential, but keep the exchange effects in the external potential i.e. use $(\beta\mu)^{(0)}$. Again we get shells at low temperatures for $r_s = 5$ at $t = 0.5, 1, 2, 5$ and 10 for 100 particles as shown in Figure 5-9. To understand the mechanism of the shell formation for degeneracy effects, we note that in the case of the

polynomial potentials, r^n, we get shells for $n > 2$ as shown in Figure 5-2. Thus as the steepness of the potentials increase we get shells. At low temperatures and densities the classical harmonic potential is modified by the strong diffraction effects, making it steeper than the harmonic potential. Also the coupling constant is large at very low temperatures which is another factor for the shell formation. Thus the quantum effects of diffraction and degeneracy produce shells at very low temperatures even in the mean field limit.

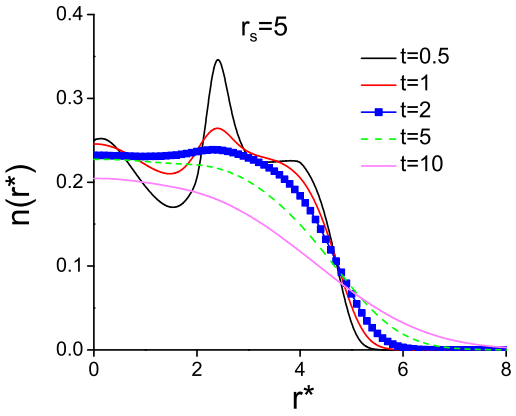

Figure 5-9. Exchange mean field approximate density profile for $r_s = 5$ and $t = 0.5, 1, 2, 5, 10$ [48].

5.4.3 N Dependence Of Radius Of The Trap

In this section we study how the radius of the trap varies as we change the average number of particles in the trap. In particular we are interested in how the quantum systems would differ from the classical systems in the way the shells are filled. The force balance condition can be used to calculate the position of the outermost shell. The dependence of the radius of the trap R on the number of particles N relates to the position of the other shells also. For classical Coulomb systems in a harmonic trap the radius of the trap (position of the outermost particles) varies as $N^{1/3}$. The same method can be applied to the effective potential to predict the R vs N behavior for the quantum systems in harmonic traps. These predictions can be compared with the experimental

data for the ultra-cold ions and the quantum dots in harmonic traps to check the validity of our formalism. To keep things simple we consider the Kelbg interaction potential $\Delta_K(r) = \frac{\Gamma}{r}\left(1 - exp(-r^2/\lambda_K^2) + \sqrt{\pi}\frac{r}{\lambda_K} erfc(r/\lambda_K)\right)$ for the effective interaction potential and the harmonic potential as the external potential. This would give us the force balance condition from the Equation (5–10) for the diffraction effects only:

$$\phi'_{ext}(\mathbf{r}) = \frac{N-1}{N}\int d\mathbf{r}' n(\mathbf{r}')\nabla\left(\Delta_K(|\mathbf{r}-\mathbf{r}'|)\right) = 0 \tag{5–21}$$

At low temperatures $\lambda \to \infty$, and as a result $\Delta_K(r) \to \frac{1}{\lambda^2}$. At the limit of high temperatures $\lambda \to 0$ we get $\Delta'_K(r) \to -1 + \frac{1}{2\lambda_K^2}r^2$. Using these results in Equation (5–21) we get

$$\lambda \to 0, \quad m\omega^2 R = (N-1)\frac{q^2}{R^2} \tag{5–22}$$

$$\lambda \to \infty, \quad m\omega^2 R = N\frac{q^2}{\lambda_K^2} \tag{5–23}$$

From the above equations, we see that in the quantum limit, the radius of the trap R depends on the total number of particles in the trap N as $R \sim N$, while in the classical limit the dependence is $R \sim N^{1/3}$. Thus the trap potential is strong compared to the Coulomb repulsion at high temperatures while at low temperatures the particles spread outward due to the stronger Coulomb repulsion.

5.5 Summary

1. We looked at classical theories that study strong correlations in shell formation: zero temperature classical DFT, shell model and finite temperature formalism by Wrighton et al.

2. The explanation behind shell formation in the classical Coulomb systems is discussed. The dependence of the number of particles in the shell and the position of the shells on the total number of particles in the trap and the coupling constant has also been discussed.

3. We extended the map to confined quantum systems using the effective potentials and the correlations of jellium from the previous chapters.

4. We studied the modifications due to the quantum exchange effects to the harmonic potential in case of the ideal Fermi gas.

5. We looked into the possible mechanism for shell formation in the quantum systems. In particular, to consider the quantum effects of diffraction we consider Kelbg potential in a harmonic trap. Similarly for degeneracy effects we consider the Coulomb interactions among the particles and an external potential modified from the harmonic form by the diffraction effects. In both cases we obtain shells at the low temperatures and densities even in the mean field limit. We explained the possible mechanism behind the shell formation due to the quantum effects.

CHAPTER 6
CONCLUSION

There exist a number of quantum many-body theories to study the correlated quantum systems at zero temperature. Either their extension to both finite temperatures and strong coupling are not straightforward or they are computationally intensive. Perrot and Dharma-wardana could successfully predict some of the thermodynamics of the uniform electron gas by using a simple classical mapping. However their model is phenomenological and the functional forms of their effective parameters were guessed from the physics of the systems. Our objective has been to provide a systematic and general formalism that would incorporate some of their ideas but would be applicable to a large class of systems.

In this thesis we have constructed a novel technique to describe the quantum correlations using the classical many-body theory, in particular using the classical DFT. The procedure has been devised to work for any quantum systems with any general interaction and external potential over a wide range of temperatures and densities. We have first constructed a classical representative system that describes the thermodynamics of a given quantum system. Its thermodynamics is described by three parameters: an effective interaction potential, local chemical potential and temperature. These parameters are determined by a map from the thermodynamics of the classical representative system to that of the quantum system. They are determined by inverting the map using classical DFT and the virial equations. The dependence of the classical parameters on each other give rise to some peculiar thermodynamics for the effective classical system.

The ideal Fermi gas and weak coupling limits of the uniform electron gas have been worked out explicitly. The ideal gas results are recovered by taking the $r_s \to 0$ limit of the interacting system. Since both our and PDW model have the same ideal gas limits, the agreement between the two is good at small r_s values. However the density

dependence of Γ_e of the PDW model effective potential at $T = 0$ is $\Gamma \propto r_s(a + b\sqrt{r_s} + cr_s)$ and for our model $\Gamma_e \propto r_s^{1/2}$ dependence. Hence the results from the two models differ at large densities and low temperatures. The effective interaction potential for our model is required to have a Coulomb tail from the perfect screening sum rule. The Kelbg form of the potential is recovered at high temperatures and low densities. The pair correlation functions have been calculated using the HNC equations and compared with the PIMC and PDW data. The agreement is good in the density range $r_s = 1$ and 10 for all temperatures. Thus this model would be able to describe well all metallic systems and warm dense matter systems. Many of the quantum theories fail to give positive pair correlation functions at these range of densities. It appears that by imposing the sum rule constraint on the effective potential we can capture the essential many body effects of the jellium. The pair correlation functions, calculated using the HNC equations for both our model and PDW theory, have good agreement even though the effective potentials are different. This may be because the non-linear equations of HNC may have multiple solutions for the same pair correlation function. The pressure of jellium becomes negative at metallic densities and low temperatures, the equivalence of the quantum and classical pressures breaks down at that regime. This would imply a negative effective temperature and we might need to refine it using some other equivalence condition.

Another application of our model has been to the confined charges in a harmonic trap. Wrighton et al. successfully predicted the shell formation for strong coupling. Their density profile calculated using the HNC equation is in good agreement with the classical Monte Carlo data. We have applied the effective potentials from our approach in the HNC equations to generate the density profile for the quantum systems. This procedure has been used to study the quantum effects on the shell formation. In the mean field limit there is no shell formation in the classical system, but there is for the quantum system. We looked into the diffraction and degeneracy effects separately.

For the diffraction, we considered the Kelbg potential in a harmonic trap. A second mechanism for shell formation is found for degeneracy effects with an effective external potential, which is the harmonic potential modified by the quantum effects of degeneracy and Coulomb interactions. At low temperatures and densities both effects produce shells even in the mean field limit. The radius of the trap for the classical quantum system has $N^{1/3}$ dependence, for N particles in the trap. For the quantum system, the radius of the trap at low temperatures has N dependence while at high temperatures we recover the classical result.

This formalism can be immediately applied to spin polarized systems, magnetic systems and lattice systems as is shown in the next chapter.

CHAPTER 7
OTHER APPLICATIONS OF THE FORMALISM

In this Chapter we consider some additional applications of the formalism for future study.

7.1 Density Profile Of Coulomb Systems In A Harmonic Trap

In Chapter 5 we see that in the mean field limit the quantum effects produce shell structure which is missing the classical systems. This does not imply that we will always have more shells in the quantum system than a classical system with the same potential. In fact we found that the Pauli potential broadens the shells and thus the exchange effects may destroy the shell formation. In Chapter 5 we have treated the two quantum effects, degeneracy and diffraction separately. If we put them all together we find that the final shell structure has a strong influence from the diffraction than the degeneracy than the diffraction effect. If we increase the number of particles in the shell, in the mean field limit, we do not necessarily get more shells.

7.2 Spin Polarized Uniform Electron Gas

When there is a magnetic field, the Hamiltonian acquires a spin dependent term. The spin in classical systems is treated as different species of particles. Thus we have different interaction potentials among the particles depending on the species they belong to. Thus for $\uparrow$ and $\downarrow$ spins in the quantum system we have four components for all the thermodynamical quantities $\uparrow\uparrow$, $\uparrow\downarrow$, $\downarrow\uparrow$ and $\downarrow\downarrow$. The Ornstein-Zernike equation splits into components too

$$h_{ij}(r) = c_{ij}(r) + \sum_k n_k \int d\mathbf{r}' h_{ik}(|\mathbf{r} - \mathbf{r}'|) c_{kj}(r') \tag{7–1}$$

where n_k is the density of the spin species k. The effective interaction potential similarly has four components [33]:

$$(\beta_c \phi_c)_{ij}(r) = (\beta_c \phi_c)^{(0)}_{ij}(r) + \triangle_{ij}(r) \tag{7–2}$$

where $ij = \uparrow\uparrow, \uparrow\downarrow, \downarrow\uparrow, \downarrow\downarrow$. For same spin species $i = j$, $(\beta_c\phi_c)_{ij}^{(0)}(r)$ is singular at the origin because of the singularity of the same spin Pauli potential, otherwise they are finite. As a result when used in the HNC equations, the pair correlation function is zero at the origin as expected for a quantum system due to the Pauli exclusion principle. The $\triangle_{ij}$ is the above equation is calculated using the RPA just like the discussion in Chapter 4. PDW assumed a spin independent form for $\triangle_{ij}$. From these results the magnetic susceptibility can be calculated as shown in Section 7.3 for the ideal Fermi gas.

7.3 Magnetic Susceptibility At Finite Temperatures Of The Ideal Fermi Gas

Let the densities of the two spin components,1 and 2 with spins $S_i = \pm S(S = \frac{1}{2})$,be

$$n_i = \frac{n}{2}(1 \pm \delta) \tag{7–3}$$

,

where n is the average density of the system. The HNC equation for the density becomes

$$ln(n_i\lambda^3) = \beta\mu - \beta BS_i + \sum_j \int d\mathbf{r}' n_j c_{ji}(r') \tag{7–4}$$

$$= \mu - BS_i + \sum_j n_j c_{ji}(k = 0) \tag{7–5}$$

$$h_{ij}(r) = c_{ij}(r) + \sum_k n_k \int d\mathbf{r}' c_{ik}(\mathbf{r} - \mathbf{r}') h_{kj}(\mathbf{r}') \tag{7–6}$$

$$\tag{7–7}$$

$$
\begin{aligned}
h_{12}(r) = h_{21}(r) = 0 \\
h_{11}(r) = h_{22}(r) \\
\Rightarrow c_{12}(r) = c_{21}(r) = 0 \\
c_{ii}(r) = \frac{h_{ii}(r)}{1 + n_i h_{ii}(r)}
\end{aligned}
\tag{7–8}
$$

,

Subtraction of density of one component from another:

$$
ln\left(\frac{n_2}{n_1}\right) = \beta B + \left(\frac{1}{1 + n_1 h_{11}(k=0)} - \frac{1}{1 + n_2 h_{11}(k=0)}\right) \tag{7–9}
$$

The magnetization is given by:

$$
M = S(n_1 - n_2) = \frac{1}{2} n\delta \ , \tag{7–10}
$$

Hence the Equation (7–4) along with the Equation (7–10) give

$$
\begin{aligned}
ln(\frac{1 - 2M/n}{1 + 2M/n}) &= \beta B + \left(\frac{1}{1 + n_1 h_{11}(k=0)} - \frac{1}{1 + n_2 h_{11}(k=0)}\right) \\
&= \beta B - \frac{n\delta h_{11}(k=0)}{(1 + \frac{1}{2} n h_{11}(k=0))^2 - (\frac{1}{2} n\delta h_{11}(k=0))^2} \\
&= \beta B - \frac{2M h_{11}(k=0)}{(1 + \frac{1}{2} n h_{11}(k=0))^2 - (M h_{11}(k=0))^2} \ ,
\end{aligned}
\tag{7–11}
$$

where $h_{11}(k=0) = -\frac{1}{2}\frac{\int d\mathrm{k} n^2(\mathrm{k})}{n^2}$ from the discussion in Chapter 3. This discussion can be easily extended to interacting systems, where we can used the spin polarized pair correlation function discussed in Section 7.2.

7.4 Crystal Lattice Systems

The theories that exist for quantum systems in a periodic potential, $\phi_{ext}(\mathbf{r} + \mathbf{R}) = \phi_{ext}(\mathbf{r})$ with lattice vectors $\mathbf{R}$, usually use independent electron model. The interactions

among the electrons are electrons are neglected. The solution of the single particle Schroedinger equation in periodic potential is a Block wavevector $\psi_{n,\mathrm{k}}$ with the property: $\psi_{n,\mathrm{k}}(\mathbf{r}) = exp(i\mathbf{k}.\mathbf{r})u_{n,\mathrm{k}}(\mathbf{r})$ with $u_{n,\mathrm{k}}(\mathbf{r}) = u_{n,\mathrm{k}}(\mathbf{r}+\mathbf{R})$ and k the crystal momentum. The energy eigenvalues are given by: $\epsilon_n(\mathbf{k}) = \epsilon_n(\mathbf{k}+\mathbf{K})$ where $\mathbf{K}$ is the reciprocal vector. The tight binding model assumes that lattice is made of weakly overlapping atomic systems. Hence the single particle wave-functions in the lattice can be written as a sum of single particle atomic orbitals.

The effective classical system still has three parameters we need to determine. Consider a quantum Coulomb system in a periodic potential ϕ_{ext}. We assume the lattice symmetry is preserved in the map. Also for simplicity we consider the effective pair potential to depend on the relative coordinates. Hence $\beta_c\phi_c(\mathbf{r}-\mathbf{r}') = \sum_R(\beta_c\phi_c)^{UEG}(\mathbf{r}-\mathbf{r}')$ where $(\beta_c\phi_c)^{UEG}$ is the effective interaction potential determined in Chapter 4 using RPA theory. The HNC equation for this non-uniform system is highly complicated. However even if we replace the non-uniform density by an uniform average density of the system, then the pair correlations does not have the periodicity of the lattice:

$$g(r) = \sum_{\mathrm{R}} g^0(|\mathbf{r}-\mathbf{R}|) \tag{7–12}$$

where g^0 are some periodic function with the periodicity of the lattice. This is because the HNC equation is a non-linear equation in ϕ_c. The same conclusion can be drawn from the density.

7.5 2D Electron Gas

For materials where electrons are confined to two dimensions like graphene, the analysis of 2D systems becomes important. Important applications are the shell formation in the quantum dots. For 2D systems the Fourier transform of the Coulomb potential is different than the 3D systems. The sum rules are also different and the form of the effective potential are completely different than the 3D case.

APPENDIX A
EXACT COUPLED EQUATIONS FOR $N_C(\mathbf{R})$ AND $G_C\left(\mathbf{R}, \mathbf{R}'\right)$

This appendix outlines the origin of the exact equations, Equations (3–31) - (3–32), for the classical density and pair correlation function from the classical density functional theory (DFT). We go from local chemical potential representations of thermodynamics through the grand potential to the density representations though free energy by the use of the Legendere transform.

$$F_c(\beta_c \mid n_c) = \Omega_c\left(\beta_c \mid \mu_c\right) + \int d\mathbf{r}\mu_c\left(\mathbf{r}\right) n_c\left(\mathbf{r}\right) \tag{A–1}$$

where the free energy is a functional of the classical density and the grand potential of $\mu_c\left(\mathbf{r}\right)$. The density and local chemical potential are conjugate to one another

$$\frac{\delta F_c}{\delta n_c(\mathbf{r})} = \mu_c(\mathbf{r}). \tag{A–2}$$

The free energy is now divided into its ideal classical gas contribution $F_c^{(0)} = -\beta_c^{-1}\int d\mathbf{r}\,[1 - \ln\left(n\left(\mathbf{r}\right)\lambda^3\right) n\left(\mathbf{r}\right)$, where $\lambda_c = \left(2\pi\hbar^2\beta_c/m\right)^{1/2}$, and the remainder $F_{c,ex}$ the interaction part, so that the Equation (A–2) becomes an equation for the density

$$\beta_c\mu_c(\mathbf{r}) = \ln\left(n_c\left(\mathbf{r};\beta_c\right)\lambda_c^3\right) - c_c^{(1)}\left(\mathbf{r};\beta_c \mid n_c\right) \tag{A–3}$$

Here $c_c^{(1)}\left(\mathbf{r} \mid n_c\right)$ is the first of a family of functions (direct correlation functions) defined by derivatives of the free energy

$$c_c^{(m)}\left(\mathbf{r}_1, .., \mathbf{r}_1; \beta_c \mid n_c\right) \equiv -\beta\frac{\delta^m F_c}{\delta n_c(\mathbf{r}_1)..\delta n_c(\mathbf{r}_m)} \tag{A–4}$$

Equation (A–3) relates the density $n_c(\mathbf{r})$ to a given external potential (recall $\mu_c(\mathbf{r}) = \mu_c - \phi_{c,ext,}(\mathbf{r})$). Now an interesting case is when one of the particles in the system is treated as an impurity at some point r'. Then the interaction potential $\phi_c(r)$ becomes the external potential for the other particles. Thus the total external potential is $\phi_{c,ext} + \phi_c$ and the density of the particles in the new external potential is related to the pair correlations

and density of the original system by

$$n_c\left(\mathbf{r},\mathbf{r}'\right)=n_c\left(\mathbf{r}\right)g_c\left(\mathbf{r},\mathbf{r}'\right). \tag{A–5}$$

The equation corresponding to Equation (A–3) for this new external potential is

$$\ln\left(n_c\left(\mathbf{r}\right)g_c\left(\mathbf{r},\mathbf{r}'\right)\lambda_c^3\right)=\beta_c\mu_c(\mathbf{r})-\beta_c\phi_c(\mathbf{r},\mathbf{r}')+c_c^{(1)}\left(\mathbf{r};\beta_c\mid n_cg_c\right). \tag{A–6}$$

Finally, subtracting Equation (A–3) from Equation (A–6) gives the desired equation for $g_c\left(\mathbf{r},\mathbf{r}'\right)$

$$\ln\left(g_c\left(\mathbf{r},\mathbf{r}'\right)\lambda_c^3\right)=-\beta_c\phi_c(\mathbf{r},\mathbf{r}')+c_c^{(1)}\left(\mathbf{r};\beta_c\mid n_cg_c\right)-c_c^{(1)}\left(\mathbf{r};\beta_c\mid n_c\right). \tag{A–7}$$

The notation used implies that the functional $c_c^{(1)}\left(\mathbf{r};\beta_c\mid\cdot\right)$ in both Equations (A–3) and (A–6) are the same. This follows from density functional theory where it is demonstrated that the free energy is a universal functional of the density, the same for all external potentials. Equations (3–31) and (3–30) now follow directly from Equations (A–3) and (A–7) and the identity

$$\begin{aligned}c_c^{(1)}\left(\mathbf{r};\beta_c\mid X\right)&=c_c^{(1)}\left(\mathbf{r};\beta_c\mid Y\right)+\int_0^1 d\alpha\partial_\alpha c_c^{(1)}\left(\mathbf{r};\beta_c\mid\alpha X+\left(1-\alpha\right)Y\right)\\&=c_c^{(1)}\left(\mathbf{r};\beta_c\mid Y\right)+\int_0^1 d\alpha\int d\mathbf{r}'\frac{\delta c_c^{(1)}\left(\mathbf{r};\beta_c\mid\alpha X+\left(1-\alpha\right)Y\right)}{\delta n_c\left(\mathbf{r}'\right)}\left(X\left(\mathbf{r}'\right)-Y\left(\mathbf{r}'\right)\right)\\&=c_c^{(1)}\left(\mathbf{r};\beta_c\mid Y\right)+\int_0^1 d\alpha\int d\mathbf{r}'c_c^{(2)}\left(\mathbf{r},\mathbf{r}';\beta_c\mid\alpha X+\left(1-\alpha\right)Y\right)\left(X\left(\mathbf{r}'\right)-Y\left(\mathbf{r}'\right)\right)\end{aligned} \tag{A–8}$$

with appropriate choices for X and Y.

The Ornstein - Zernicke equation, Equation (3–32), is an identity obtained as follows. The second functional derivative of the grand potential is related to the pair correlation function by

$$\frac{\delta^2\left(-\beta_c\Omega_c\right)}{\delta\mu_c\left(\mathbf{r}\right)\mu_c\left(\mathbf{r}'\right)}=\frac{\delta n_c\left(\mathbf{r}'\right)}{\delta\mu_c\left(\mathbf{r}\right)}=\beta_c n_c\left(\mathbf{r}'\right)\left[\delta\left(\mathbf{r}-\mathbf{r}'\right)+n_c\left(\mathbf{r}\right)\left(g_c\left(\mathbf{r},\mathbf{r}'\right)-1\right)\right], \tag{A–9}$$

Similarly, the second derivative of the free energy is

$$\frac{\delta^2 F_c}{\delta n_c\left(\mathbf{r}'\right)\delta n_c\left(\mathbf{r}\right)}=\frac{\delta\mu_c(\mathbf{r})}{\delta n_c\left(\mathbf{r}'\right)}=\beta_c^{-1}n_c\left(\mathbf{r}\right)^{-1}\left[\delta\left(\mathbf{r}-\mathbf{r}'\right)-n_c\left(\mathbf{r}\right)c_c^{(2)}\left(\mathbf{r},\mathbf{r}'\mid n\right)\right]. \tag{A–10}$$

Then the chain rule

$$\int d\mathbf{r}''\frac{\delta n_c\left(\mathbf{r}\right)}{\delta\mu_c\left(\mathbf{r}''\right)}\frac{\delta\mu_c(\mathbf{r}'')}{\delta n_c\left(\mathbf{r}'\right)}=\delta\left(\mathbf{r}-\mathbf{r}'\right) \tag{A–11}$$

can be written

$$\int d\mathbf{r}''\left[\delta\left(\mathbf{r}-\mathbf{r}''\right)+n_c\left(\mathbf{r}\right)\left(g_c\left(\mathbf{r},\mathbf{r}''\right)-1\right)\right]\left[\delta\left(\mathbf{r}''-\mathbf{r}'\right)-n_c\left(\mathbf{r}''\right)c_c^{(2)}\left(\mathbf{r}'',\mathbf{r}'\mid n\right)\right]=\delta\left(\mathbf{r}-\mathbf{r}'\right). \tag{A–12}$$

This gives the Ornstein-Zernicke equation, Equation (3–32).

APPENDIX B
INHOMOGENEOUS IDEAL FERMI GAS

The thermodynamic and structural properties of an inhomogeneous ideal Fermi gas are straightforward to calculate in a representation that diagonalizes the effective single particle Hamiltonian

$$\left(\frac{\widehat{p}^2}{2m} - \mu(\widehat{\mathbf{r}})\right)\psi_{\mathsf{k}}(\mathbf{r}) = \epsilon_{\mathsf{k}}\psi_{\mathsf{k}}(\mathbf{r}) \tag{B–1}$$

where $\mathbf{k}$ labels the corresponding quantum numbers. For Fermions with spin s, the quantum numbers are labeled by $\kappa = (s, \mathbf{k})$. The Hamiltonian in second quantized form is then simply

$$H = \sum_{\kappa} \epsilon_{\mathsf{k}} a_{\kappa}^{\dagger} a_{\kappa}, \tag{B–2}$$

where $a_{\kappa}^{\dagger}$, a_{κ} are the creation and annihilation operators for occupation of the states $\{\psi_{\mathsf{k}}\}$. Then the pressure is found directly from evaluation of the grand potential Ω_c

$$\begin{aligned} p(\beta \mid \mu) V &= \sum_{\kappa} \ln\left(1 + e^{-\beta\epsilon_{\mathsf{k}}}\right) = Tr^{(1)} \ln\left(1 + e^{-\beta\left(\frac{\widehat{p}^2}{2m} - \mu(\widehat{\mathbf{r}})\right)}\right) \\ &= (2s+1)\,\beta^{-1} \int d\mathbf{r}\, \langle \mathbf{r}| \ln\left(1 + e^{-\beta\left(\frac{\widehat{p}^2}{2m} - \mu(\widehat{\mathbf{r}})\right)}\right) |\mathbf{r}\rangle \end{aligned} \tag{B–3}$$

where a coordinate representation has been used in the last expression.

The local density and pair correlation function are obtained from the one a two particle density matricies. In the diagonal representation these are

$$\rho^{(1)}(\kappa_1; \kappa_2) = \left\langle a_{\kappa_1}^{\dagger} a_{\kappa_2} \right\rangle = \left\langle a_{\kappa_1}^{\dagger} a_{\kappa_1} \right\rangle \delta_{\kappa_1,\kappa_2} \tag{B–4}$$

$$\rho^{(2)}(\kappa_1, \kappa_2; \kappa_3, \kappa_4) = \left\langle a_{\kappa_1}^{\dagger} a_{\kappa_2}^{\dagger} a_{\kappa_4} a_{\kappa_3} \right\rangle = \left(\delta_{\kappa_1,\kappa_3}\delta_{\kappa_2,\kappa_4} - \delta_{\kappa_1,\kappa_4}\delta_{\kappa_2,\kappa_3}\right) \left\langle a_{\kappa_1}^{\dagger} a_{\kappa_1} \right\rangle \left\langle a_{\kappa_2}^{\dagger} a_{\kappa_2} \right\rangle \tag{B–5}$$

where the mean occupation number is

$$\left\langle a_{\kappa}^{\dagger} a_{\kappa'} \right\rangle = \delta_{\kappa,\kappa'} \left(e^{\beta\epsilon_{\mathsf{k}}} + 1\right)^{-1}. \tag{B–6}$$

The coordinate representations are

$$\rho^{(1)}\left(\mathbf{r},\sigma_1;\mathbf{r}',\sigma_2\right)=\sum_{\mathsf{k}_1,\mathsf{k}_2}\psi^*_{\kappa_1}\left(\mathbf{r}\right)\psi_{\kappa_2}\left(\mathbf{r}'\right)\left\langle a^\dagger_{\kappa_1}a_{\kappa_2}\right\rangle=\delta_{\sigma_1,\sigma_2}\left\langle\mathbf{r}\right|\ln\left(e^{\beta\left(\frac{\hat{\mathbf{p}}^2}{2m}-\mu(\hat{\mathbf{r}})\right)}+1\right)^{-1}\left|\mathbf{r}'\right\rangle$$
$$\equiv\delta_{\sigma_1,\sigma_2}n\left(\mathbf{r},\mathbf{r}'\right) \tag{B–7}$$

$$\rho^{(2)}\left(\mathbf{r}_1,\sigma_1,\mathbf{r}_2,\sigma_2;\mathbf{r}'_1,\sigma_3,\mathbf{r}'_2,\sigma_4\right)=\sum_{\mathsf{k}_1..\mathsf{k}_6}\psi^*_{\kappa_1}\left(\mathbf{r}_1\right)\psi^*_{\kappa_2}\left(\mathbf{r}_2\right)\psi_{\kappa_3}\left(\mathbf{r}'_1\right)\psi_{\kappa_4}\left(\mathbf{r}'_2\right)\left\langle a^\dagger_{\kappa_1}a^\dagger_{\kappa_2}a_{\kappa_4}a_{\kappa_3}\right\rangle$$
$$=\delta_{\sigma_1,\sigma_3}\delta_{\sigma_2,\sigma_4}\sum_{\mathsf{k}_1}\psi^*_{\kappa_1}\left(\mathbf{r}_1\right)\psi_{\kappa_1}\left(\mathbf{r}'_1\right)\left\langle a^\dagger_{\kappa_1}a_{\kappa_1}\right\rangle\sum_{\mathsf{k}_2}\psi^*_{\kappa_2}\left(\mathbf{r}_2\right)\psi_{\kappa_2}\left(\mathbf{r}'_2\right)\times$$
$$\left\langle a^\dagger_{\kappa_2}a_{\kappa_2}\right\rangle-\delta_{\sigma_1,\sigma_4}\delta_{\sigma_2,\sigma_3}\sum_{\mathsf{k}_1}\psi^*_{\kappa_1}\left(\mathbf{r}_1\right)\psi_{\kappa_1}\left(\mathbf{r}'_2\right)\left\langle a^\dagger_{\kappa_1}a_{\kappa_1}\right\rangle\sum_{\mathsf{k}2}\psi^*_{\kappa_2}\left(\mathbf{r}_2\right)\times$$
$$\psi_{\kappa_2}\left(\mathbf{r}'_1\right)\left\langle a^\dagger_{\kappa_2}a_{\kappa_2}\right\rangle \tag{B–8}$$

The diagonal elements are

$$\rho^{(1)}\left(\mathbf{r},\sigma_1;\mathbf{r},\sigma_1\right)=n\left(\mathbf{r},\mathbf{r}\right) \tag{B–9}$$

$$\rho^{(2)}\left(\mathbf{r}_1,\sigma_1,\mathbf{r}_2,\sigma_2;\mathbf{r}_1,\sigma_1,\mathbf{r}_2,\sigma_2\right)=\rho^{(1)}\left(\mathbf{r}_1,\sigma_1;\mathbf{r}_1,\sigma_1\right)\rho^{(1)}\left(\mathbf{r}_2,\sigma_2;\mathbf{r}_2,\sigma_2\right)$$
$$-\delta_{\sigma_1,\sigma_2}\rho^{(1)}\left(\mathbf{r}_1,\sigma_1;\mathbf{r}_2,\sigma_1\right)\rho^{(1)}\left(\mathbf{r}_2,\sigma_2;\mathbf{r}_1,\sigma_2\right) \tag{B–10}$$

Finally, the density and pair correlation function are identified from the summation over spin states

$$n(\mathbf{r})=\sum_{\sigma_1}\rho^{(1)}\left(\mathbf{r},\sigma_1;\mathbf{r},\sigma_1\right)=\left(2s+1\right)n\left(\mathbf{r},\mathbf{r}\right) \tag{B–11}$$

$$n(\mathbf{r}_1)n(\mathbf{r}_2)g\left(\mathbf{r}_1,\mathbf{r}_2\right)=\sum_{\sigma_1,\sigma_2}\rho^{(2)}\left(\mathbf{r}_1,\sigma_1,\mathbf{r}_2,\sigma_2;\mathbf{r}_1,\sigma_1,\mathbf{r}_2,\sigma_2\right)=n(\mathbf{r}_1)n(\mathbf{r}_2)-\left(2s+1\right)n\left(\mathbf{r}_1,\mathbf{r}_2\right)\times$$
$$n\left(\mathbf{r}_2,\mathbf{r}_1\right) \tag{B–12}$$

This gives the results Equations (3–60) and (3–61).

The local density and pair correlation function are determined from the function $n(\mathbf{r},\mathbf{r}')$ obtained from the single particle density matrix from the Equation (B–7),

$$n(\mathbf{r},\mathbf{r}') = \langle \mathbf{r}| \left(e^{\beta\left(\frac{\hat{p}^2}{2m}-\mu(\hat{\mathbf{r}})\right)} + 1 \right)^{-1} |\mathbf{r}'\rangle \,. \tag{B–13}$$

In the local density approximation of the text, $\mu(\hat{\mathbf{r}}) \to \mu(\mathbf{R})$, where $\mathbf{R} = (\mathbf{r}+\mathbf{r}')/2$, this becomes Equation (3–68)

$$n(\mathbf{r},\mathbf{r}') = \frac{1}{h^3}\int d\mathbf{p}\, e^{\frac{i}{\hbar}\mathrm{p}\cdot(\mathrm{r}-\mathrm{r}')} \left(e^{\beta(\frac{p^2}{2m}-\mu(\mathrm{R}))} + 1 \right)^{-1}. \tag{B–14}$$

Further simplification is possible to get

$$n(\mathbf{r},\mathbf{r}')\lambda^3 = \frac{2\lambda}{\pi\,|\mathbf{r}-\mathbf{r}'|}\int_0^\infty dx x \left(z^{-1}(\mathbf{R})e^{x^2} + 1 \right)^{-1} \sin\left(2\sqrt{\pi}x\,|\mathbf{r}-\mathbf{r}'|/\lambda\right), \tag{B–15}$$

with

$$z(\mathbf{R}) = e^{\beta\mu(\mathrm{R})} \tag{B–16}$$

Accordingly the density and pressure simplify to

$$n(\mathbf{r})\lambda^3 = (2s+1)\, n(\mathbf{r},\mathbf{r})\lambda^3 = (2s+1)\, f_{3/2}(z(\mathbf{r})), \tag{B–17}$$

$$\beta p\lambda^3 = \frac{1}{V}\int d\mathbf{r}\,(2s+1)\, f_{5/2}(z(\mathbf{r})), \tag{B–18}$$

with the definitions

$$f_{3/2}(z) = \frac{4}{\sqrt{\pi}}\int_0^\infty dx x^2 \left(z^{-1}e^{x^2} + 1 \right)^{-1}, \quad f_{5/2}(z) = \frac{8}{3\sqrt{\pi}}\int_0^\infty dx x^4 \left(z^{-1}e^{x^2} + 1 \right)^{-1}. \tag{B–19}$$

A fitting function for the density in terms of the local chemical potential is given by

$$f_{3/2}(e^{\nu}) = \left[e^{-\nu} + \epsilon_{1/2}(\nu)\right]^{-1}$$
$$\epsilon_{1/2}(\nu) = 3\sqrt{\frac{\pi}{2}}\left[(\nu + 2.13) + \left(|\nu - 2.13|^{2.4} + 9.6\right)^{5/12}\right]^{-3/2} \quad \text{(B–20)}$$

APPENDIX C
QUANTUM PRESSURE

Here we derive the expression for pressure for an inhomogeneous Fermi gas. We consider a quantum system in a volume V with the interaction potential $\Phi(r)$ and external potential Φ_{ext}.

$$\beta pV = ln\left(Tr(e^{-\beta\widehat{H}})\right) \tag{C–1}$$

where $\widehat{H} = \widehat{K} + \widehat{\Phi} + \widehat{\Phi}_{ext}$

$$\begin{aligned} P &= \frac{1}{\beta}\partial_V\left(ln\left(Tr(e^{-\beta\widehat{H_V}})\right)\right) \\ &= \left\langle \partial_V\widehat{H_V}\right\rangle \end{aligned} \tag{C–2}$$

$$Tr\left(e^{-\beta\widehat{H}}\right) = \int \Pi_i d\mathbf{q}_i^* \left\langle \mathbf{q}_1^*, \mathbf{q}_2^{*}.., \mathbf{q}_N^* | e^{-\beta\widehat{H}}\widehat{S}|\mathbf{q}_1^{*}..\mathbf{q}_N^*\right\rangle \tag{C–3}$$

where we have introduced complete set of kets q_i^* such that $|q_i^*| = 1$. Hence the wavefunctions are independent of the volume of the system.

We can define the hamiltonian in terms of dimensionless momentum and position operators $\widehat{p^*} = V^{1/3}\widehat{p}$ and $\widehat{q^*} = \widehat{q}/V^{1/3}$:

$$\begin{aligned} \widehat{H} &= \sum_i^N \frac{\widehat{p_i}^2}{2m} + \frac{1}{2}\int d\mathbf{r}_1 d\mathbf{r}_2 \Phi(\mathbf{r}_1, \mathbf{r}_2)\widehat{g}(\mathbf{r}_1, \mathbf{r}_2) - \int d\mathbf{r}\mu(\mathbf{r})\widehat{\rho}(\mathbf{r}) \\ &= \frac{1}{V^{2/3}}\sum_i^N \frac{\widehat{p_i^*}^2}{2m} + \frac{1}{2}\int d\mathbf{q}_1^* d\mathbf{q}_2^* \Phi(\mathbf{q}_1^* V^{1/3}, \mathbf{q}_2^* V^{1/3})\widehat{g}(\mathbf{q}_1^*, \mathbf{q}_2^*) - \int d\mathbf{q}^*\mu(\mathbf{q}^* V^{1/3})\widehat{\rho}(\mathbf{q}^*) \end{aligned} \tag{C–4}$$

where $\mathbf{r}_i = V^{1/3}\mathbf{q}_i^*$.

$$e^{-\beta\widehat{H}_{V+\Delta V}} = e^{-\beta\widehat{H_V}} - \Delta V \int_0^\beta d\beta' e^{-(\beta-\beta')\widehat{H_V}} \partial_V \widehat{H_V} e^{-\beta'\widehat{H_V}} + O(\Delta^2 V) \tag{C–5}$$

Using this we can prove:

$$\partial_V Tr\left(e^{-\beta\widehat{H_V}}\right) = \left\langle \partial_V \widehat{H_V} \right\rangle \tag{C–6}$$

$$\partial_V \widehat{H_V} = -\frac{2}{3V}\sum_i^N \frac{\widehat{p_i}^2}{2m} + \frac{1}{3V}\int d\mathbf{r}_1 d\mathbf{r}_2 r_1 \partial_{r_1}\Phi(\mathbf{r}_1,\mathbf{r}_2)\widehat{g}(\mathbf{r}_1,\mathbf{r}_2) - \frac{1}{3V}\int d\mathbf{r} r \partial_r \mu(\mathbf{r})\widehat{\rho}(\mathbf{r}) \ , \tag{C–7}$$

$$\beta p = -\frac{2\bar{n}}{3}\left\langle \frac{\widehat{p_i}^2}{2m} \right\rangle + \frac{1}{3V}\int d\mathbf{r}_1 d\mathbf{r}_2 r_1 \partial_{r_1}\Phi(\mathbf{r}_1,\mathbf{r}_2) n(\mathbf{r}_1) n(\mathbf{r}_2) g(\mathbf{r}_1,\mathbf{r}_2) - \frac{1}{3V}\int d\mathbf{r} r \partial_r \mu(\mathbf{r}) n(\mathbf{r}) \ , \tag{C–8}$$

APPENDIX D
STATIC STRUCTURE FACTOR IN RPA

There are two equivalent representations of the RPA static structure factor as given in references [1]:

$$S^{RPA}(k) = -\frac{\hbar}{n}\int \frac{d\omega}{\pi}\frac{1}{1-e^{-\beta\hbar\omega}}\mathcal{I}\chi(\omega, k) \tag{D–1}$$

where $\chi(\omega, k) = \frac{1}{V(k)(1-V(k)\chi^{(0)}(\omega,k))}$ and $V(k) = \frac{4\pi e^2}{k^2}$. The $\chi^{(0)}(\omega, k)$ is the non-interacting response:

$$\chi^{(0)}(\omega, k) = lim_{\eta\to 0}\frac{(2s+1)\beta}{4\sqrt{\pi}\lambda^3\kappa}\int_{-\infty}^{\infty} dx ln(1+ze^{-x^2})\left(\frac{1}{\nu-x-\kappa+i\eta}-\frac{1}{\nu-x+\kappa+i\eta}\right) \tag{D–2}$$

where $\kappa = \frac{q\lambda}{4\sqrt{\pi}}$ and $\nu = \frac{\beta\hbar\omega}{4\kappa}$.

Another representation of the RPA static structure factor follows from converting the frequency integral in the above equation to a sum of discrete frequencies [39].

$$S^{RPA}(x = k/k_F) = \frac{3}{2}\theta\sum_{l=-\infty}^{l=\infty}\frac{\Phi(x, l)}{1+(2\Gamma\theta/\pi\lambda x^2)\Phi(x, l)} \tag{D–3}$$

where

$$\Phi(x, l) = \frac{1}{2x}\int_0^{\infty} dy\frac{y}{exp[(y^2/\theta)-\alpha]+1} ln\left|\frac{(2\pi l\theta)^2+(x^2+2xy)^2}{(2\pi l\theta)^2+(x^2-2xy)^2}\right| \tag{D–4}$$

The constant α is determined from the normalization conditions. $I_{1/2}(\alpha) = \frac{2}{3}\theta^{-3/2}$ with $I_\nu(\alpha) = \int_0^{\infty} dt\frac{t^\nu}{exp(t-\alpha)+1}$.

To prove that the RPA structure factor satisfies the exact screening sum rule, we look at $S^{RPA}(k)$ for small values of k. The integrand in Equation (D–1) for small k values becomes sharply peaked around two specific frequencies $\pm\nu_p$ [1]. We will try to find out the functional form of the integrand around those frequencies and do the frequency integral to prove the sum rule. For small k, the integrand is sharply peaked because the

denominator of χ in Equation (D–1), $\epsilon(\kappa,\nu) = (1 - V(k)\chi^{(0)}(\omega,k))$ becomes very small. These frequencies are actually the zeros of the real part of $\epsilon(\kappa,\pm\nu_p) = 0$. The reason is that since the imaginary part of ϵ is a fast decaying function, if the real part is zero the denominator becomes small.

$$\begin{aligned}
&\Re\epsilon(\kappa,\pm\nu_p) = 0 \Rightarrow 1 - \frac{\beta V(k)(2s+1)}{\lambda^3}\Re\chi^{(0)^*}(k,\nu_p) = 0 \\
&\Im\epsilon(\kappa,\pm\nu_p) = \eta
\end{aligned} \tag{D–5}$$

For small k values some simplifications can be made to the functional form of $\chi^{(0)}$

$$\begin{aligned}
lim_{\kappa\to 0}\chi^{(0)}(\kappa,\nu) &\approx -\frac{1}{2\sqrt{\pi}}\int dx ln(1+ze^{-x^2})\left(\frac{1}{(\nu-x)^2+i\eta}\right) \\
\Re\chi^{(0)}(\kappa,\nu) &\approx -\frac{1}{\sqrt{\pi}}\mathcal{P}\int dx ln(1+ze^{-x^2})\frac{1}{(\nu-x)^2} \\
\Im\chi^{(0)}(\kappa,\nu) &\approx \sqrt{\pi}\nu n_\nu
\end{aligned} \tag{D–6}$$

$$\tag{D–7}$$

We can expand $\epsilon(\kappa,\nu)$ about ν_p

$$\begin{aligned}
\epsilon(\kappa,\nu) &\approx \epsilon(\kappa,\nu_p) + \frac{\partial}{\partial\nu}\epsilon|_{\nu=\nu_p}(\nu-\nu_p) + \mathcal{O}((\nu-\nu_p)^2) \\
&= i\eta - \frac{\beta V(k)(2s+1)}{\lambda^3}\frac{\partial}{\partial\nu}\Re\chi^{(0)}(k,\nu_p)(\nu-\nu_p) \\
\frac{\partial}{\partial\nu}\Re\chi^{(0)}(k,\nu_p) &\approx \frac{2}{\sqrt{\pi}}\mathcal{P}\int dx\frac{ln(1+ze^{-x^2})}{(\nu_p-x)^3} \\
&\approx \frac{2}{\nu_p\sqrt{\pi}}\mathcal{P}\int dx\frac{ln(1+ze^{-x^2})}{(\nu_p-x)^2} + \frac{2}{\nu_p\sqrt{\pi}}\mathcal{P}\int dx\frac{xln(1+ze^{-x^2})}{(\nu_p-x)^3} \\
&= \frac{2\Re\chi(\kappa,\nu_p)}{\nu_p} + \mathcal{O}(\frac{1}{\nu_p^4}) \\
\frac{\beta V(k)(2s+1)}{\lambda^3}\frac{\partial}{\partial\nu}\Re\chi^{(0)}(k,\nu_p) &= \frac{\partial}{\partial\nu}\epsilon|_{\nu=\nu_p} \approx \frac{2}{\nu_p} \\
\epsilon(\kappa,\nu) &\approx \frac{2}{\nu_p}(i\eta + (\nu-\nu_p))
\end{aligned} \tag{D–8}$$

$$\tag{D–9}$$

For small k values the main contribution to the integrand in equation (D–1) comes from around the peaks around $\pm\nu_p$

$$\begin{aligned} S^{RPA}(k) &= -\frac{4\kappa}{n\beta V(k)}\int_{-\infty}^{\infty}\frac{d\nu}{\pi}\frac{1}{1-e^{-4\kappa\nu}}\Im(\frac{1}{\epsilon(\kappa,\nu)}) \\ &= -\frac{4\kappa}{n\beta V(k)}\int_{\nu_p-\epsilon}^{\nu_p+\epsilon}\frac{d\nu}{\pi}\frac{1}{1-e^{-4\kappa\nu}}\Im(\frac{1}{\epsilon(\kappa,\nu)}) \\ &\quad -\frac{4\kappa}{n\beta V(k)}\int_{-\nu_p+\epsilon}^{\nu_p-\epsilon}\frac{d\nu}{\pi}\frac{1}{1-e^{-4\kappa\nu}}\Im(\frac{1}{\epsilon(\kappa,\nu)}) \end{aligned} \tag{D–10}$$

Lets look at the integral around the peak around ν_p.

$$\begin{aligned} S(k) &= -\frac{4\kappa}{n\beta V(k)}\int_{\nu_p-\epsilon}^{\nu_p+\epsilon}\frac{d\nu}{\pi}\frac{1}{1-e^{-4\kappa\nu}}\Im\left(\frac{1}{\epsilon(\kappa,\nu)}\right) \\ &= \frac{2\kappa}{n\beta V(k)}\int_{\nu_p-\epsilon}^{\nu_p+\epsilon}\frac{d\nu}{\pi}\frac{1}{1-e^{-4\kappa\nu}}\nu_p\delta(\nu-\nu_p) \\ &= \frac{2}{n\beta V(k)}\frac{\kappa\nu_p}{1-e^{-4\kappa\nu_p}} \end{aligned} \tag{D–11}$$

(D–12)

Similarly we get contribution from another peak at $-\nu_p$ by replacing $\nu_p \rightarrow -\nu_p$ and adding the two we get:

$$\begin{aligned} \text{S(k).around.peaks} &= \frac{2}{n\beta V(k)}\frac{\kappa\nu_p}{1-e^{-4\kappa\nu_p}} - \frac{2}{n\beta V(k)}\frac{\kappa\nu_p}{1-e^{4\kappa\nu_p}} \\ &= \frac{1}{n\beta V(k)}2\kappa\nu_p coth(2\kappa\nu_p) \end{aligned} \tag{D–13}$$

The exact screening sum rule:

$$\begin{aligned} \beta n\int d\mathbf{r}\,d\mathbf{r}'\frac{S(\mathbf{r}|\mathbf{r}')}{|\mathbf{r}|} &= \frac{\hbar\beta\Omega_p}{2}coth(\frac{\hbar\beta\Omega_p}{2}) \\ \beta V(\mathbf{k})nS(\mathbf{k}) &= 2\kappa\nu_p coth(2\kappa\nu_p) \end{aligned} \tag{D–14}$$

where the definition of dimensionless frequency : $\nu_p = \beta\hbar\omega_p/(4\kappa)$ has been used above.

To prove at high temperature $t >> 1$ the structure factor goes to the Debye limit, we define $\alpha_0 = \frac{\alpha}{2\sqrt{t}}$ and then take limit $\alpha_0 \rightarrow 0$ for $\chi^{(0)}$. We change the momentum scaling

from $\kappa = \frac{\lambda k}{4\sqrt{\pi}}$ to $k^* = kr_s$ and redefine the dimensionless frequency as $\nu = \frac{\beta\hbar\omega}{4k^*}$ in $\chi^{(0)}$

$$\chi^{(0)^*}(\kappa,\nu) = -\frac{1}{4\sqrt{\pi}\kappa}\int dx ln(1+ze^{-x^2})\left(\frac{1}{\nu-(x-\kappa)+i\eta}-\frac{1}{\nu-(x+\kappa)+i\eta}\right)$$
$$\chi^{(0)^*}(k^*\alpha_0,\nu'/\alpha_0) = -\frac{1}{4\sqrt{\pi}k^*\alpha_0}\int dx ln(1+ze^{-x^2})\times$$
$$\left(\frac{1}{\nu/\alpha_0-(x-k^*\alpha_0)+i\eta}-\frac{1}{\nu/\alpha_0-(x+k^*\alpha_0)+i\eta}\right) \tag{D–15}$$

The susceptibility can be expressed in terms of the dimensionless susceptibility as shown below

$$\chi^{(0)}(k,\omega) = \frac{\beta(2s+1)}{\lambda^3}\chi^{(0)^*}(k^*\alpha_0,\nu/\alpha_0) \tag{D–16}$$

In the high temperature limit $z << 1$, hence the dimensionless susceptibility in Equation (D–15) can be written as

$$\begin{aligned} lim_{\alpha_0\to 0}\chi^{(0)}(k^*\alpha_0,\nu/\alpha_0) &= -\frac{1}{2\sqrt{\pi}}\int dx z e^{-x^2}\left(\frac{1}{(\nu/\alpha_0-x)^2+i\eta}\right) = \frac{z}{\sqrt{\pi}}\int dx x e^{-x^2}\left(\frac{1}{\nu/\alpha_0-x+i\eta}\right) \\ &= \frac{z}{\sqrt{\pi}}\mathcal{P}\int dx x e^{-x^2}\left(\frac{1}{\nu/\alpha_0-x}\right) - iz\sqrt{\pi}\nu/\alpha_0 e^{-(\nu/\alpha_0)^2} \\ &= -zG(\nu/\alpha_0) - iz\sqrt{\pi}\nu/\alpha_0 e^{-(\nu/\alpha_0)^2} \end{aligned} \tag{D–17}$$

The RPA structure factor (D–1) in this limit becomes

$$\begin{aligned} S^{RPA}(k^*) &= -\frac{4k^{*3}}{3\pi\Gamma}\int d\nu \frac{1}{1-e^{-4k^*\nu}}\Im\chi^*(k^*\alpha_0,\nu/\alpha_0) \\ &= -\frac{4k^{*3}\alpha_0}{3\pi\Gamma}\int d\nu \frac{1}{1-e^{-4k^*\alpha_0\nu}}\Im\chi^*(k^*\alpha_0,\nu) \\ &\approx -\frac{k^{*2}}{3\pi\Gamma}\int d\nu \frac{1}{\nu}\Im\chi^*(k^*\alpha_0,\nu) \\ &= -\frac{k^{*2}}{3\pi\Gamma}\int d\nu \frac{1}{\nu}\Im\left(\frac{1}{1+\frac{3\Gamma}{k^{*2}}G(\nu)+i\frac{3\Gamma}{k^{*2}}\sqrt{\pi}\nu e^{-\nu^2}}\right) \\ &= -\frac{k^{*2}}{3\pi\Gamma}\Re\left(\frac{1}{1+\frac{3\Gamma}{k^{*2}}G(0)}-1\right) \\ &= \frac{k^{*2}}{k^{*2}+3\Gamma} \end{aligned} \tag{D–18}$$

where the Kramer-Kronig equations [51], $z \approx \frac{n\lambda^3}{2s+1}$ and $G(0) = 1$ have been used in the last equation.

Here we show that at large k the RPA structure factor behaves like k^{-4} [57]. At this limit $V(k)$ is small, and we can expand in powers of $V(k)$:

$$
\begin{aligned}
S^{RPA}(k) &= -\frac{\hbar}{n}\int_{-\infty}^{\infty}\frac{d\omega}{\pi(1-e^{-\beta\hbar\omega})V(k)}Im\left(\frac{1}{1-V(k)(2s+1)\chi^{(0)}(k,\omega)}\right)\\
&= -\frac{\hbar}{n}\int_{-\infty}^{\infty}\frac{d\omega}{\pi(1-e^{-\beta\hbar\omega})}Im\left((2s+1)\chi^{(0)}(k,\omega)+V(k)(2s+1)^2{\chi^{(0)}}^2(k,\omega)+..\right)\\
&\approx 1-\frac{\hbar}{n}V(k)(2s+1)^2\int_{-\infty}^{\infty}\frac{d\omega}{\pi(1-e^{-\beta\hbar\omega})}\Im(\chi^{(0)}(k,\omega))^2\\
&\approx 1-\frac{\hbar}{n}V(k)(2s+1)^2\frac{4\kappa}{\beta\hbar}\int_{-\infty}^{\infty}\frac{d\nu}{\pi(1-e^{-4\nu\kappa})}\Im(\chi^{(0)}(\kappa,\nu))^2\\
&\approx 1-\frac{1}{n}V(k)(2s+1)^2\frac{1}{\beta}\int_{-\infty}^{\infty}\frac{d\nu}{\pi\nu}\Im(\chi^{(0)}(\kappa,\nu))^2\\
&\approx 1-\frac{1}{n}V(k)(2s+1)^2\frac{1}{\beta}\Re(\chi^{(0)}(\kappa,0))^2\\
&= 1-\frac{1}{n}V(k)(2s+1)^2\frac{1}{\beta}(\Re\chi^{(0)}(\kappa,0))^2\\
Re\chi^*(\kappa,0,z) &= -\frac{1}{2\sqrt{\pi}\kappa}g(\kappa) = -\frac{1}{2\sqrt{\pi}\kappa}P(\int_{-\infty}^{\infty}dx\frac{ln(1+ze^{-x^2})}{\kappa-x}\\
&= \frac{1}{2\sqrt{\pi}\kappa}P(\int_{-\infty}^{\infty}dx\frac{ln(1+ze^{-x^2})}{x}-\frac{1}{2\sqrt{\pi}}P(\int_{-\infty}^{\infty}dx\frac{ln(1+ze^{-x^2})}{\kappa-x}\\
&\sim \frac{f_{3/2}(z)}{4\kappa}\\
S^{RPA}(\kappa) &\sim 1-\frac{\Gamma(2s+1)^2f_{3/2}^2(z)}{4^3n\lambda^3}\frac{1}{\kappa^4}
\end{aligned}
\tag{D–19}
$$

Again the Kramers-Kronig relations has been used.

APPENDIX E
PROPERTIES OF EFFECTIVE INTERACTION POTENTIAL FOR RPA SYSTEMS

The integral representation of the RPA structure factor will be used in this section to prove that at very low densities and high temperatures, Δ in Equation (4–10) would look like a Kelbg potential. In this limit the fugacity, z, is very small, $z << 1$. Thus we can expand the response function, Equation (D–1), in powers of z.

$$\begin{aligned}
S^{RPA}(k) &= -\frac{\hbar}{n}\int_{-\infty}^{\infty}\frac{d\omega}{\pi(1-e^{-\beta\hbar\omega})V(k)}Im\left(\frac{1}{1-V(k)(2s+1)\chi^{(0)}(k,\omega)}\right)\\
&= -\frac{\hbar}{n}\int_{-\infty}^{\infty}\frac{d\omega}{\pi(1-e^{-\beta\hbar\omega})}Im\left((2s+1)\chi^{(0)}(k,\omega)+V(k)(2s+1)^2{\chi^{(0)}}^2(k,\omega)+..\right)\\
&= S^{(0)}(k)-\frac{\hbar}{n}V(k)(2s+1)^2\int_{-\infty}^{\infty}\frac{d\omega}{\pi(1-e^{-\beta\hbar\omega})}Im(\chi^{(0)}(k,\omega))^2\\
&= S^{(0)}(k)-\frac{2\hbar}{n}V(k)(2s+1)^2\int_{-\infty}^{\infty}\frac{d\omega}{\pi(1-e^{-\beta\hbar\omega})}Im\chi^{(0)}(k,\omega)Re\chi^{(0)}(k,\omega)\\
&= S^{(0)}(k)+\beta V(k)f(k) \qquad \text{(E–1)}
\end{aligned}$$

where $f(k) = -\frac{2\hbar}{\beta n}(2s+1)^2\int_{-\infty}^{\infty}\frac{d\omega}{\pi(1-e^{-\beta\hbar\omega})}Im\chi^{(0)}(k,\omega)Re\chi^{(0)}(k,\omega)$. The expression for f can be simplified:

$$\begin{aligned}
f(\kappa) &= -\frac{2\hbar}{\beta n}(2s+1)^2\frac{4\kappa}{\beta\hbar}\frac{\beta^2}{\lambda^6}\int_{-\infty}^{\infty}\frac{d\nu}{\pi(1-e^{-4\kappa\nu})}Im\chi^{(0)}(\kappa,\nu)Re\chi^{(0)}(\kappa,\nu)\\
&= \frac{2\hbar}{\beta n}(2s+1)^2\frac{4\kappa}{\beta\hbar}\frac{\beta^2}{\lambda^6}\int_{-\infty}^{\infty}\frac{d\nu}{\pi(1-e^{-4\kappa\nu})}\frac{1}{4\sqrt{\pi}\kappa}z(e^{-(\nu+\kappa)^2}-e^{-(\nu-\kappa)^2}) \qquad \text{(E–2)}\\
&\times\frac{\sqrt{\pi}}{4\kappa}z(g(\kappa+\nu)-g(\kappa-\nu))\\
&= \frac{n}{2\pi\kappa}(2s+1)^2\int_{-\infty}^{\infty}\frac{d\nu}{\pi}e^{-(\kappa-\nu)^2}(g(\nu+\kappa)-g(\nu-\kappa))
\end{aligned}$$

(E–3)

$$\begin{aligned}\widetilde{\Delta}(\kappa) &= \frac{S^{RPA}(\kappa)}{S^{RPA}(\kappa)-1} - \frac{S^{(0)}(\kappa)}{S^{(0)}(\kappa)-1} \\ &= \frac{S^{(0)}(\kappa)+\beta V(\kappa)f(\kappa)-1}{S^{(0)}(\kappa)+\beta V(\kappa)f(\kappa)} - \frac{S^{(0)}(\kappa)}{S^{(0)}(\kappa)-1} \\ &\approx \frac{\beta V(\kappa)f(\kappa)}{S^{(0)}(\kappa)} \\ &= \frac{\beta V(\kappa)f(\kappa)}{(S^{(0)})^2(\kappa)}\end{aligned} \tag{E–4}$$

since $S^{(0)}(\kappa) = 1 + n\lambda^3 h^*(\kappa) \approx 1 + \mathcal{O}(z)$. Hence:

$$\widetilde{\Delta}(\kappa) = \beta V(\kappa) f(\kappa) \tag{E–5}$$

$$\begin{aligned}f(\kappa)\kappa &\sim \int_{-\infty}^{\infty} d\nu e^{-\nu^2}(g(\nu+2\kappa)-g(\nu)) \\ &= \int_{-\infty}^{\infty} \frac{d\nu}{\pi} e^{-\nu^2} Re \int_{-\infty}^{\infty} e^{-x^2}\left(\frac{1}{\nu+2\kappa-x+i\eta} - \frac{1}{\nu-x+i\eta}\right) \\ &= \int_{-\infty}^{\infty} d\nu e^{-\nu^2} Re \int_{-\infty}^{\infty} e^{-(x+\nu)^2}\left(\frac{1}{2\kappa-x+i\eta} - \frac{1}{0-x+i\eta}\right) \\ &= \int_{-\infty}^{\infty} dx e^{-x^2/2} Re \int_{-\infty}^{\infty} d\nu e^{-(x/2+\nu)^2}\left(\frac{1}{2\kappa-x+i\eta} - \frac{1}{0-x+i\eta}\right) \\ &= \int_{-\infty}^{\infty} dx e^{-x^2/2} \frac{\sqrt{\pi}}{\sqrt{2}} Re\left(\frac{1}{2\kappa-x+i\eta} - \frac{1}{0-x+i\eta}\right) \\ &= \sqrt{\frac{\pi}{2}}\left(g(\sqrt{2}\kappa)-g(0)\right) \\ &= \sqrt{\frac{\pi}{2}} g(\sqrt{2}\kappa)\end{aligned} \tag{E–6}$$

Hence we have from Equation (E–5):

$$\begin{aligned}\widetilde{\Delta}(\kappa) &= \beta V(\kappa) f(\kappa) \\ &\sim \frac{g(\sqrt{2}\kappa)}{\kappa^3}\end{aligned} \tag{E–7}$$

which can be shown to be the Fourier transform of the Kelbg potential $\triangle_K(x) = \frac{1}{x}(1 - exp(-x^2/\lambda_K^2) + \sqrt{\pi}x/\lambda_K(1 - erf(x/\lambda_K)))$. Hence we have proved that at high temperatures and low densities, Δ behaves like a Kelbg potential.

In this section, we will show that the effective interaction potential has a Coulomb tail and how it follows from the perfect screening sum rule. We are going to use an important fact: the large distance behavior of a function is governed by the small momentum behavior of its Fourier transform. From Equation (4–10):

$$\widetilde{\Delta(k)} = \frac{1}{n}\left(\frac{1}{S^{RPA}(k)} - \frac{1}{S^{(0)}(k)}\right) \tag{E–8}$$

In the small k limit $S(k) = \frac{\hbar k^2}{2m\omega_p} coth(\beta\hbar\omega_p/2)$, where ω_p is the plasma frequency. But $S^{(0)}(k)$ goes to a finite number. Thus $\frac{1}{S^{RPA}(k)} >> \frac{1}{S^{(0)}(k)}$ for small k values. Hence:

$$\widetilde{\Delta}(k) \approx \frac{2m\omega_p}{n\hbar k^2 coth(\beta\hbar\omega_p/2)} \tag{E–9}$$

Writing $\widetilde{\Delta}(k) = \frac{4\pi r_0 \Gamma_{eff}}{k^2}$, we get as was to be proved in Equation (4–12):

$$\begin{aligned} \Gamma_{eff} &= \frac{2}{\beta\hbar\omega_p coth(\beta\hbar\omega/2)}\Gamma \\ \Gamma &= \frac{\beta q^2}{r_0} \end{aligned} \tag{E–10}$$

APPENDIX F
IDEAL FERMI GAS IN A HARMONIC TRAP

Here we derive the LDA form Equation (3–67) of the density profile for the ideal Fermi gas in a harmonic trap at zero temperature.

$$
\begin{aligned}
n^{(0)}(\mathbf{x})r_0^3 &= \frac{1}{(2\pi)^3}\int d\mathbf{k}^* \frac{1}{exp(\frac{\beta q^2 a_0 (k^*)^2}{2r_0^2} + \frac{1}{2}\beta\frac{q^2}{r_0}x^2)/z + 1} \\
&= \frac{1}{(2\pi)^3}\int d\mathbf{k}^* \Theta\left(\frac{(k^*)^2}{2r_s^2} + \frac{1}{2r_s}x^2 - \epsilon_F\right) \\
&= \frac{1}{2\pi^2}\int dk^* k^{*2} \Theta\left(\frac{(k^*)^2}{2r_s^2} + \frac{1}{2r_s}x^2 - \epsilon_F\right) \\
&= \frac{\sqrt{2}r_s^3}{3\pi^2}(\epsilon_F - \frac{x^2}{2r_s})^{3/4} \qquad \text{(F–1)}
\end{aligned}
$$

(F–2)

The parameter ϵ_F is obtained by integrating the density in Equation (F–1) to get the total number of particles in the trap.

$$
\begin{aligned}
f_{3/2}(\nu) &= \frac{4}{3\sqrt{\pi}}\nu^{3/2} \\
n^{(0)}(r) &= 2\lambda^{-3} f_{3/2}(exp(\beta\mu^{(0)}(r))) \approx \frac{8}{3\sqrt{\pi}}\frac{(\beta\mu^{(0)}(r))^3}{\lambda^3} \\
\int n^{(0)}(r)d\mathbf{r} &= N \\
\Rightarrow N &= \frac{16}{3\sqrt{2}}(\frac{m\omega}{\hbar})^3 \int_0^{\epsilon_F} (\epsilon_F/(m\omega^2) - r^2)^{3/2} r^2 dr \\
\Rightarrow \epsilon_F &= \hbar\omega\left(\frac{3N}{\pi}\right)^{1/3} \qquad \text{(F–3)}
\end{aligned}
$$

The exact equation for density for a non-interacting Fermi system is given in terms of the single particle wave functions by

$$\begin{aligned} n(\mathbf{r}) &= \langle \sum_i \delta(q_i - \mathbf{r}) \rangle = \sum_{\epsilon,\epsilon'} \langle \epsilon' | \delta(\widehat{q} - r) | \epsilon \rangle \langle a^+_{\epsilon'} a_\epsilon \rangle \\ &= \sum_{\epsilon,\epsilon'} \int d\mathbf{r}' \langle \epsilon' | \mathbf{r}' \rangle \delta(\mathbf{r}' - \mathbf{r}) \langle \mathbf{r}' | \epsilon \rangle \langle a^+_\epsilon a_\epsilon \rangle \delta_{\epsilon,\epsilon'} \\ &= \sum_\epsilon |\psi_\epsilon(\mathbf{r})|^2 n_\epsilon \end{aligned} \tag{F–4}$$

(F–5)

where ψ is the single particle non-interacting wave function and n_ϵ is the Fermi distribution with energy ϵ. At T=0, the density equation becomes:

$$n(r) = \sum_{klm} \sqrt{\frac{2\nu^3}{\pi}} \frac{2^{k+2l+3} k! \nu^l r^{2l} e^{-2\nu r^2}}{(2k+2l+1)!!} (L_k^{(l+1/2)}(2\nu r^2))^2 Y_{lm}^2(\theta, \phi) \ , \tag{F–6}$$

where $\nu = \frac{m\omega^2}{2\hbar}$. Using the force balance condition we get an equality $2\nu r_0^2 = \sqrt{r_s}$. Hence in terms of dimensionless distance $x = r/r_0$, the density equation becomes

$$\begin{aligned} n(r) = \sum_{klm,k'l'm'} \sqrt{\frac{r_s^{3/2}}{\pi}} \sqrt{\frac{2^{k+l+2} k! r_s^{l/2} x^{2l} e^{-\sqrt{r_s}x^2}}{(2k+2l+1)!!}} \sqrt{\frac{2^{k'+l'+2} k'! r_s^{l'/2} x^{2l'} e^{-\sqrt{r_s}x^2}}{(2k'+2l'+1)!!}} L_k^{(l+1/2)}(\sqrt{r_s}x^2) \times \\ L_{k'}^{(l'+1/2)}(\sqrt{r_s}x^2) Y_{lm}(\theta, \phi) Y_{l'm'}(\theta, \phi) \end{aligned} \tag{F–7}$$

If the angular symmetry is not broken, the angular integrals can be performed:

$$\begin{aligned} n(r) &= \sum_{klm} \sqrt{\frac{r_s^{3/2}}{\pi}} \frac{2^{k+l+2} k! r_s^{l/2} x^{2l} e^{-\sqrt{r_s}x^2}}{(2k+2l+1)!!} (L_k^{(l+1/2)}(\sqrt{r_s}x^2))^2 \\ &= \sum_{kl} \sqrt{\frac{r_s^{3/2}}{\pi}} \frac{2^{k+l+2} k! r_s^{l/2} x^{2l} e^{-\sqrt{r_s}x^2}}{(2k+2l+1)!!} (2l+1)(L_k^{(l+1/2)}(\sqrt{r_s}x^2))^2 \\ &= \sum_{nl} \sqrt{\frac{r_s^{3/2}}{\pi}} \frac{2^{n/2+l/2+2} (n/2-1/2)! r_s^{l/2} x^{2l} e^{-\sqrt{r_s}x^2}}{(n+l+1)!!} (2l+1)(L_{n/2-1/2}^{(l+1/2)}(\sqrt{r_s}x^2))^2 \end{aligned} \tag{F–8}$$

In the above equation we replace quantum number k by the quantum number n by the relationship $2k = n - l$. To figure out what values of (n, l) to sum over, we consider the case of $N = 100$ particles and try to figure out how many of these (n, l) are filled up. Due to spin degeneracy we need to consider $N/2 = 50$ particles filling up the states. The constraints on l and m are: $-m \leq l \leq m$ and $l = 0, 2, .., n-2, n$ for n even and $l = 1, 3, .., n-2, n$. The degeneracy calculation gives : $n = 0, 1, ..4$ are completely filled and the rest of the 15 electrons fill up the following quantum numbers $(k = (n-l)/2, l) \rightarrow (1, 3), (2, 1)$ in the $n = 5$ level.

The Fermi energy in this case is the energy of the highest electron:$\epsilon_F = \hbar\omega(n + 3/2) = \hbar\omega(5 + 3/2) = \hbar\omega 6.5$. This is higher than predicted by the LDA in Equation (F–3). The number of particles the shell with quantum number n can hold is $\frac{(n+1)(n+2)}{2}$. Hence if shells till $n0$ are completely filled, then the total number of particles in the system is $\sum_{n=0}^{n0} \frac{(n+1)(n+2)}{2} = \frac{1}{6}(n_0 + 1)(n_0 + 2)(n_0 + 3)$. If we have N particles in the system, then for large number of particles:$n_0 \approx (6N)^{1/3}$. Hence the Fermi energy for large non-interacting system is $\epsilon_F \approx \hbar\omega(6N)^{1/3}$. LDA in Equation (F–3): $\epsilon_F = (\frac{3N}{\pi})^{1/3}\hbar\omega$ underestimates the Fermi energy.

REFERENCES

[1] G. Giuliani and G. Vignale, *Quantum Theory of the Electron Liquid*, (Cambridge U. Press, Cambridge, 2005).

[2] L. D. Landau, Theory of the Fermi liquid, Soviet Physics JETP **3**, 920925, (1957).

[3] L. D. Landau, On the theory of the Fermi liquid, Sov. Phys. JETP **8**, 7074, (1959).

[4] P. Hohenberg and W. Kohn, Phys. Rev. **136**, B864 (1964)

[5] W. Kohn, L. J. Sham, Phys. Rev. **140**, A1133 (1965).

[6] N. D. Mermin, Phys. Rev. **137**, A1441 (1965).

[7] C. Jones and M. Murillo, High Energy Density Physics **3**, 379 (2007).

[8] F. Graziani et al, High Energy Density Physics **8**,105 (2012).

[9] R. Rozner, D. Hammer, and T. Rothman *Basic Research Needs in High Energy Density Laboratory Physics*, (U.S. Dept. of Energy, 2010), Chapter 6 and references therein.

[10] R.P. Drake,"High Energy Density Physics", Phys. Today 63, 28-33 (2010) and refs. therein.

[11] E. Brown, B. Clark, J. DuBois, D. Ceperley, *Path Integral Monte Carlo Simulation of the Warm-Dense Homogeneous Electron Gas* , cond mat arXiv:1211.6130, 2012.

[12] Richard W. Lee, presentation *Plasma and warm dense matter studies*, LCLS Stanford.

[13] K. Singwi, A. Sjolander, M. Tosi, and R. Land, Phys. Rev. **B1**, 1044 (1970).

[14] A. Georges, G. Kotliar, W. Krauth and M. Rozenberg, Rev. Mod. Phys. **68**, 13 (1996).

[15] A. Georges and G.Kotliar, Phys. Rev. B **45**, 6479 (1992).

[16] W. Metzner and D. Vollhardt Phys. Rev. Lett. **62**, 324 (1989).

[17] G. Kotliar, S. Y. Savrasov, K. Haule, V. S. Oudovenko, O. Parcollet, and C. A. Marianetti, Rev. Mod. Phys. **78**, 865 (2006).

[18] P.W. Anderson, Phys. Rev. **124**, 41 (1961).

[19] G.E. Uhlenbeck, L. Gropper, Phys. Rev. **41** (1932) 79.

[20] G. Kelbg, Ann. Phys. **12**, 219 (1963).

[21] C. Deutsch, Phys. Lett. A **60,** 317 (1977).

[22] H. Minoo, M. Gombert, and C. Deutsch, Phys. Rev. A **23**, 924 (1981).

[23] T. Dunn and A. Broyles, Phys. Rev. **157**, 1 (1967).

[24] F. Lado, J. Chem. Phys. **47**, 5369 (1967).

[25] M.A. Pokrant, J. Chem. Phys. 62 (1975) 4959.

[26] T. Morita, Prog. Theor. Phys. **20**, 920 (1958); **23**, 829 (1960).

[27] For additional early references see W. Ebeling, A. Filinov, M. Bonitz, V. Filinov, and T. Pohl, J. Phys. A **39**, 4309 (2006).

[28] A. Filinov, V. Golubnychiy, M. Bonitz, W. Ebeling, and J. Dufty, Phys. Rev. E **70,** 046411 (2004).

[29] M. W. C. Dharma-wardana, Int. J. Quant. Chem. **112**, **53** (2012).

[30] J. Dufty, S. Dutta, M. Bonitz, and A. Filinov, Int. J. Quant. Chem. **109**, 3082 (2009).

[31] J. W. Dufty and S. Dutta, Contrib. Plasma Phys. **52**, 100 (2012).

[32] J-P Hansen and I. MacDonald, *Theory of Simple Liquids*, (Academic Press, San Diego, CA, 1990).

[33] M. W. C. Dharma-wardana and F. Perrot, Phys. Rev. Lett. **84**, 959 (2000).

[34] F. Perrot and M. W. C. Dharma-wardana, Phys. Rev. B **62**, 16536 (2000).

[35] J. Dufty and S. Dutta, *Classical Representation of a Quantum System at Equilibrium: Theory* , (to appear in Phys. Rev. E), arXiv:1211.5177.

[36] J. M. Luttinger, An exactly soluble model of a many-fermion system, Journal of Mathematical Physics **4**, 11541162, (1963).

[37] R. Kubo,J. Phys. Soc,Japan, **12**, 570 (1957).

[38] H. B. Callen and T. A. Welton , Phys. Rev. **83**, 34 (1951).

[39] S. Tanaka and S. Ichimaru, J. Phys. Soc. Japan **55**, 2278 (1986).

[40] K. S. Singwi, M. P. Tosi, R. H. Land, and A. Sjlander, Phys. Rev. 176, 589 (1968).

[41] P. Vashista and K. S. Singwi, Phys. Rev. B 6, 875 (1972).

[42] J. Hubbard, Proceedings of the Royal Society of London **276** (1365): 238257, (1963).

[43] *Density Functional Theory: An Advanced Course*, E. Engel and R.M. Dreizler (Springer, Heidelberg, 2011).

[44] J. Lutsko, *Recent Developments in Classical Density Functional Theory*, Adv. Chem. Phys. **144**, S. Rice, ed. (J. Wiley, Hoboken, NJ, 2010).

[45] M. Baus and J.P. Hansen, Phys. Rep. **59**, 1 (1980).

[46] J. Wrighton, J. W. Dufty, H. Kählert, and M. Bonitz, Phys. Rev. E **80**, 066405 (2009).

[47] Huang, Kerson (1990), *Statistical Mechanics*, Wiley, John Sons, ISBN 0-471-81518-7, OCLC 15017884.

[48] S. Dutta and J. Dufty, *Classical Representation of a Quantum System at Equilibrium: Applications*, Phys. Rev. E (to appear), arXiv:1211.5185.

[49] J. Wrighton, H. Kählert, T. Ott, P. Ludwig, H. Thomsen, J. Dufty, and M. Bonitz, Contrib. Plasma Phys. **52**, 45 (2012).

[50] D. Brydges and Ph. Martin, J. Stat. Phys. **96,** 1163 (1999).

[51] D. Pines and Ph. Nozieres, *The Theory of Quantum Liquids*, (Benjamin, NY, 1966).

[52] D. Kremp, M. Schlanges, W. Kraeft, *Quantum Statistics of Nonideal Plasmas*, (Springer-Verlag, Berlin, 2005).

[53] F. Perrot and M. W. C. Dharma-wardana, Phys. Rev. A **30**, 2169 (1984).

[54] P. Attard, J. Chem. Phys. **91**, 3072 (1989), equation (18).

[55] J. W. Dufty and S. Trickey, Phys. Rev. B **84**, 125118 (2011).

[56] G. Ortiz and P. Ballone, Phys. Rev. B **50**, 1391 (1994).

[57] J. Kimball, Phys. Rev. A **7**, 1648 (1973); A. Rajagopal, J. Kimball, and M. Banerjee, Phys. Rev. B **18**, 2339 (1978).

[58] K-C Ng, J. Chem. Phys. **61**, 2680 (1974).

[59] S. Dutta and J. Dufty, *Jellium at Warm, Dense Matter Conditions*, arXiv:1302.4507.

[60] C. Henning, H. Baumgartner, A. Piel, P. Ludwig, V. Golubnychiy, M. Bonitz, and D. Block, Phys. Rev. E **74**, 056403 (2006).

[61] C. Henning, P. Ludwig, A. Filinov, A. Piel, and M. Bonitz, Phys. Rev. E **76**, 036404 (2007).

[62] H. Totsuji, Journal of Physics A: Mathematical and General , vol. **39**, 45654569, (2006).

[63] K. Tsuruta and S. Ichimaru, Physical Review A , **48**, 1339, (1993).

[64] R. W. Hasse and V. V. Avilov, Physical Review A, **44**, 4506, (1991).

[65] W. D. Kraeft and M. Bonitz: Thermodynamics of a correlated confined plasma II. Mesoscopic system. Journal of Physics: Conference Series (2006), vol. 35:pp. 94109

BIOGRAPHICAL SKETCH

Sandipan Dutta was born in India. He had his final exam at University of Florida on April 15, 2013.